

# **Measuring the Mechanical Forces of Elongation Factor G Mediated Translocation**

by  
Miriam Nicolette Gavriiuc

**A dissertation submitted to the Department of Biology and Biochemistry,  
College of Natural Sciences and Mathematics  
in partial fulfillment of the requirements for the degree of**

Doctor of Philosophy

in Biochemistry

**Chair of Committee: Yuhong Wang**

**Committee Member: James Briggs**

**Committee Member: Loi Do**

**Committee Member: Preethi Gunaratne**

University of Houston  
May 2022

## **DEDICATION**

This dissertation is dedicated to my family. My parents, Paul and Luminita Gavriiuc. My siblings, Lucian and his wife Liliana Gavriiuc, Michelle and her husband Alex Constantinescu, Octavian and his wife Leslie Gavriiuc. My nieces and nephews, Timmy, Emma, Lizzie, Edy, Michael, Jacob, and Ella. My best friend Dr. Diane Dreucean. Thank you to all of my family for your love and support. I would not have made it here without each one of you.

“FOR I KNOW THE PLANS I HAVE FOR YOU,” DECLARES THE LORD, “PLANS TO PROSPER YOU AND NOT TO HARM YOU, PLANS TO GIVE YOU HOPE AND A FUTURE.”

JEREMIAH 29:11

## ACKNOWLEDGMENTS

I would like to acknowledge my advisor Dr. Yuhong Wang for her guidance and support for these past six years. Thank you for giving me my first full time job, and for giving me the opportunity to grow as a scientist during my graduate studies. I will always appreciate the support and guidance that I received during this time. I would also like to acknowledge my committee members, Dr. James Briggs, Dr. Margaret Cheung, Dr. Loi Do, Dr. George Fox, and Dr. Preethi Gunaratne. Thank you for your guidance and encouragement during my graduate studies. I would also like to acknowledge Dr. Ted Wensel, as well as the HAMBP steering committee. The HAMBP fellowship greatly impacted my development as scientist, and I will always be grateful for the opportunities given to me by this fellowship. To my labmates and friends, Haopeng Yang, Jordan Johnson, Jacob Steele, Heng Yin, and Yujia Mao. Thank you for the support and kindness you showed me during my graduate studies. Without each one of you, I would not have made it to this point and I will always be grateful for the opportunity to have become friends with you. I also would like to acknowledge Dr. Victor Stepanov, I will always appreciate the kindness and patience you showed me during my graduate studies. To my labmate and good friend, Dr. Ran Lin, thank you for your support during my studies, I couldn't have made here without out you, and I'm grateful to have made a lifelong friend. Thank you Rosezelia Jackson for all of the support you have given me in these past five years. I will always cherish the times I spent chatting with you in your office. I would also like to acknowledge my friends Rintu, Riya, Fei, and Taher, Zeinab, Shravasti, Brandon, and Stewart. To Nabina Paudyal and Josh Rosario-Sepulveda, I am very grateful to have met both of you through HAMBP. I would also like to acknowledge Dr. William

Widger. Thank you for your support and mentorship during my undergraduate and graduate studies. Visiting with you was always a highlight in my day, and I will always think of you when I make cinnamon rolls. To my good friend Dr. Jonathan Rangel, thanks for putting up with me.

## ABSTRACT

The ribosome is the ribonucleoprotein complex that is responsible for the correct translation of mRNA into protein. This complex is associated with the GTPase elongation factor G (EF-G), which catalyzes translocation on the ribosome, however, the mechanism is poorly understood. Crystallographic studies revealed a previously unknown compact conformation of EF-G, implying large conformational changes. The biological relevance of this change was not revealed, however, because of the artificial crystal lattice present in x-ray studies. To explore this, an EF-G mutant carrying only two cysteines (M5 EF-G) was generated and internally crosslinked to itself, using two lengths of crosslinker. One that restricted EF-G from fully extending (BM(PEG)<sub>6</sub>) and one that allowed EF-G to undergo full conformational changes (BM(PEG)<sub>11</sub>). BM(PEG)<sub>11</sub> crosslinked EF-G functioned comparably to wild type, while BM(PEG)<sub>6</sub> crosslinked EF-G resulted in a lower force exerted. The BM(PEG)<sub>6</sub> crosslinker also reduced ribosomal translocation efficiency to half, compared to that of the longer crosslinker and non-crosslinked EF-G. This force reduction did not result in frameshifting, confirming that EF-G does exert a force, but does not contribute to reading frame maintenance. Studying the overall conformational changes was important for understanding EF-G mechanism, however, it was also important to observe the details leading to the full conformational changes. In a second exploration of EF-G, the effector loop region was studied. The effector loop region spans approximately 7 residues within the GTPase center, the region where GTP is bound and hydrolyzed, on domain I of EF-G and contains important interactions for the function of EF-G. By introducing single site substitutions in the effector loop, the role of each residue was examined. Six variants were produced, and of the

six, one was completely unable to hydrolyze GTP, while another exhibited reduced GTPase activity. Not a single of the six was able to promote translocation at a rate comparable to M5 EF-G, effectively abolishing the function of EF-G on the ribosome. By studying the effector loop of EF-G, further understanding of the roles of the residues within this region, and how they contribute to the overall function of EF-G was obtained.

## TABLE OF CONTENTS

<b>DEDICATION.....</b>	<b>II</b>
<b>ACKNOWLEDGMENTS.....</b>	<b>III</b>
<b>ABSTRACT.....</b>	<b>V</b>
<b>LIST OF TABLES.....</b>	<b>IX</b>
<b>LIST OF FIGURES.....</b>	<b>X</b>
<b>LIST OF ABBREVIATIONS.....</b>	<b>XII</b>
<b>I. CHAPTER ONE: INTRODUCTION AND LITERATURE REVIEW.....</b>	<b>1</b>
1.1 The Ribosome and Translation.....	1
1.1.1 The Ribosome and its Structure.....	1
1.1.2 rRNA Structure and Function.....	4
1.1.3 Ribosomal Proteins.....	5
1.1.4 tRNA Structure and Function.....	6
1.1.5 The Steps of Translation.....	7
1.1.6 Ribosomal Targets of Antibiotics.....	9
1.2 Elongation Factor G (EF-G).....	11
1.2.1 EF-G Structure.....	11
1.2.2 The Function of EF-G.....	12
1.2.3 The GTPase Center.....	14
1.2.4 The Effector Loop of EF-G and eEF2.....	15
1.2.5 EF-G Targets of Antibiotics.....	17
1.3 Translocation.....	18
1.3.1 The Steps and Mechanisms of Translocation.....	18
1.3.2 The Translocation Debate.....	19
<b>II. CHAPTER TWO: MATERIALS AND METHODS.....</b>	<b>21</b>
2.1 Methods.....	21
2.1.1 Elongation Factor G Mutagenesis.....	21
2.1.2 Protein Purification.....	23
2.1.3 Elongation Factor G Crosslinking.....	24
2.1.4 Crosslinked Elongation Factor G Purification.....	25
2.1.4.1 Electro-Elution (Model 491 Prep Cell).....	25
2.1.4.2 Bead Purification.....	25
2.1.4.3 Phenyl Column Purification.....	27
2.1.5 Force Induced Remnant Magnetization Spectroscopy (FIRMS).....	27
2.1.6 Polyphenylalanine Assay.....	30
2.1.7 GTP Hydrolysis Assay.....	31
2.1.8 In Vitro RNA Transcription.....	32
2.1.9 tRNA Preparation and Charging.....	32
2.1.10 Ribosome Complex Preparation.....	33
2.1.11 Total tRNA Synthetase Purification.....	33
2.2 Materials.....	34

<b>III. CHAPTER THREE: ELONGATION FACTOR G CROSSLINKING, AND ITS ROLE IN TRANSLOCATION FIDELITY.....</b>	<b>36</b>
3.1 Introduction.....	36
3.2 Results.....	37
3.2.1 Site-Directed Mutagenesis and Crosslinking of Elongation Factor G.....	37
3.2.2 Visualization of Crosslinked M5 Elongation Factor G.....	43
3.2.3 Purification of Crosslinked M5 Elongation Factor G via Electro-Elution.....	51
3.3 Modulation and Visualization of EF-G Power Stroke During Ribosomal Translocation...53	
3.3.1 Power Stroke and Translocation Measurements of Maleimide Crosslinked EF-G.....	53
3.4 Discussion.....	56
<b>IV. CHAPTER FOUR: THE EFFECTS OF FUSIDIC ACID BINDING POCKET MUTATIONS.....</b>	<b>60</b>
4.1 Introduction.....	60
4.2 Results.....	61
4.2.1 Site-Directed Mutagenesis and Crosslinking of F95C/M682C Elongation Factor G in the Fusidic Acid Binding Pocket.....	61
4.2.2 Purification of F95C/M682C Elongation Factor G via Hydrophobic Interaction Chromatography and Bead Purification.....	65
4.3 Discussion.....	72
<b>V. CHAPTER FIVE: CHARACTERIZATION OF THE EFFECTOR LOOP OF EF-G.....</b>	<b>74</b>
5.1 Introduction.....	74
5.2 Results.....	76
5.2.1 GTP Hydrolysis Analysis of Effector Loop Mutants of EF-G.....	76
5.2.2 Translocation Activity of Effector Loop Mutants of EF-G.....	80
5.3 Discussion.....	82
<b>VI. CHAPTER SIX: CONCLUSIONS AND FUTURE DIRECTIONS.....</b>	<b>85</b>
6.1 Major Conclusions.....	85
6.1.1 EF-G Crosslinking and FIRMS Measurements.....	85
6.1.2 Crosslinking in the Fusidic Acid Binding Pocket.....	86
6.1.3 Characterization of the Effector Loop of EF-G.....	87
6.2 Future Directions.....	88
6.2.1 Crosslinking to Study Protein Conformational Changes.....	88
6.2.2 Fusidic Acid Resistance.....	89
6.2.3 Continued Studies of the Effector loop.....	89
Bibliography.....	91

## LIST OF TABLES

2.1.1	Mutagenesis Primers.....	22
2.1.2	PCR Parameters for Methylation and Mutagenesis.....	23
3.2.1	Residues in <i>T. thermophilus</i> Elongation Factor G Selected for Mutation to Cysteine and Their Distances in the Pre-translocation and Post-Translocation Complex.....	38
4.2.1	Residues in <i>T. thermophilus</i> Elongation Factor G Fusidic Acid Binding Pocket Selected for Mutation to Cysteine and Their Distances in the Pre-Translocation and Post-Translocation Complex.....	61

## LIST OF FIGURES

1.1.1	The Structure of the 70S Ribosome.....	3
1.1.2	2D Structure of Phenylalanine-tRNA.....	7
1.1.3	The Steps of Translation.....	9
1.2.1	Structure of EF-G.....	12
1.2.2	Structure of EF-G with Ordered Effector Loop.....	16
1.2.3	The Steps of Translocation.....	19
3.2.1	Site-Directed Mutagenesis of F411C/Y534C EF-G.....	39
3.2.2	Structures of F411C/Y534C (M5) EF-G.....	40
3.2.3	Crosslinking of E413C/G528C and M5 EF-G.....	41
3.2.4	Visualization of M5 BM(PEG) <sub>2</sub> Crosslinked EF-G Using Tris-Glycine SDS-PAGE..	44
3.2.5	Visualization of M5 BM(PEG) <sub>2</sub> Crosslinked EF-G Using Stacking and Native Gels..	46
3.2.6	Visualization of M5 BM(PEG) <sub>2</sub> Crosslinked EF-G Using Bis-Tris SDS-PAGE.....	48
3.2.7	Purification of Crosslinked EF-G via Electro-elution and Mass Spectrometry Confirmation of Crosslinking.....	52
3.2.8	Measurements of EF-G Power-stroke and Translocation Efficiencies.....	55
4.2.1	Site-Directed Mutagenesis and Crosslinking of F95C/M682C EF-G.....	63
4.2.2	Purification of F95C/M682C EF-G via Hydrophobic Interaction Chromatography....	66
4.2.3	Purification of F95C/M682C Crosslinked EF-G Via Thiol Sepharose 4B and Sulfolink Coupling Resin Bead Binding.....	68
4.2.4	Purification of F95C/M682C Crosslinked EF-G Via PureCube Maleimide Bioclone Iodoacetyl Bead Binding.....	70

5.2.1	Structure of the Effector Loop of EF-G.....	77
5.2.2	Effector Loop Mutants of EF-G.....	78
5.2.3	GTP Hydrolysis Activities of M5 EF-G and Effector Loop Mutants of EF-G.....	79
5.2.4	Polyphenylalanine Assays of M5 EF-G and Mutants of M5 EF-G.....	81

## LIST OF ABBREVIATIONS

Å	Angstrom
BME	Beta-mercaptoethanol
BM(PEG) <sub>2</sub>	1,8-bismaleimido-diethyleneglycol
BM(PEG) <sub>3</sub>	1,11-bismaleimido-triethyleneglycol
BM(PEG) <sub>6</sub>	Bis-Maleimide (Polyethylene Glycol) <sub>6</sub>
BM(PEG) <sub>11</sub>	Bis-Maleimide (Polyethylene Glycol) <sub>11</sub>
bp	Base pairs
DEPC	Diethyl pyrocarbonate
DNA	Deoxyribonucleic acid
EDTA	Ethylenediaminetetraacetic acid
EF-Tu	Elongation factor Tu
EF-G	Elongation factor G
<i>E. coli</i>	<i>Escherichia coli</i>
eEF2	Eukaryotic elongation factor 2
FIRMS	Force induced remnant magnetization spectroscopy
fmet	Formyl methionine
FPLC	Fast protein liquid chromatography
GTP	Guanosine-5'-triphosphate
IPTG	Isopropyl β-D-1-thiogalactopyranoside
LSU	Large subunit
M5 EF-G	F411C/Y534C EF-G
MES	2-ethanesulfonic acid
MgAc	Magnesium acetate
mRNA	Messenger RNA
MRSA	Methicillin-resistant <i>Staphylococcus aureus</i>
μL	Microliter
μm	Micrometer
μM	Micromolar
mg	Milligram
mL	Milliliter
mm	Millimeter
mM	Millimolar
M	Molar
MWCO	Molecular weight cut-off
MOPS	N-morpholino propanesulfonic acid
NF Water	Nuclease Free Water
ng	Nanogram
nmol	Nanomole
OD	Optical density
Pi	Inorganic phosphate
PBS	Phosphate buffered saline
PEP	Phosphoenolpyruvate

PK	Pyruvate kinase
RFU	Relative fluorescence unit
r-proteins	Ribosomal proteins
RRF	Ribosome recycling factor
rRNA	Ribosomal RNA
smFRET	Single-molecule Förster resonance energy transfer
SSU	Small subunit
<i>str</i>	Streptomycin operon
TCA	Trichloroacetic acid
<i>T. thermophilus</i>	<i>Thermus thermophilus</i>
TCEP	Tris(2-carboxyethyl) phosphine

# **CHAPTER ONE: INTRODUCTION**

## **1.1 The Ribosome and Translation**

### **1.1.1 The Ribosome and its Structure**

The ribosome is the complex molecular machine that is responsible for translating messenger RNA (mRNA) into protein. Ribosomes are present in all domains of life and are essential for the survival of an organism (1). For translation to occur, the step-by-step instructions for making protein must first be transcribed from nuclear or mitochondrial DNA (2). The transcribed mRNA is then translated into protein by free floating ribosomes in the cytosol, or endoplasmic reticulum attached ribosomes, in the case of eukaryotic organisms (3). When the ribosome has finished translating the mRNA, the newly made protein moves on to be fully folded, post-translationally modified, or directly to begin its function. Once the protein is made, the ribosome can then be recycled through dissociation of its subunits to continue the translation cycle (4). Decades of studies have gone into uncovering the details of ribosomal translation, and yet more work still remains to be done to fully understand this complex process.

Crystal structures of the ribosome reveal that it is made up of two major subunits, the small and large subunits consisting of ribosomal RNA (rRNA) (Figure 1.1.1) (5,6). In bacteria, the small subunit (SSU) is referred to as the 30S subunit, while the large subunit (LSU) is the 50S subunit. The combined subunits come together to form one single 70S subunit. In eukaryotes, the small and large subunits are the 40S and 60S subunits, respectively, and the 80S subunit combined. The individual subunits are quite flexible and movement occurs both within the subunits, and relative to each other, termed inter-subunit rotation (7). Studies of this rotation determined that it was critical for the ribosome to carry

out its function in translation (8). Individually, the subunits serve their own specific functions. The SSU is responsible for mediating interactions between the codon of the mRNA and the anticodon of the corresponding tRNA. The LSU contains the peptidyl transferase center, which is the region that the peptide bond is catalyzed, and the binding sites for the multiple GTPases that bind to the complex (9). When combined, the 70S ribosome can rapidly and accurately translate mRNA to protein. In order to accommodate incoming tRNAs, the ribosome contains three tRNA docking sites. The aminoacyl site (A site) accepts new aminoacyl-tRNAs (tRNAs containing their amino acid). The tRNA then advances to the peptidyl site (P site) with the peptide chain, and once the chain has been handed to the next tRNA, the P site tRNA will move to the exit site (E site). From here, the now deacylated tRNA can depart from the ribosome to be re-charged and cycle through again. These three sites are formed in the ribosome by the rRNA themselves and span both subunits, with the anticodon stem loop of the tRNA in the 30S and the acceptor stem in the 50S. In addition to the rRNA aspects of the subunits, many proteins (r-proteins) are also associated with this complex. The bacterial ribosome contains approximately 56 r-proteins, while the number is about 80 in eukaryotes (10,11). The ribosome is also associated with several transient proteins that catalyze specific functions on the ribosome, then dissociate. They include the GTPases elongation factor Tu (EF-Tu), which is responsible for delivering charged tRNAs, and elongation factor G (EF-G), which catalyzes translocation. Through the coordination of rRNA, tRNA, mRNA, and protein, the ribosomal complex is tasked with manufacturing each needed polypeptide for use in the cell. If this process cannot occur as it should, the results can be devastating to the organism; but, deep understanding of this sophisticated process can also provide the key to solving a multitude of human health complications (12).

In November and December of 2020, two mRNA vaccines were approved to aid in the prevention of COVID-19 infections. The first vaccines of their kind function by utilizing the essential process conducted by the ribosome. The mRNA vaccine is injected into the body, where it eventually makes its way to the cells. The instructions for making COVID spike proteins is then translated by our bodies' own ribosomes, and this foreign protein is then recognized by the immune system, which mounts a full response (13). After the body has taken care of the foreign protein, the body will file away the information needed to fight the infection, should the spike protein ever be spotted again (14). The introduction of mRNA vaccines is a huge step for future disease prevention and treatments. Although using the bodies' own machinery is not a new method in medicine, as several immunotherapies already exist, it shows the potential that something as small as the ribosome holds.

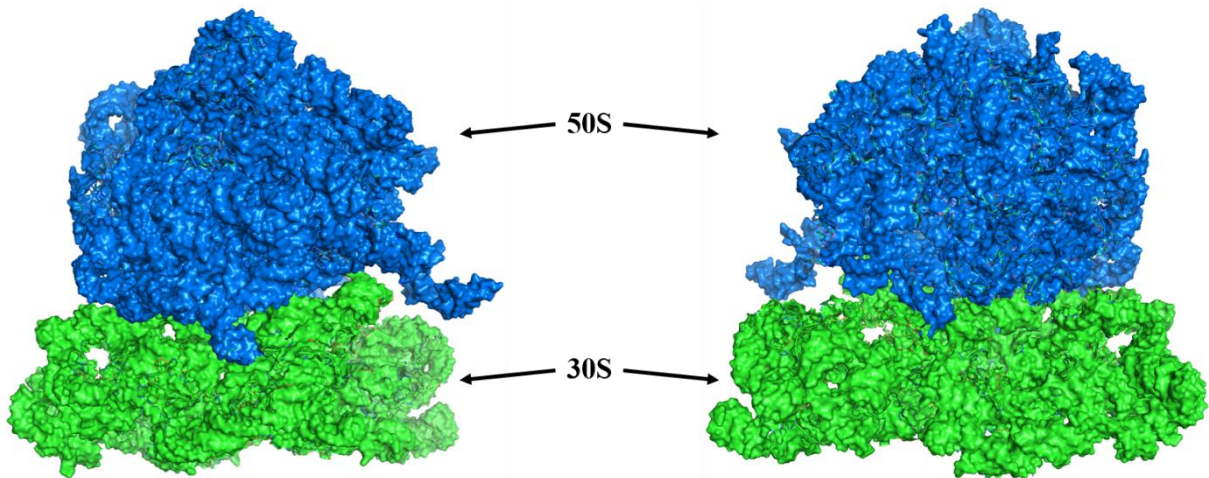


**Figure 1.1.1 The Structure of the 70S Ribosome.** Surface view of the 70S *E. coli* ribosome. 30S subunit (green), 50S subunit (blue) (PDB: 4V7B (15)).

### 1.1.2 rRNA Structure and Function

Approximately two-thirds of the weight of the ribosome is made up of rRNA. rRNAs are categorized by their size, which is determined by their sedimentation coefficients (how the particle sediments during centrifugation) (16). The sedimentation coefficients are given in units of Svedbergs (S), and this is reflected in the naming of the rRNAs. The bacterial SSU consists of 16S rRNA, while the LSU is made up of 5S and 23S rRNA (9). Eukaryotic ribosomes are similar to their bacterial counterparts and the SSU contains 18S rRNA, while the LSU is made up of 5S, 5.8S, and 28S rRNA (17,18). Due to a lack of membrane bound organelles, bacteria produce their rRNA in the cytoplasm. Eukaryotes, on the other hand, make rRNA in the nucleolus, located within the nucleus (19). Following transcription of the rRNA molecules, the RNA will base pair to itself and fold into its correct secondary structure. Reconstitution of 30S subunits *in vitro* revealed that the information needed for correct folding of the ribosome is inherent to the ribosomal particles (20). Once the ribosome has fully assembled with rRNA and protein, it is ready to begin translating. Following years of work and debate, thorough analysis of the ribosome structure finally led to the conclusion that the rRNA portion itself is responsible for catalyzing peptide bond formation, and the phrase “the ribosome is a ribozyme” was termed (21). Decades of studies had shown that the peptidyl transferase site was located in the 50S subunit, but it wasn’t until high resolution structures of this region revealed that none of the several dozen ribosomal proteins side chains were close enough to catalyze peptide bond formation (21,22). The rRNA itself was the only species in this complex capable of this feat.

### 1.1.3 Ribosomal Proteins

Protein accounts for the remaining one-third of the weight of the ribosome. As mentioned, 56 r-proteins and 80 r-proteins are associated with bacterial and eukaryotic ribosomes, respectively. To distinguish which subunit the protein is associated with, the protein is denoted by the letter L for large subunit, and S for small subunit. Within all three domains of life, 15 SSU proteins and 18 LSU proteins are universally conserved (11). Many of the proteins are tasked with structural support of the flexible ribosomal complex, however, several do have specific functions, though, their identification was quite difficult due to the size and cooperativity of the ribosomal complex. Nonetheless, multiple roles for r-proteins have been identified, and various r-proteins involved in the elongation cycle are outlined. For example, the bacterial small subunit proteins S3, S4, and S5 form an entry tunnel for the mRNA on the ribosome. Studies of these proteins revealed that when S3 and S4 were mutated, it resulted in an impairment of helicase activity on the ribosome, although the ribosome itself was still the primary executor of this activity (23). A second trio on the small subunit consisting of S12, S4, and S5 are responsible for assisting in the accuracy of translation. Studies on the ribosome revealed that streptomycin resistant mutations in S12 correct the error inducing effect of the antibiotic (24,25). S4 and S5 stabilized the movement of the 30S subunit into the closed form upon cognate tRNA binding, which was shown to have an effect on translational accuracy compared to cases in which stabilization did not occur (26). Together the S12, S4, and S5 collaboration assisted in ensuring accurate translation. On the large subunit, the dimer of the nearly identical proteins L7/L12 binds two copies plus one L10 to the ribosome to form what's known as the L12 stalk. This complex was determined to be involved in elongation factor binding and subsequent activation, and

deletions of the flexible hinge region in L12 resulted in total inactivation in polyphenylalanine synthesis assays (27,28). While the rRNA portion of the ribosome is the primary conductor of activity, r-proteins were shown to also be critical in translation.

#### **1.1.4 tRNA Structure and Function**

Delivery of amino acids to the ribosome for incorporation into the growing peptide chain is handled by the transfer RNAs (tRNAs), together with the GTPase EF-Tu. Detailed studies of protein synthesis led to the discovery of a soluble RNA, later called tRNA, that could transfer amino acids for incorporation into peptides (29). tRNAs are generally pictured in their secondary structure form, however the tertiary structure reveals that tRNAs are “L-shaped” in order to be accommodated into the ribosome (30). tRNAs contain four helical sections, a 5' phosphate, a 3' CCA tail, and is structurally highly conserved (Figure 1.1.2). The 5' and 3' ends come together to form the acceptor stem, containing the CCA tail that interacts with EF-Tu•GTP to form the amino acid delivery complex ready to bind to the ribosome (31). The D-loop and TΨC loop contain dihydrouridine and pseudouridine, respectively, and form the turn of the L shaped tRNA (32). The anticodon loop sits across the hypotenuse relative to the acceptor stem and pairs with the codon of the mRNA (33). The discovery of wobble base pairing of the first of the three bases on the tRNA explains why multiple codons can be paired with a limited number of tRNAs (34,35). Once the correct amino acid is delivered to the growing peptide, the tRNA exits the ribosome and is recharged with a new amino acid by specific tRNA synthetases for continued use. The segments of the tRNA each come together to form an essential component of the translation complex, and along with other factors, provides each amino acid needed to produce every peptide the cell requires.

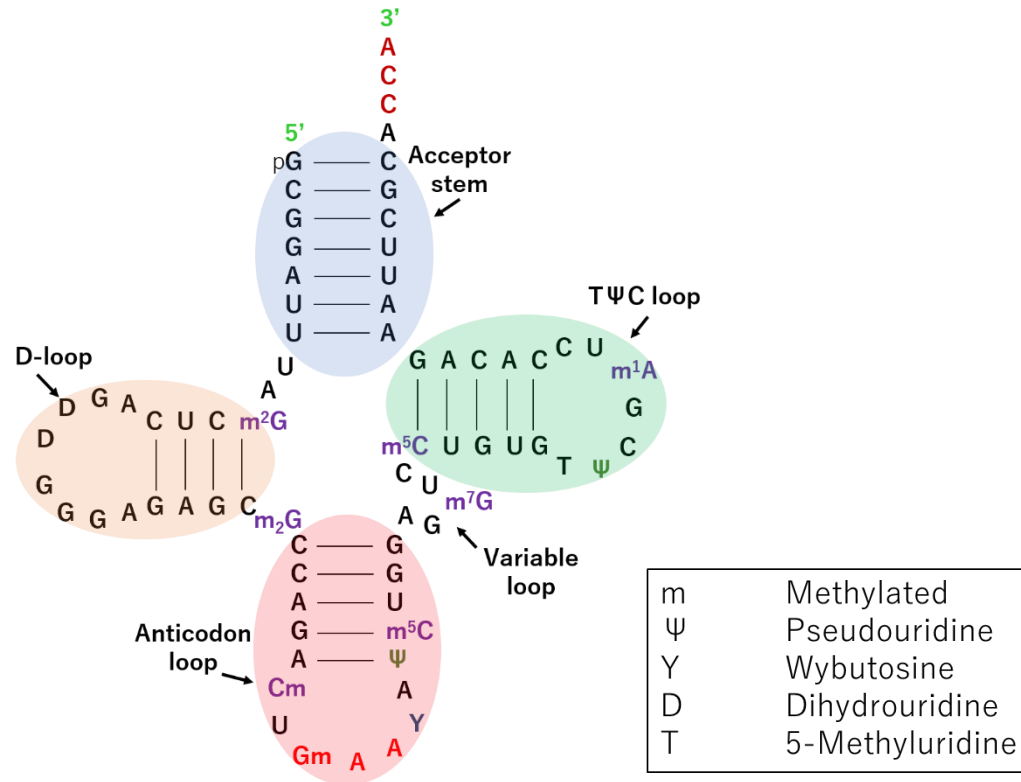


**Figure 1.1.2 2D Structure of Phenylalanine-tRNA.**

### 1.1.5 The Steps of Translation

Translation occurs in three major steps: initiation, elongation, and termination, followed by ribosome recycling (Figure 1.1.3). In bacterial translation, initiation begins with the formation of the 30S initiation complex. Approximately eight nucleotide bases upstream of the start codon of the mRNA (most often AUG) resides the Shine-Dalgarno sequence which is complementary to a portion of the 16S rRNA of the 30S subunit (36). At this time the initiator tRNA, usually an fmet-tRNA<sup>fmet</sup>, also binds to the 30S initiation complex in the P site. In addition to the RNA aspects, three initiation factors are also part of this complex. Studies have revealed that IF1 binds to the A site of the SSU and assists in initiator tRNA selection (37,38). IF3 is involved in initiator tRNA selection fidelity, and ensuring the correct start codon is chosen. Unlike the other factors, IF2 is a GTPase that binds to the initiator

tRNA to help shuttle it to the correct position on the P site (39). Upon 50S subunit association, the factor hydrolyzes its GTP and the subunits can fully combine, becoming the 70S subunit. All three initiation factors work together to ensure accuracy at the start of the translation reaction. Once the full 70S complex has formed correctly, it is ready to begin protein synthesis.

During the elongation phase of translation, amino acids are incorporated into the growing peptide chain. To begin elongation, EF-Tu•GTP shuttles charged tRNAs (tRNAs bound with their corresponding amino acid) to the A site. Upon GTP hydrolysis, EF-Tu dissociates from the complex. After peptide bond formation is catalyzed by the ribosome, the peptide linked A site, deacylated P site, and the E site tRNAs can begin their movement to the next position. This initial movement happens spontaneously, and results in hybrid position tRNAs. EF-G•GTP is now free to bind the ribosome at the A site to catalyze the completion of the tRNAs' journey. The peptide-linked tRNA will now be in the P site, the deacylated tRNA in the E site, and the previous E site tRNA will have left the complex. The ribosome will also have shifted three nucleotides (one codon) down the mRNA so the next amino acid can be incorporated (15,40). New residues will be added to the chain until a STOP codon is reached to start termination.

Termination most often occurs when a STOP codon is reached, although other modes of termination exist. To begin termination, the empty A site containing UAG, UGA, or UAA is recognized by either release factor 1 (RF1) or 2 (RF2) which binds that site, and is followed by peptide ester bond hydrolysis (41,42). The GTPase release factor 3 (RF3) can now proceed to bind. Studies of RF3 were initially contradictory to each other, however experiments have revealed that post GDP exchanged RF3•GTP's main function is to promote dissociation of

RF1 and RF2 from the ribosome to be recycled. RF3 dissociation then follows (43). Directly after termination, ribosome recycling occurs to prepare for the next round of translation.

Although ribosome recycling could be considered a fourth step, here it will be included within termination. Recent in-depth studies of ribosome recycling have revealed that through the combined actions of ribosome recycling factor (RRF), EF-G, and the tRNA occupying the P site, the promotion of subunit splitting is achieved (4). After the translation complex has been fully separated into its components, the cycle can begin once again with a new protein to be produced.

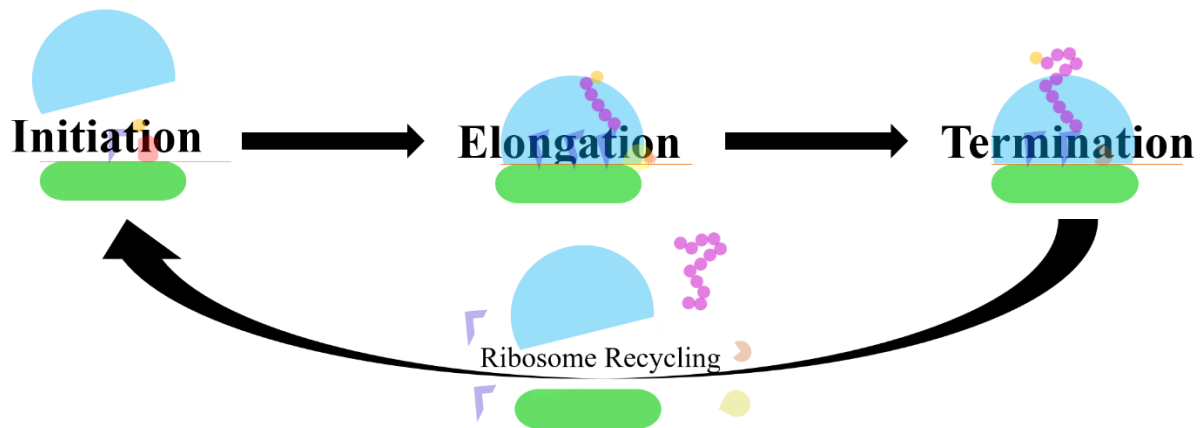


**Figure 1.1.3 The Steps of Translation.**

### **1.1.6 Ribosomal Targets of Antibiotics**

The ribosome is responsible for the production of proteins across all domains of life, and the interruption of ribosomal function results in organism death. The presence of ribosomes in bacteria, therefore, makes them a significant target for antibiotics. And while the bacterial and eukaryotic ribosomes are similar, their differences provide the needed room for antibiotics to be designed in a way that lowers their toxicity to humans, and the result is several classes of antibiotics targeting this complex. Despite the large size of this complex, drugs tend to target specific areas. For the 30S subunit, the primary location is the

mRNA/tRNA interface, while the peptidyl transferase center is the target on the 50S subunit (44). With all of the added players, the elongation phase of translation is a prime spot for stopping an infection. Of the 30S subunit targeting antibiotics, tetracycline is a well-known example that is used to treat a variety of infections, as well as acne. This drug binds the 16S rRNA and prevents aminoacyl-tRNAs from binding to the A-site, effectively halting translation (45,46). Of the 50S binding drugs, chloramphenicol is an important antibiotic used to treat serious bacterial infections. This molecule binds in the peptidyl transferase center at the aminoacyl side of the A site, blocking protein synthesis (44,47,48). Both of these antibiotics target the elongation phase of translation when the complex is in full swing. Yet, this is only a small sample of the antibiotics that target the ribosome, and many more still remain to be discovered or engineered to address the growing problem of antibiotic resistance. When studying antibiotics, resistance has to be considered, and in the case of ribosome targeting drugs, resistance has become a frequent issue. There are a variety of modes of resistance, but one significant way that the bacterial ribosome can confer resistance is through mutations. Mutations of rRNA at these binding sites can lead to decreased affinity for the antibiotic leading to increased resistance (49). Mutations happen naturally, but pressure from drugs like chloramphenicol can push for more resistant strains to dominate, leading to infections that are no longer treatable. To address this problem, more studies of the ribosome complex are required to produce new and efficient antibiotics. In addition to discovering modes of resistance, detailed studies on ribosome movement during translation can result in the development of antibiotics that can target specific intermediate states in this process, thus reducing the likelihood of resistance developing. The concerted efforts in studying translation will continue to be necessary to combat antibiotic resistance.

## 1.2 Elongation Factor G (EF-G)

### 1.2.1 EF-G Structure

Elongation factor G (EF-G) is a 78 kDa, five-domain bacterial GTPase that binds to the ribosome and catalyzes translocation. In *E. coli*, the sequence for EF-G is located on the *fus* gene within the streptomycin operon (*str*) (50). Domain I, also called the G domain, binds and hydrolyzes GTP. The structure of this domain is similar to that of other GTPases, but unlike other members of this family EF-G does not require a specific exchange factor for a GDP/GTP swap to occur, although the ribosome itself could fill this role (51). Domain I contains both beta strands and alpha helices (52). Studies of EF-G have shown that this enzyme has similar affinities for GDP and GTP, which can potentially be explained structurally by a difference in the hydrogen bonding partner of the conserved P loop lysine (53). The similar affinities would explain why a specific exchange factor is not needed for EF-G. Domain II, also called the G' domain, has a distinctive  $\beta$ -barrel or  $\beta$ -sandwich structure. Domains III-IV are characterized by  $\alpha$ - $\beta$  sandwich structures, with domain IV containing an additional type of each secondary structure (54). The Fusidic acid binding pocket is located in a compartment formed by domains I-III. Domain IV contains the active site of EF-G and extends out from the enzyme (55). This region interacts with the ribosome and tRNA<sub>2</sub>/mRNA complex to promote translocation. Domain V has been shown to be necessary for both translocation and EF-G turnover (55). Each domain within EF-G is essential for EF-G to hydrolyze GTP, catalyze translocation, and to be able to dissociate from the ribosome to continue during the elongation phase. Looking at the overall structure of EF-G, Czworkowski *et al.* describes, quite accurately, the shape as resembling a “tadpole”, with domain IV protruding out to resemble the tail. This conformation of EF-G has been well

known, but in 2015 a study reported a never-before-seen compact conformation of EF-G (56). The biological relevance of this state remained, however, and newer studies suggest that this conformation may not occur to the extent it was originally thought during elongation. Nonetheless, EF-G itself still undergoes significant and necessary conformational changes within the switch regions, regardless if the global changes do not occur as suggested, or when suggested. In ribosome recycling, the compact conformation is seen when bound to ribosome recycling factor (56). It's possible that EF-G assumes this extremely compact conformation only in this instance. Regardless, the ability for structural rearrangements to occur is critical for EF-G function, and this has been supported by multiple studies (57,58).

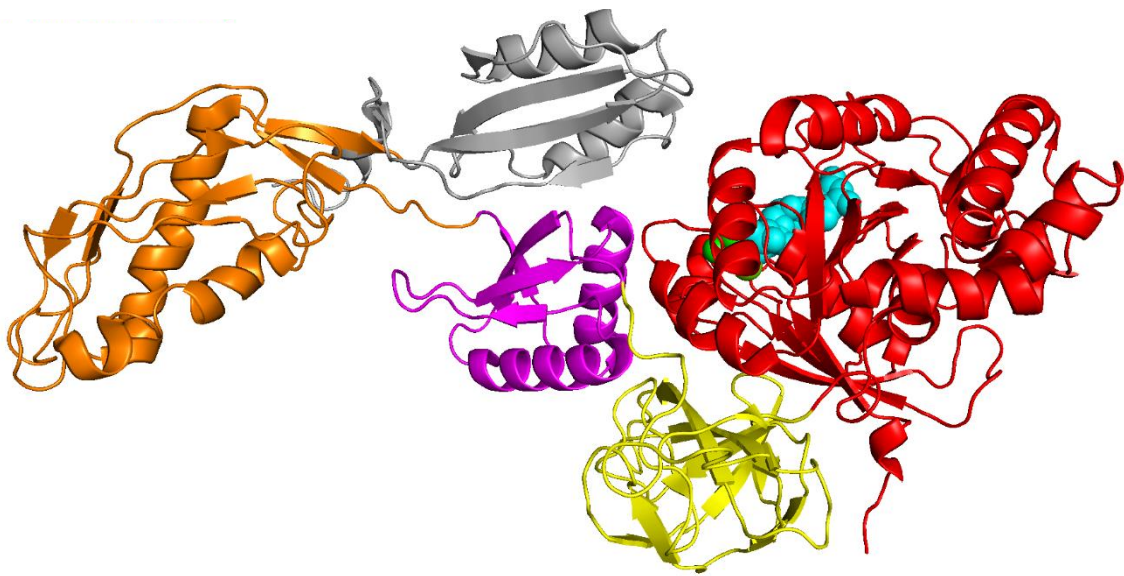


**Figure 1.2.1 Structure of EF-G.** Cryo-EM structure of EF-G. domain I (red), domain II (yellow), domain III (magenta), domain IV (orange), domain V (grey). GDP (cyan) and Pi (green) shown as spheres (PBD: 7PJV (59)).

### 1.2.2 The Function of EF-G

Catalysis during translocation and ribosome recycling are the two known functions of EF-G. During translocation, EF-G binds to the ribosome and GTP hydrolysis is rapidly induced (53). Although the ribosome can spontaneously translocate, the rate is improved

approximately 50,000 fold with the inclusion of EF-G, through stabilization of the hybrid ribosome state and lowering of the activation barrier (60). After translocation occurs and phosphate is released, EF-G dissociates from the ribosome, and translation continues beginning the cycle again. From previous studies, the binding of GTP by EF-G had been long known, however, the function of GTP hydrolysis for this enzyme was realized much later. Initial conclusions of the function of GTP pointed towards hydrolysis being used to dissociate EF-G from the ribosome after translocation had occurred (61). However, kinetic studies of this reaction revealed that the hydrolysis of GTP occurs before the catalysis of translocation, and from this study speculation that EF-G may exert a force arose (62). Regardless of mechanism, the function of EF-G to catalyze translocation is well understood. EF-G binds to the ribosome and stabilizes the ratcheted conformation in the initial stages of translocation, after the tRNAs have moved into their hybrid states (movement on the LSU, but not on the SSU). Hydrolysis of GTP occurs quickly after binding followed by ribosomal rearrangements. To complete translocation, the tRNAs move fully into their next positions and the mRNA shifts three nucleotides (one codon) down. The tip of domain IV of EF-G was shown to interact tightly with the tRNA<sub>2</sub>/mRNA complex, 30S, and 50S subunits during this process (15,59,63). The function of EF-G is clear, but questions of how it's carried out still remains.

EF-G's second function occurs during ribosome recycling, for which deeper understanding has been achieved more recently. During this phase, ribosome recycling factor (RRF) and EF-G combine together to form a large complex that can then bind the ribosome at the termination stage. EF-G induces large conformational changes in RRF, as well as undergoing its own. GTP hydrolysis and subsequent movement to the elongated conformation of EF-G result in further changes in RRF allowing the ribosome to be fully split into its

subunits (4). Taken together, the diverse functions of EF-G reveal the extensive potential for mechanistic understandings that studying this enzyme holds.

### **1.2.3 The GTPase Center**

Within domain I of EF-G lies the GTPase center. This region is responsible for the binding and hydrolyzing of GTP to be used during translation. Studies of the protein synthesis reaction reported the specificity of EF-G only for the triphosphate GTP. While ITP binding did occur, ITP results in a very reduced amount of activity. The remaining nucleotide triphosphates had shown no activity (64). Early studies of the function of GTP use by EF-G concluded that hydrolysis occurred after translocation and was used to remove the enzyme from the ribosome. Later studies, however, proved this incorrect and revealed that GTP hydrolysis does precede translocation (61,62). Experiments on the requirements for EF-G GTP hydrolysis revealed that binding to the ribosome was essential (65). Studies of GTPases have reported several major functional units within the center including switch I, switch II, and the p-loop. The effector loop is also considered part of the GTPase center and is explained in greater detail in the following section and in Chapter 5. To be able to hydrolyze GTP, the molecule must first bind to the enzyme and this is achieved through the phosphate binding loop (p-loop), which interacts with the  $\beta$  and  $\gamma$  phosphates of the bound nucleotide (66). A large number of the p-loops contain the motif GXXXXGK, though this motif can be variable, with the exception of the lysine which is extremely conserved (67). The lysine is shown to interact with the  $\gamma$  phosphate of the nucleotide throughout the reaction (68). The remaining portions of the GTPase center are made up by switch I and II. The switch regions of G proteins have been studied extensively and the simplest definition is that these regions are considered to be “on” or “off” depending on the bound nucleotide, and that these regions

propagate protein-wide conformational changes (69). The boundaries of the switch regions are fairly arbitrary, though they can be set based on secondary structural groups. Structures of *E. coli* EF-G during translation reveal that switch I is in a compact position following GTP hydrolysis and before Pi release (59). Several points of interaction of the switch regions with Pi, GDP, and the rRNA of the ribosome occur. Conserved threonine 61 of switch I is coordinated by Pi, along with glycine 90 and histidine 91 of switch II. Switch I arginine 58 and the mentioned switch II histidine 91 both contact the sarcin-ricin loop of the 50S subunit in this phase. The release of Pi from EF-G activates conformational changes in EF-G which commences ribosome unlocking and results in tRNA translocation on the 30S subunit. The switch regions undergo large conformational changes and switch I eventually reaches the elongated or “relaxed” position. Through the cooperation of each piece of the GTPase center, the energy from hydrolysis can be converted into global rearrangements of the entire translational complex resulting in the completion of translocation.

#### **1.2.4 The Effector Loop of EF-G and eEF2**

The effector loop region of EF-G encompasses about seven residues within the switch I region, as mentioned previously, and is important for the function of EF-G on the ribosome during translocation. This segment is often disordered in crystal structures, though recent studies have been able to capture this area in high resolution. From just sequence comparisons alone, aspartate residue 51 in *E. coli* is conserved across all domains of life, as well as in EF-Tu, while glycine 46 is conserved only within bacteria. Studies in EF-Tu have revealed that the aspartate residue coordinates with a magnesium ion via a water bridge, and this residue in EF-G may potentially do the same (59,70). Although they are similar, studies that replaced the effector loop of EF-G with the loop of EF-Tu resulted in a total abolishment of EF-G function

(71). This affirms that while the loops are similar in function, they each have their own distinctive design specific for their assignment. In the human homolog of EF-G, eEF2, phosphorylation at threonine 56 by eEF2 kinase occurs (72). Phosphorylation shuts down the function of eEF2, and to date, this translational control mechanism has only been seen in this example. It should be noted, though, that while T56 is the primary phosphorylation site, studies show two additional sites that also become phosphorylated, though T56 phosphorylation is sufficient to arrest function (73). The likely consequence of T56 phosphorylation is halting of enzyme function after GTPase activity has occurred, but before translocation (74,75). Though this is not yet seen in bacterial EF-G, studies of the effector loop continue and results obtained by our lab are presented in Chapter 5.

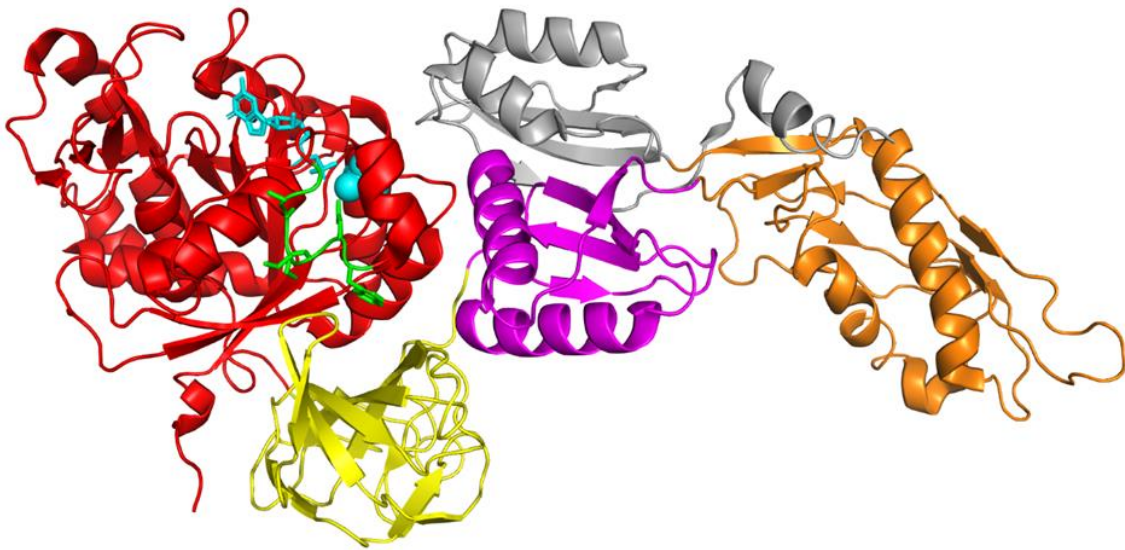


**Figure 1.2.2 Structure of EF-G with Ordered Effector Loop.** Crystal structure of EF-G with effector loop highlighted in green. domain I (red), domain II (yellow), domain III (magenta), domain IV (orange), domain V (grey). GDP and Pi shown in cyan (PDB: 7PJV (59)).

### 1.2.5 EF-G Targets of Antibiotics

Like the ribosome, EF-G is also a target for antibiotics due to its role in protein synthesis. One notable drug is Fusidic acid, which binds to the aptly named Fusidic Acid binding pocket on EF-G and prevents EF-G from dissociating from the ribosome after translocation has occurred (76). Fusidic Acid is currently banned in the United States for use in humans, however, it is used extensively for research purposes to lock EF-G in a post-translational state on the ribosome. The reason for its banning is unclear, however, resistance is the most likely candidate (77,78). Nonetheless, it is still approved for use in other countries and recently has been brought up again for its potential to be used to treat MRSA, which has become a tremendous problem in this day of antibiotic overuse (79). If human use in the US remains impossible, however, the research applications of this antibiotic can still exist and continue to be utilized. A second drug, Dityromycin, is an antibiotic that is currently not approved for humans and is used to trap EF-G in the pre-translocation complex (56). Before the use of dityromycin, the pre-translocation complex of EF-G had never been seen. This antibiotic, though, does not bind to EF-G, but instead to r-protein S12 to block EF-G from undergoing its conformational changes during translocation (80). Compared to the ribosome, the number of regions in EF-G to be targets of antibiotics is substantially lower, thus not many drugs exist for the purpose of targeting EF-G. Greater understanding of EF-G mechanism and conformational changes could potentially open the door for newer antibiotics targeting this region.

## 1.3 Translocation

### 1.3.1 The Steps and Mechanisms of Translocation

Movement of the tRNA<sub>2</sub>/mRNA complex driven by large scale rearrangements in EF-G and the ribosome occurs during a process called translocation. A series of coordinated steps transpire to achieve this, and while translocation can occur spontaneously, meaning the ribosome inherently contains the ability, the rate is increased significantly by the addition of EF-G to the reaction (60,81). The early stages of translocation are marked by movement directly solely by the ribosome complex itself. The movement of the 30S subunit relative to the 50S subunit termed “ratcheting” occurs first. Evidence for this movement came in the form of structural studies when it was found that the 30S subunit fully rotates counterclockwise (7). After this step, but before EF-G catalysis, rotation within the 30S subunit shifts the tRNAs into their hybrid positions. This state is characterized by movement of the acceptor stem of the tRNAs on the 50S subunit from its current position into the next position, while the anticodon stem loop remains in the same site on the 30S subunit. Early studies using chemical footprinting inferred that this state was taking place, and EF-G with GTP could drive the tRNAs back into their classical states (82). Structural evidence of the hybrid state of the tRNAs revealed that they move into an intermediate position referred to as a chimeric hybrid state in which the tRNAs are between the sites on the SSU and fully in the next site on the LSU (83). Rotation or swiveling of the 30S head occurs and the anticodon stem loops of the tRNAs move into a chimeric state characterized by shifting between sites, as the acceptor stems have done, to accommodate the entrance of EF-G (84). Once the complex has entered this hybrid state, EF-G•GTP can bind to stabilize it. Confirmed by kinetic studies, the preference of EF-G is to bind the pre-translocation hybrid conformation of the ribosome,

which in turn supported EF-G's role in stabilizing the hybrid state (15,60,85). EF-G rapidly hydrolyzes GTP upon ribosome binding, and induces global rearrangements in the translocation complex. The movement of the mRNA was found to occur with the back rotation of the 30S subunit, and this was supported further when cryo-EM was used to capture structures containing two tRNAs (15,86). These studies affirmed the importance of inter- and intra- subunit movements, which had already been proven to be necessary for ribosomal function (8). Studies have shown that the ribosome itself is capable of translocation, albeit not at a sustainable level. Nonetheless, the inherent properties of this large multi-complex machine that has been studied for so many decades will certainly require several more to fully understand it.

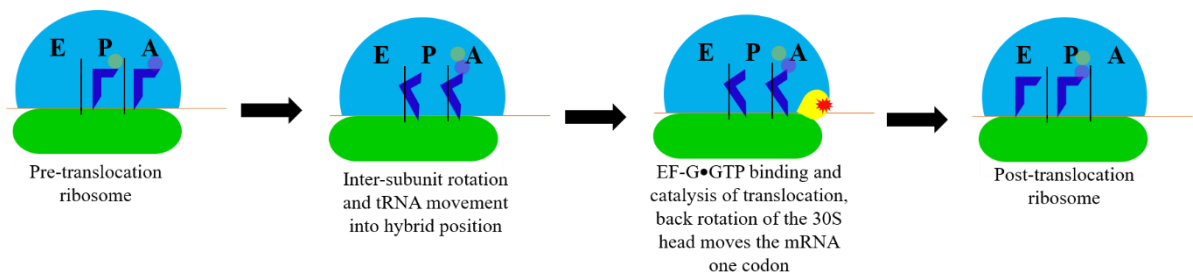


**Figure 1.2.3 The Steps of Translocation.**

### 1.3.2 The Translocation Debate

In the search for the mechanism of EF-G mediated translocation, multiple theories have arisen. Prior to the discovery that GTP is hydrolyzed before translocation occurs, it was thought that EF-G potentially used the energy from GTP to dissociate from the ribosome. When the order of hydrolysis was ascertained, this sparked the idea that EF-G could function through a power stroke mechanism as other motor proteins do. Early studies, however, disagreed with this idea. Using an optical tweezer method, the force generation by the ribosome was measured to be ~13 pN, which would be consistent with a Brownian motion

mechanism (87). Based on the Brownian model, EF-G uses the energy from GTP to tightly bind to the A-site of the ribosome after the tRNA has moved to the P-site, and no mechanical force by EF-G is generated. On the other hand, studies directly measuring EF-G force displayed a much larger number, that of ~89 pN generated on the ribosome (88). Structures of the ribosome with EF-G and two tRNAs in hybrid positions revealed that A-site tRNA movement exceeded the movement distance possible with the Brownian model (84). When the existence of a never-before-seen compact conformation of EF-G was discovered, the idea that this enzyme could generate a large force was sustained (56). Addition of internal crosslinkers into EF-G decreased the generated force, indicating that the compact state may occur *in vivo* (56,58). When the structural and force data are examined together, the power stroke model is favored.

With the contradicting ideas, the discovery of new evidence was inevitable. In many models, the role of EF-G dissociation assistant was assigned to Pi. The function of Pi release and switch I movement, though, have now been studied in greater detail (63). The notion that switch I conformational changes propagated by GTP hydrolysis result in large scale ribosomal complex movement was not widely accepted at the time it was reported due to the use of two different bacterial species for different states (89). Recent studies, however, have not only backed this but have also been able to reveal an in-depth snapshot of the function of Pi in this reaction. Structures at multiple stages of translocation have now made known that conformational changes in switch I occur after Pi release, and then subsequent global rearrangements can occur (59). Where this leaves the mechanism of EF-G is still up for debate, and studies will certainly continue to work out the complex system by which EF-G, and translocation as whole, occurs.

## CHAPTER TWO: MATERIALS AND METHODS

This chapter contains work from the publication “Modulation and Visualization of EF-G Power Stroke During Ribosomal Translocation” published in ChemBioChem. Necessary permissions were obtained from ChemBioChem for this work to be used in this dissertation.

### 2.1 Methods

#### 2.1.1 Elongation Factor G Mutagenesis

Mutation sites were selected using the three-dimensional structure of *Thermus thermophilus* (*T. thermophilus*) elongation factor G (EF-G) (PDB files 4V7B and 4WQU). Using a sequence alignment, the residues in *Escherichia coli* (*E. coli*) were determined. All subsequent experiments were performed using *E. coli* EF-G. The GeneArt™ Site-Directed Mutagenesis PLUS System (ThermoFisher Scientific) was used to generate each double mutant. Beginning with a cysteine free variant of EF-G (vector: pET24b (+)), forward and reverse primers were designed for mutagenesis (Table 2.1.1). Each PCR reaction mix contained a final concentration of 1X Accuprime™ *pfx* reaction buffer, 1X enhancer, 4.8 units DNA methylase, 1X SAM, 1.5 units Accuprime™ *pfx*, 0.5µM forward primer, 0.5 µM reverse primer, and 28 ng of plasmid DNA containing the cysteine-free EF-G sequence (Table 2.1.2). After each PCR piece was produced, the short and long pieces were recombined. The recombination mix contained PCR water, equal amounts of PCR product 1 and PCR product 2, and 1X GeneArt® enzyme mix. The mix was incubated at room temperature for 15 min. The reaction was stopped with the addition of 0.5 M EDTA pH 8.0 (GE Healthcare). 3 µL of recombination reaction was used to transform one tube of MAX Efficiency® DH5α™-T1<sup>R</sup> cells (ThermoFisher Scientific) using heat shock. The sample was incubated for 15 min on ice, put into a 42 °C water bath for 30 s, and then transferred back to the ice for 2 min. 250 µL

of S.O.C (ThermoFisher Scientific) media was added, and the sample was shaken at 37 °C for 1 h. The cells were plated on LB-kan agar plates and incubated at 37 °C overnight. Colonies were selected for inoculation and plasmid was isolated using the QIAprep Spin Miniprep Kit (Qiagen) or the PureLink™ HQ Mini Plasmid Purification Kit (Invitrogen).

**Table 2.1.1 Mutagenesis Primers**

Mutation Site (In <i>E. coli</i> )	Forward Primer	Reverse Primer
Phenylalanine 411	5' - TGGAACGTATGGAATGCCCTGAGCC GGTAAT - 3'	5' - ATTACCGGCTCAGGGCATTCCATAC GTTCCA - 3'
Tyrosine 534	5' - CAAACCCGAAAGGCTGCGAGTTCAT CAACGA - 3'	5' - TCGTTGATGAACTCGCAGCCTTTCG GGTTTG - 3'
Phenylalanine 95	5' - CGGGGCACGTTGACTGCACAATCGA AGTAGA - 3'	5' - TCTACTTCGATTGTGCAGTCAACGT GCCCG - 3'
Methionine 682	5' - CGTGCATCATACTTGCGAATTCCT GAAGTAT - 3'	5' - ATACTTCAGGAATTCGCAAGTGTATG ATGCACG - 3'
Threonine 62	5' - CAGGAACGTGGTATTTGCATCACTTC CGCTGC - 3'	5' - GCAGCGGAAGTGATGCAAATACCACG TTCCTG - 3'
Valine 93	5' - GACACCCCGGGGCACTGTGACTTCAC AATCGA - 3'	5' - TCGATTGTGAAGTACAGTGCCCCGG GGTGTC - 3'
Glycine 91	5' - ATCATCGACACCCCGTGCCACGTTGA CTTCACA - 3'	5' - TGTGAAGTCAACGTGGCACGGGGTGTG GATGAT - 3'
Asparagine 369	5' - GTTCAGATGCACGCTTGCAAACGTGA AGAGAT - 3'	5' - ATCTCTTCACGTTTGCAAGCGTGCAT CTGAAC - 3'

**Table 2.1.2 PCR Parameters for Methylation and Mutagenesis**

Temperature (°C)	Duration	# of cycles
37	20 mins	1
94	2 mins	
94	20 s	18
57	30 s	
68	<u>Phenylalanine 411/Tyrosine 534</u> Long piece: 3.5 min Short piece: 11 s	
	<u>Phenylalanine 95/Methionine 682</u> Long piece: 2 min 53 s Short piece: 58 s	
	<u>Threonine 62/Valine 93</u> Long piece: 3 min 50 s Short piece: 5 s	
	<u>Glycine 91/Asparagine 369</u> Long piece: 3 min 25 s Short piece: 28 s	
68	5 minutes	1
4	Hold	-

**2.1.2 Protein Purification**

30-40 ng of purified plasmid was used to transform 1 tube of One Shot™ BL21(DE3) pLysS cells (ThermoFisher Scientific). The cells were inoculated overnight in LB-kan media at 37 °C. The overnight culture was then separated equally into flasks of LB-kan. The flasks were incubated, with shaking, at 37 °C until the optical density (OD) reached ~0.8. 1 M IPTG was used to induce. The flasks were shaken, undisturbed, for 3 h. The culture was spun down at 4424  $\times$  g for 10 min. The supernatant was discarded and the cells were resuspended with B-per™ (ThermoFisher Scientific). DNase I (ThermoFisher Scientific) and lysozyme (Sigma) were added to the resuspended cells. Resuspended cells were stored at -20 °C. For purification, the cells were thawed and sonicated on ice for 5 min, with 20 s sonication on and 40 s sonication off, amplitude 80%. The cell lysate was spun down at 15,000  $\times$  g for 2 h, until

the supernatant was clear. The supernatant was collected and run through a PTFE 0.45  $\mu\text{m}$  30 mm diameter syringe filter (Denville Scientific INC.). The sample was purified using an ÄKTApurifier FPLC system with a HisTrap<sup>TM</sup> HP column (GE Healthcare Life Sciences). Sample was loaded onto the column using protein lysis buffer (50 mM NaH<sub>2</sub>PO<sub>4</sub>, 0.3 M NaCl, 4 mM BME, pH 8.0), and eluted using a gradient of protein elution buffer (50 mM NaH<sub>2</sub>PO<sub>4</sub>, 0.3 M NaCl, 4 mM BME, 1 M imidazole, pH 8.0). Purified sample was collected and concentrated using Pierce<sup>TM</sup> protein concentrators PES, 10 K or 30 K MWCO (Thermo Scientific) at 4300  $\times$  g for 30 min to 1 h. The sample was buffer exchanged to protein dialysis buffer (20 mM Tris-HCl, 10 mM MgCl<sub>2</sub>, 0.5 mM EDTA, 800  $\mu\text{M}$  BME, 400 mM KCl, pH 7.5) using a Nap<sup>TM</sup>-5 column (GE Healthcare Life Sciences) for long term storage. Collected protein was flash frozen with liquid nitrogen and stored at -80 °C.

### **2.1.3 Elongation Factor G Crosslinking**

Double-cysteine EF-G, in protein dialysis buffer, was reduced for 1 h with 5 mM TCEP. The EF-G sample was buffer exchanged to PBS buffer (137 mM NaCl, 2.7 mM KCl, 8 mM Na<sub>2</sub>HPO<sub>4</sub>, 2 mM KH<sub>2</sub>PO<sub>4</sub>, pH 7.4). The crosslinkers used were: bis-maleimide-(PEG)<sub>2</sub> and (PEG)<sub>3</sub> (Thermofisher Scientific), and bis-maleimide-(PEG)<sub>6</sub> and -(PEG)<sub>11</sub> (BroadPharm). The crosslinkers were made to a 20 mM final concentration in DMSO. The crosslinker was incubated with EF-G at room temperature for 2 h, and a ratio of 2:1 crosslinker:protein (cl/p) was used. The reaction was stopped with 1  $\mu\text{L}$  of 14.7 M BME (Sigma). The sample was flash frozen and stored at -80 °C. The sample was run on 5% tris-glycine SDS-PAGE gels for confirmation of crosslinking and determination of crosslinking efficiency.

## **2.1.4 Crosslinked Elongation Factor G Purification**

### **2.1.4.1 Electro-elution (Model 491 Prep Cell)**

The Bio-Rad Model 491 Prep Cell was used to purify crosslinked EF-G from non-crosslinked EF-G. The crosslinked sample was run on a 6 cm long, 5% tris-glycine SDS polyacrylamide gel in the prep cell. The sample was run at 15 W for 9 h. The upper chamber contained electro-elution buffer A (375 mM tris-HCl, 192 mM glycine, 0.2% SDS), and the lower tank contained electro-elution buffer B (50 mM MOPS pH 7.2, 1 mM EDTA). The non-crosslinked EF-G and crosslinked EF-G were eluted separately and collected in two fractions. Running times for each band was determined by eluting sample and running the eluted sample on a 5% SDS-PAGE gel to determine sample contents. Purified sample was stored at -80 °C.

### **2.1.4.2 Bead Purification**

#### Activated Thiol Sepharose 4B:

0.5 g of activated thiol sepharose 4B (GE Healthcare Life Sciences) beads were mixed with 4 mL of thiol sepharose 4B binding buffer (137 mM NaCl, 2.7 mM KCl, 8 mM Na<sub>2</sub>HPO<sub>4</sub>, 2 mM KH<sub>2</sub>PO<sub>4</sub>, 1 mM EDTA, 0.2% Tween 20, pH 7.5). 1 mL of the slurry was added to a micro-spin column (Denville Scientific) and washed with thiol sepharose 4B binding buffer until A280 was 0.0. The crosslinked EF-G was reduced with 1 mM TCEP for 1 h and buffer exchanged to thiol sepharose 4B binding buffer. 1 or 2 nmol of crosslinked EF-G was added to the column and incubated at 30 °C for 2 h, then incubated at 4 °C overnight. To collect the protein, thiol sepharose 4B elution buffer (137 mM NaCl, 2.7 mM KCl, 8 mM Na<sub>2</sub>HPO<sub>4</sub>, 2 mM KH<sub>2</sub>PO<sub>4</sub>, 1 mM EDTA, 0.2% Tween 20, 30 mM BME, pH 7.5) was added in 1 mL amounts and fractions were collected.

#### Sulfolink Coupling Resin:

3.2 mL of sulfolink coupling resin (Thermo Scientific) was added into micro-spin columns (Denville Scientific). Columns were washed with sulfolink coupling resin coupling buffer (50 mM Tris-HCl, 5 mM EDTA, pH 8.5) until A280 was 0.0. Crosslinked EF-G was reduced with 1 mM TCEP and added to the column. The columns were rocked for 30 min at room temperature. Protein was collected by running 5 mL of sulfolink coupling resin coupling buffer through the column.

#### Purecube Maleimide Magnetic Beads:

100  $\mu$ L of purecube maleimide magnetic beads (Cube Biotech) were added to a tube. The beads were washed three times with purecube maleimide bead buffer (137 mM NaCl, 2.7 mM KCl, 8 mM Na<sub>2</sub>HPO<sub>4</sub>, 2 mM KH<sub>2</sub>PO<sub>4</sub>, 1 mM EDTA, 1% Tween 20, pH 7.2). Crosslinked EF-G was reduced with 2 mM TCEP for 1 h. Excess buffer was removed after the third wash and 200  $\mu$ L of purecube maleimide bead buffer was added to the beads and vortexed. Crosslinked protein was added to the columns, and the columns were rotated overnight at 4 °C. The excess solution was collected. The beads were then washed twice and the wash, containing the crosslinked EF-G, was collected.

#### Purecube Maleimide Activated Agarose:

1 mL of purecube maleimide activated agarose (Cube Biotech) was spun down at 500  $x$  g and excess liquid was removed. The agarose was washed three times with 1 mL of purecube maleimide agarose buffer (137 mM NaCl, 2.7 mM KCl, 8 mM Na<sub>2</sub>HPO<sub>4</sub>, 2 mM KH<sub>2</sub>PO<sub>4</sub>, 1 mM EDTA, pH 7.2). The agarose was resuspended with 500  $\mu$ L of purecube maleimide agarose buffer. Crosslinked EF-G was reduced with 1 mM TCEP for 1 h at room temperature, then added to the resuspended agarose and rotated overnight at 4 °C. The

agarose was spun at 500  $x g$  and the supernatant was collected. The agarose was washed twice with purecube maleimide agarose buffer and the wash was collected in a separate tube.

#### Iodoacetyl Magnetic Beads:

30 mg of iodoacetyl magnetic beads (Bioclone Inc.) were resuspended in iodoacetyl magnetic bead buffer (50 mM tris, 5 mM EDTA, pH 8.5) and vortexed. The supernatant was removed and the beads were washed twice with 1 mL of iodoacetyl magnetic bead buffer. Crosslinked EF-G was reduced with 2 mM TCEP for 30 min at room temperature. The crosslinked EF-G was added to the beads and rotated at room temperature for 2 h. The supernatant was collected. The beads were washed once with 1 mL iodoacetyl magnetic bead buffer and the wash was collected in a separate tube.

#### **2.1.4.3 Phenyl Column Purification**

Crosslinked EF-G was buffer exchanged into phenyl column buffer A (40 mM tris-HCl, 1 mM EDTA, 5 mM BME, 650-850 mM  $(\text{NH}_4)_2\text{SO}_4$ , pH 7.6). The sample was run on a HiTrap Phenyl HP (GE Healthcare Life Sciences) using a gradient of phenyl column buffer B (40 mM tris-HCl, 1 mM EDTA, 5 mM BME, pH 7.6). Various concentrations of  $(\text{NH}_4)_2\text{SO}_4$  in buffer A were tested (650 mM, 680 mM, 700 mM, 715 mM, 850 mM, 1M, and 2 M). Buffer pH's tested with 1 M  $(\text{NH}_4)_2\text{SO}_4$  were pH 6.5, pH .0, and pH 7.6.

#### **2.1.5 Force Induced Remnant Magnetization Spectroscopy (FIRMS) and Microscope Detection**

##### **Power Stroke – Magnetic Detection:**

Biotin-coated glass was glued to the bottom surface of a sample well with dimensions of  $4 \times 3 \times 2 \text{ mm}^3$  (L $\times$ W $\times$ D). 20  $\mu\text{L}$  of a  $0.25 \text{ mg mL}^{-1}$  aqueous solution of streptavidin was loaded into the sample well and incubated for 40 min. The sample well was rinsed twice with

TAM10 buffer (20 mM tris pH 7.5, 10 mM MgAc, 30 mM NH<sub>4</sub>Cl, 70 mM KCl, 5 mM EDTA, 7 mM BME, 0.05% Tween 20). 20  $\mu$ L of 1  $\mu$ m Biotinylated probing DNA strand was added and incubated for 1 h. After rinsing twice with TAM10 buffer, 20  $\mu$ L of 0.1  $\mu$ m ribosome complexes were immobilized on the surface and incubated for 1.5 h. The magnetic beads were incubated with the long DNA strand at room temperature for 1 h. A vortex shaker was used to enhance conjugation. Each initial volume was 1  $\mu$ L. The initial DNA concentration was 100  $\mu$ m. The mixture was diluted to 100  $\mu$ L by TAM10 buffer, so the final concentration of the magnetic beads was approximately  $3.2 \times 10^7$  particle mL<sup>-1</sup>. The sample was washed with buffer three times. The DNA-conjugated beads were then added into the sample well and incubated for another 1.5 h. Nonspecifically bound magnetic particles were removed from the surface by applying centrifugal force at 84 x g for 2 min. The magnetic signal of the samples was measured by a home-built atomic magnetometer. Percentages of remnant magnetic beads were obtained by dividing the magnetic signal after EF-G addition by the signal before EF-G addition. The percentages were normalized to 100% for the strongest ruler (17 bp) and 0% for the weakest ruler (11 bp). Typical error was  $\pm 5\%$ . All experiments were repeated to ensure the reproducibility of the percentage profile, based on which power stroke was extracted.

### **Power Stroke – Microscope Detection:**

The sample preparation was the same as in magnetic detection, except the density of magnetic beads was reduced to approximately  $6.5 \times 10^6$  particle mL<sup>-1</sup>. For each sample well, six images were captured using a 20x objective with an inverted microscope (Amscope, Model ME1400TC). The dimensions of each image were 4098 $\times$ 3288 pixels, equivalent to 0.215 mm<sup>2</sup> in area. Subsequently, 2  $\mu$ L of EF-G solution (20  $\mu$ m EF-G, 4 mM GTP, 4 mM

PEP, 0.2 mg mL<sup>-1</sup> PK) in TAM10 buffer was added into the sample well and incubated for 20 min at 37 °C. Both BM(PEG)<sub>6</sub> and BM(PEG)<sub>11</sub> had the same concentration as the wild type EF-G. For the Fusidic acid experiment, 2.5 mM Fusidic acid was incubated with wild type EF-G before adding onto the surface. The nonspecifically bound magnetic particles were removed from the surface by applying centrifugal force at 84 x g for 2 min. Then another six images were captured for the same sample well. The position of the sample well was maintained the same before and after adding EF-G by using a high-resolution motor (Thorlabs Z725B, resolution: 40 nm). The number of particles on each image was counted using ImageJ. The decreasing percentage was calculated by averaging the six images, and scaled to 100% for the strongest ruler (17 bp) and to 0% for the weakest ruler (11 bp). Typical error in percentage was ±7–8%.

#### **Translocation Efficiency – Magnetic Detection:**

Magnetic signal of the samples was measured by an atomic magnetometer as a function of mechanical forces. The atomic magnetometer had a sensitivity of  $\approx 200$  fT/(Hz)<sup>1/2</sup>. The force was provided by a centrifuge (Eppendorf, Model 5427R). The dissociation of the DNA-mRNA duplexes was indicated by a decrease in the magnetic signal, which occurred when the centrifugal force reached the dissociation force of the DNA-mRNA duplex. The typical force range in this work was 90 pN, after which the residual magnetic signal was taken as the background. The FIRMS profiles were obtained by normalizing the overall magnetic signal decrease ( $B_0$ ) to be 100% and then plotting the relative magnetic signal decrease ( $B/B_0$ ) versus the external force. The force values were calculated according to  $m\omega^2r$ , in which  $m$  is the buoyant mass of M280 magnetic beads ( $4.6 \times 10^{-15}$  kg),  $\omega$  is the centrifugal speed, and  $r$  is the distance of the magnetic beads from the rotor axis (7.5 cm for

5427R). The typical force resolution was 3–4 pN. Each profile reported in this work was repeated at least three times to ensure reproducibility.

### 2.1.6 Polyphenylalanine Assay

The A-mix, ribosome mix, and G mixes were prepared separately. The A mix contained 100 mM tris pH 7.5, 1 mM EDTA, 20 mM MgAc, 4 mM ATP, 7 mM BME, 5  $\mu$ M yeast phenylalanine-tRNA, 50  $\mu$ M  $^{14}$ C-phenylalanine, 10% total volume yeast total synthetase (25 mM Tris-HCL (pH 7.45), 35 mM  $\text{NH}_4\text{Cl}$ , 15 mM KCl, 5 mM  $\text{MgCl}_2$ , 0.25 mM EDTA, 3 mM BME), and nuclease-free water. The ribosome mix contained 1  $\mu$ M *E. coli* MRE600 70S ribosome complex, 3 mg/mL of polyU, 1  $\mu$ M of NAc-Phenylalanine, 10X TAM10, and 1X TAM10 (20 mM tris-HCl pH 7.5, 10 mM MgAc, 30 mM  $\text{NH}_4\text{Cl}$ , 70 mM KCl, 0.5 mM EDTA, 7 mM BME, 0.05% Tween 20). Each G mix contained 3  $\mu$ M EF-Tu, 0.5 mM GTP, 0.5 mM PEP, 0.2 mg/mL of PK, and 1X TAM10. EF-G was added to the G mixes (except for the blank which contained no EF-G) to a final concentration of 6  $\mu$ M. The separate A-mix, ribosome mix, and G mixes were incubated at 37 °C for 10 min. The A-mix, G mix, and ribosome mix were combined together in a 2:2:1 ratio. The combined sample was incubated for 10 min at 37 °C and 10  $\mu$ L aliquots were taken at 20 s, 3 min, and 10 min. The aliquots were incubated with 10  $\mu$ L 0.4 M NaOH at 37 °C for 10 min. The sample was then added to 500  $\mu$ L of ice cold 10% TCA. The samples were then incubated at 90 °C for 10 min, and filtered on Supor® 450 Membrane Disc Filters, 0.45  $\mu$ m - 25 mm (Pall Life Sciences). The filters were submerged in Scintlogix™ U scintillation fluid (LabLogic) and radioactivity was counted using a HIDEX 300 SL scintillation counter (LabLogic).

### **2.1.7 GTP Hydrolysis Assay**

GTP hydrolysis activity was measured using the Transcreener GDP FI Assay (BellBrook Labs) for both the real-time and end point assays.

#### Real-Time Assay:

The antibody-tracer mix contained 90 µg/mL GDP-antibody, 4 nM GDP-Alexa fluor 594, 100 µM GTP, and milliQ water. The GTPase mix contained 0.75 µM EF-G, 0.125 µM ribosome complex, and protein dialysis buffer (20 mM Tris-HCl, 10 mM MgCl<sub>2</sub>, 0.5 mM EDTA, 4 mM BME, 40 mM KCl, pH 7.5). The antibody-tracer mix was prepared and incubated for 1 h at room temperature. The GTPase mix was prepared and incubated at 37 °C for 10 min. Fluorescence was measured using a DeNovix QFX Fluorometer with excitation at 525 nm and emission 560-650 nm. The GTPase mix was added to the cuvette, followed by the antibody-tracer mix to begin the reaction. Measurements were taken at 15 s, 30 s, 1 min, 1.5 min, 2 min, 2.5 min, 3 min, 4 min, 5 min, 6 min, 7 min, 8 min, 9 min, 11 min, 13 min, and 15 min.

#### End Point Assay:

The antibody-tracer mix contained 90 µg/mL GDP-antibody, 4 nM of GDP-Alexa fluor 594, 0.5X of 10X stop & detect buffer, and milliQ water. The GTPase mix contained 0.75 µM EF-G, 0.125 µM ribosome complex, and protein dialysis buffer (20 mM tris-HCl, 10 mM MgCl<sub>2</sub>, 0.5 mM EDTA, 4 mM BME, 40 mM KCl, pH 7.5). The GTPase mix, with the addition of GTP, had a final volume of 50 µL. The antibody-tracer mix was prepared at room temperature. The GTPase mix was prepared and incubated at 37 °C for 10 min. Fluorescence was measured using a DeNovix QFX Fluorometer with excitation at 525 nm and emission 560-650 nm. To begin the reaction, GTP was added to a final concentration of 100 µM. The

reaction was stopped at 20 s, 3 min, and 10 min by taking 50 uL aliquots and adding them to 50 µL of antibody-tracer mix. The reaction mix was incubated at room temperature for 1 h, then fluorescence was measured with a DeNovix QFX Fluorometer.

### **2.1.8 *In Vitro* RNA Transcription**

To prepare linear template DNA, 1 µg of circular plasmid DNA was digested with NdeI (ThermoFisher Scientific) restriction enzyme. The digested plasmid was run on a 0.8% agarose gel and the linear plasmid band was extracted using the GeneJET Gel Extraction Kit (ThermoFisher Scientific). +1 frameshifting mRNA was made using the HiScribe™ T7 Quick High Yield RNA Synthesis Kit (New England Biolabs Inc.), with 658.8 ng of linear template DNA. Phenol:chloroform extraction followed by ethanol precipitation was done to collect the mRNA. mRNA was resuspended in nuclease-free water with 0.1 mM EDTA and stored at -20 °C.

### **2.1.9 tRNA Preparation and Charging**

Phenylalanine tRNA was charged using the following mix: 25 mM tris-HCl pH 7.8, 10 mM ATP, 20 mM MgCl<sub>2</sub>, 1 mM EDTA, 7 mM BME, 80 µM <sup>14</sup>C-Phenylalanine, 10 A/mL phenylalanine-tRNA, total tRNA synthetase equal to 10% total volume, and nuclease-free water. The mix was incubated at 37 °C for 20 min. 20% potassium acetate was added to the mix. The tRNA was purified via phenol:chloroform extraction, followed by ethanol precipitation. The tRNA was collected and resuspended in a buffer solution of 0.2% potassium acetate in DEPC water. The tRNA was then run through a Sephadex® G-25 (Sigma) column. Sample was eluted by adding more buffer and collecting the tRNA immediately. Purified tRNA was stored at -20 °C.

### 2.1.10 Ribosome Complex Preparation

Three mixtures were prepared: the ribosome mix, Tu0G mix, Leu mix. The ribosome mix contained 1  $\mu\text{M}$  ribosome, 1.5  $\mu\text{M}$  each of IF1, IF2, IF3, 2  $\mu\text{M}$  of mRNA coding for “ML” at the first two codons, 4  $\mu\text{M}$  charged fMet-tRNA<sup>fMet</sup>, and 4 mM GTP. The Tu0G mix contained 6  $\mu\text{M}$  EF-Tu, 4 mM GTP (4 mM), 4 mM PEP, and 0.02 mg mL<sup>-1</sup> pyruvate kinase. The Leu mix contained 100 mM tris pH 7.5, 20 mM MgAc<sub>2</sub>, 1 mM EDTA, 4 mM ATP, 7 mM BME, 0.1 mg mL<sup>-1</sup> total synthetase, 50 A<sub>260</sub> mL<sup>-1</sup> total tRNA, and 0.25 mM leucine. All mixtures were in TAM10 buffer. The mixtures were incubated at 37 °C for 25 min. The ML-Pre complex was formed by incubating the ribosome mix, Tu0G mix and Leu mix in the volume ratio of 1:2:2, at 37 °C for 2 min. The resulting ribosome complex was added on 1.1 m sucrose cushion and purified by ultra-centrifuge.

### 2.1.11 Total tRNA Synthetase Purification

MRE600 *E. coli* cells were grown overnight at 37 °C. The overnight inoculation was divided equally into flasks of LB and grown until an OD of ~0.7 was reached. The cells were spun down and the dry cell pellet was stored at -20 °C. The cell pellet was resuspended with DEAE Solution 0 (10 mM tris-HCl, pH 7.5, 10 mM MgCl<sub>2</sub>, 6 mM BME). The resuspension was sonicated for 30 min (10 s on, 20 s off, amplitude 50%). DNase I (ThermoFisher Scientific) was added after sonication and the cell lysate was incubated for 1 h at 4 °C. The cell lysate was centrifuged at 15,000  $\times g$  to remove cell debris. The cell lysate supernatant was collected and ultracentrifuged overnight at 40,000  $\times g$ . 180 mL of DEAE Solution 0 was added to 30 g of pre-swollen DEAE Sepharose<sup>TM</sup> (GE Healthcare Life Sciences). The DEAE was washed with DEAE Solution 0 until pH was 7.0. 30 mL of the DEAE slurry was taken and allowed to settle. 15 mL of DEAE slurry supernatant was removed from the settled

DEAE and replaced with the cell lysate supernatant that was collected after overnight centrifugation. The slurry was rocked overnight at 4 °C, and then packed into a chromatography column (Pharmacia) and washed with 50 mL of DEAE Solution 0. The column was then washed with 20 mL DEAE Solution I (10 mM tris-HCl, pH 7.5, 10 mM MgCl<sub>2</sub>, 6 mM BME, 30 mM NH<sub>4</sub>Cl) and collected. For fraction collection, DEAE solution I was added until 10, 8 mL fractions were collected. This process was repeated with DEAE Solutions II (10 mM tris-HCl, pH 7.5, 10 mM MgCl<sub>2</sub>, 6 mM BME, 60 mM NH<sub>4</sub>Cl) and III (10 mM tris-HCl, pH 7.5, 10 mM MgCl<sub>2</sub>, 6 mM BME, 120 mM NH<sub>4</sub>Cl). For elution, 20, 3 mL fractions were collected using DEAE Elution buffer (10 mM tris-HCl, pH 7.5, 10 mM MgCl<sub>2</sub>, 6 mM BME, 250 mM NH<sub>4</sub>Cl). Fractions with an A280/A260 between 1.100-1.500 and a peak at A280 were combined and ultracentrifuged at 139,750 *x g* overnight. The supernatant was collected and stored at -80 °C.

## **2.2 Materials**

0.5 M EDTA pH 8.0 (GE Healthcare) (15575020)

Agarose (Bio-Rad) (1613100)

Ambion™ NF water (Thermo Fisher Scientific) (AM9932)

ATP (Sigma) (1.30195)

BME (Sigma) (M6250)

BM(PEG)<sub>2</sub> (Thermo fisher Scientific) (22336)

BM(PEG)<sub>3</sub> (Thermo fisher Scientific) (22337)

BM(PEG)<sub>6</sub> (BroadPharm) (BP-22152)

BM(PEG)<sub>11</sub> (BroadPharm) (BP-22151)

GTP (Sigma) (11140957001)

Imidazole (Sigma) (I5513)

KCl (Sigma) (P3911)

KH<sub>2</sub>PO<sub>4</sub> (Sigma) (P0662)

MgCl<sub>2</sub>•6H<sub>2</sub>O (Sigma) (M9272)

NaCl (Sigma) (S9888)

Na<sub>2</sub>HPO<sub>4</sub> (Sigma) (S9763)

NH<sub>4</sub>Cl<sub>2</sub> (Sigma) (213330)

Polyacrylamide 40% 37.5:1 (Bio-Rad) (1610148)

Tris base (Sigma) (93352)

Tween 20 (Sigma) (P9416)

Yeast phe-tRNA (Sigma) (R4018)

Yeast Total tRNA Synthetase (purified using the protocol described by Lagerkvist U & Waldenstrom J. (1964) (90))

*E. coli* MRE600 70S ribosome complex (purified using the protocol described by Rodnina, M.V. & Wintermeyer, W. (1995) (91))

# **CHAPTER THREE: ELONGATION FACTOR G CROSSLINKING, AND ITS ROLE IN TRANSLOCATION FIDELITY**

This chapter contains work from the publication “Modulation and Visualization of EF-G Power Stroke During Ribosomal Translocation” published in ChemBioChem (58). Some figures in this chapter have been reproduced or modified relative to the original published work. Necessary permissions were obtained from ChemBioChem for this work to be used in this dissertation.

## **3.1 Introduction**

Elongation Factor G (EF-G) is the GTPase that is responsible for catalyzing ribosomal translocation during the process of translation. EF-G has been observed in two conformations, a compact and an elongated conformation. While the elongated conformation has been observed since the 1990s, the compact conformation was only recently discovered in 2015 (52,56). The mechanism of EF-G mediated translocation is hotly debated, and studies on how EF-G uses the hydrolysis of GTP are divided (87,88). It is well known that GTP hydrolysis precedes translocation, but how EF-G precisely contributes to the movement of the tRNAs is still not well understood (62,92). To study the biological relevance of the large conformational change that is now shown to occur in EF-G, various internal crosslinkers were introduced into EF-G to restrict its movement.

Beginning with a cysteine free variant of EF-G (wild type contains three), two cysteines were introduced via site-directed mutagenesis, and maleimide crosslinkers were used to crosslink EF-G to itself (93). If a large conformational change does indeed occur, then

by introducing varying lengths of crosslinkers EF-G can be restricted in its degree of movement between the conformations. The shorter crosslinker, BM(PEG)<sub>6</sub>, had a length of 27.1 Å, while the longer linker, BM(PEG)<sub>11</sub>, had a length of 42.6 Å. The issue that arose, however, was in the efficiency of crosslinking. Different residue pairs exhibit different crosslinking efficiencies, due to steric hindrance and accessibility of the crosslinker. This poses a problem for experimentation because non-crosslinked EF-G left in the sample can continue to catalyze translocation, and any amount left will result in normal translocation on the ribosome. To prevent this, the crosslinked EF-G was purified from non-crosslinked protein. Using polyacrylamide gel electrophoresis (PAGE) and maleimide beads, a purification protocol for the separation of crosslinked and non-crosslinked EF-G was designed. After purification, power stroke and translocation efficiency experiments with crosslinked EF-G were conducted. If the force exerted by EF-G is dependent on the ability of EF-G to fully extend into the elongated conformation, then addition of the shorter crosslinker would result in a decrease of exerted force. After force and translocation measurements, the data revealed a decrease in force and the conformational changes to be true.

## **3.2 Results**

### **3.2.1 Site-Directed Mutagenesis and Crosslinking of Elongation Factor G**

To determine the location of the mutations to be introduced, the crystal structure of *T. thermophilus* EF-G was examined in Pymol. Mutation points were selected based on distances between the residues in the pre- and post- translocation complex, and after elimination of residues important for EF-G function. The sequence was aligned to that of *E. coli* EF-G, and the correct *E. coli* residues were determined. Valine 404 of *T. thermophilus* EF-G is phenylalanine 411 (F411) of *E. coli*, and phenylalanine 523 of *T. thermophilus* EF-G is

tyrosine 534 (Y534) of *E. coli*. The distance between the selected residues in the pre-complex is 12.83 Å, and 38.41 Å in the post-complex (Table 3.2.1). Site-directed mutagenesis via PCR was done, and samples were confirmed using an agarose gel (Figure 3.2.1 A and B). The long piece was 6982 base pairs (bp) and the short piece was 365 bp. They were recombined and the mutation was confirmed via DNA sequencing. The F411C/Y534C mutant EF-G (referred to as M5 EF-G) was purified via a Ni-NTA column (Figure 3.2.1 C). The structures of M5 EF-G in the pre- and post- translocation conformations are shown in Figure 3.2.2. M5 EF-G was crosslinked with the 1,8-bis(maleimido)diethylene glycol (BM(PEG)<sub>2</sub>), BM(PEG)<sub>3</sub>, BM(PEG)<sub>6</sub>, and BM(PEG)<sub>11</sub> crosslinkers, and efficiency was determined using SDS-PAGE (Figure 3.2.3 A). Multiple crosslinker lengths were tested to determine the lengths that were suitable for internal crosslinking and purification. To increase crosslinking efficiency, the ratios of crosslinker to protein (cr/p) tested were 2:1, 4:1, 8:1, and 10:1. Increasing the ratio of the crosslinker did not increase crosslinking efficiency (Figure 3.2.3 B). A ratio of 2:1 of crosslinker to protein was selected. Reduction of the EF-G sample with TCEP was tested to increase crosslinking efficiency. Different concentrations of TCEP, as well as reduction times, were done. A final concentration of 5 mM TCEP, reduced for 30 min at room temperature was chosen. Larger concentrations of TCEP resulted in precipitation of EF-G, while longer reduction times produced no difference in crosslinking efficiency (Figure 3.2.3 B).

**Table 3.2.1 Residues in *T. thermophilus* Elongation Factor G Selected for Mutation to Cysteine and Their Distances in the Pre-Translocation and Post-Translocation Complex**

Residue 1	Residue 2	Pre – Distance (Å)	Post – Distance (Å)	Difference (Å)
Valine 404	Phenylalanine 523	12.83	38.41	25.58

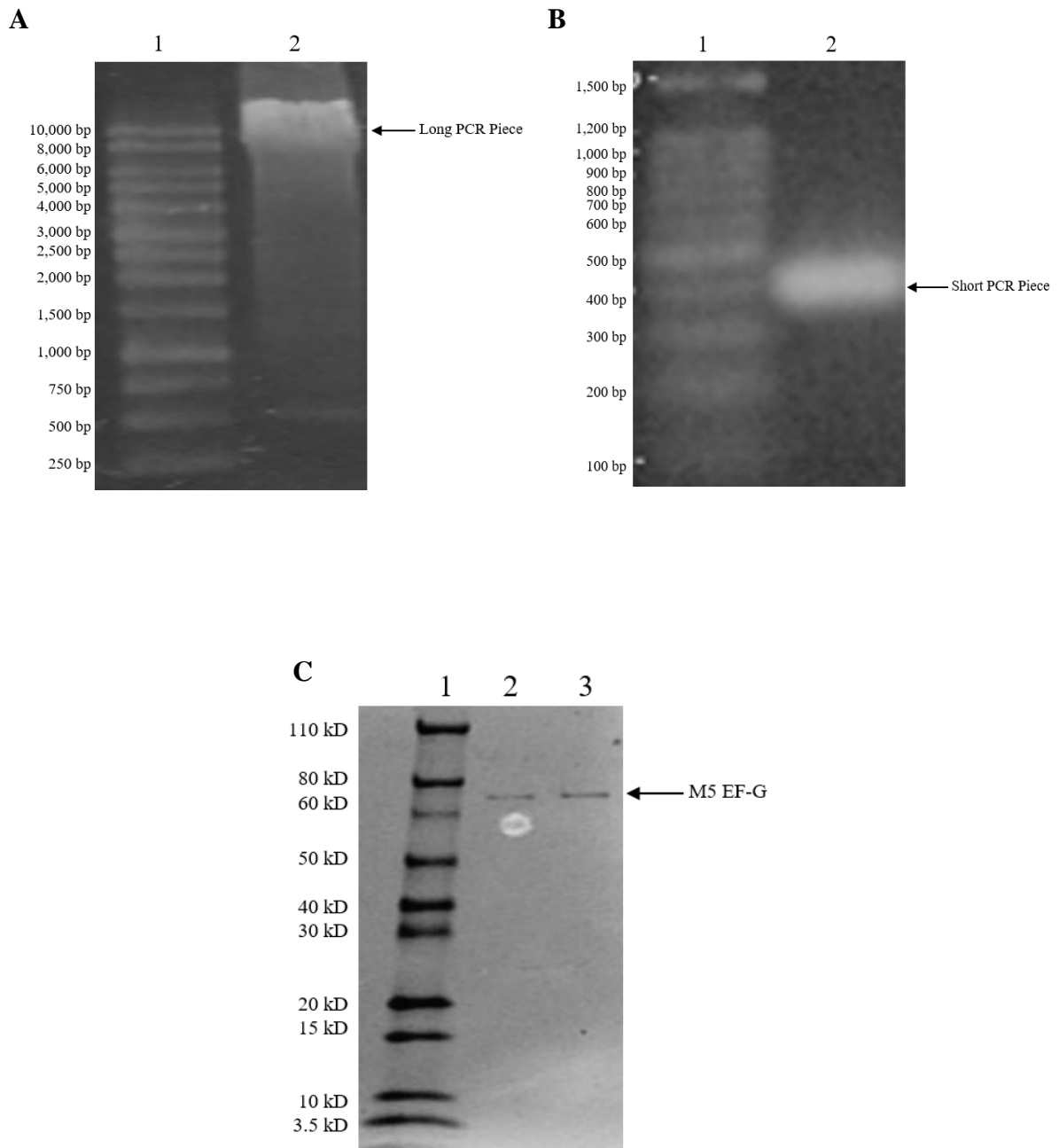


**Figure 3.2.1 Site-Directed Mutagenesis of F411C/Y534C EF-G.**

**A**, 1.0% agarose gel. *Lane 1* 1 Kb ladder, *lane 2* F411C/Y534C EF-G long PCR piece  
**B**, 3.0% Agarose gel. *Lane 1* 100 bp ladder, *lane 2* F411C/Y534C EF-G short PCR piece  
**C**, 5% PAGE gel. *Lane 1* Novex sharp protein ladder, *lane 2* M5 EF-G, *lane 3* M5EF-G

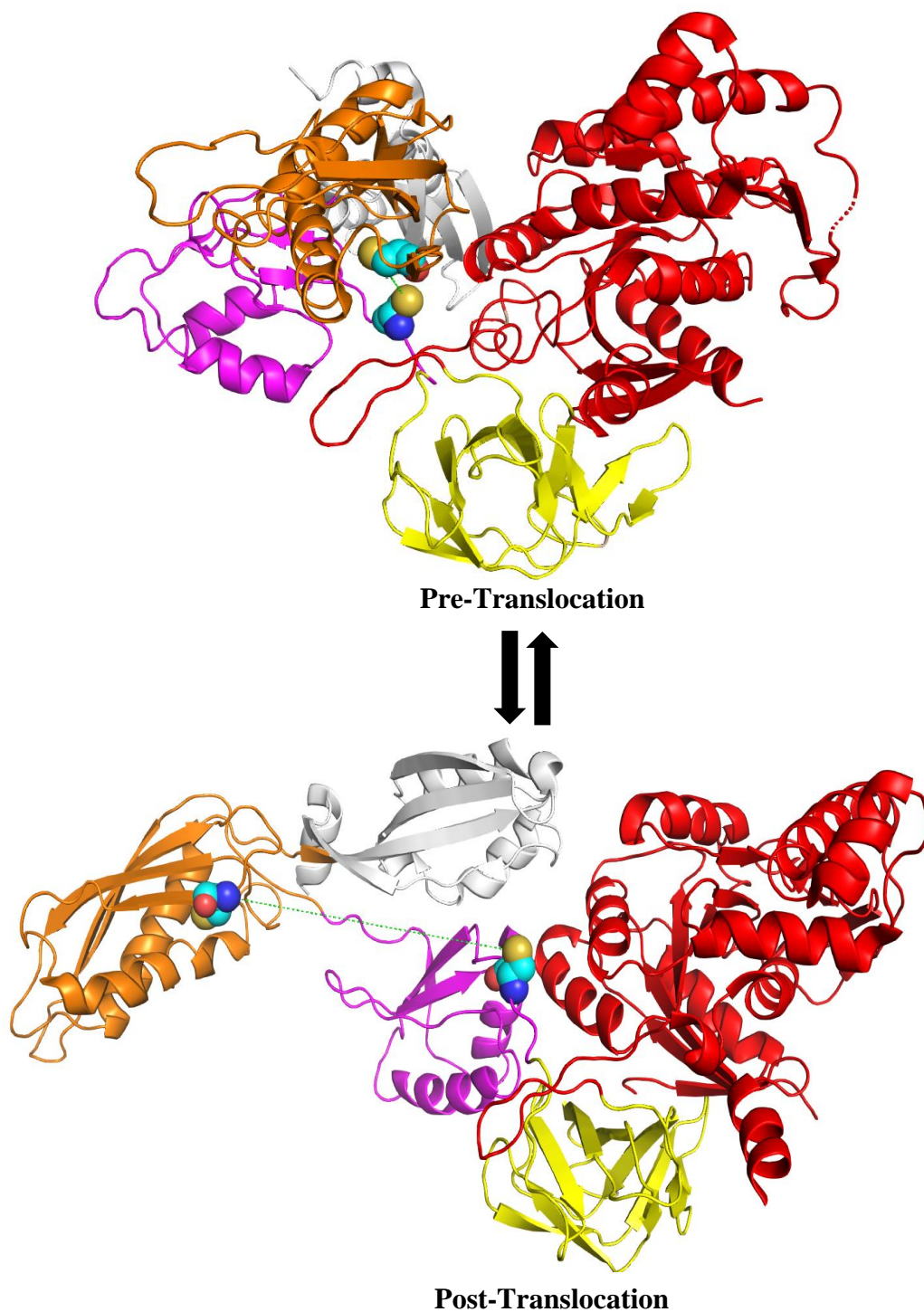


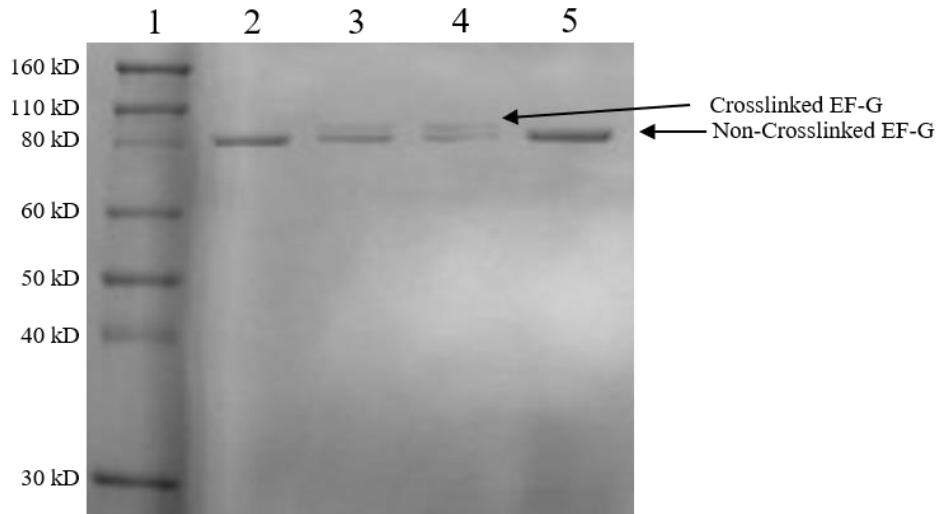
**Figure 3.2.2 Structures of F411C/Y534C (M5) EF-G.** Pre-translocation and post-translocation crystal structures of M5 EF-G with cysteine residues shown as spheres (PBD: 4WQU and 4WQF (56)).

**Figure 3.2.3 Crosslinking of E413C/G528C and M5 EF-G.**

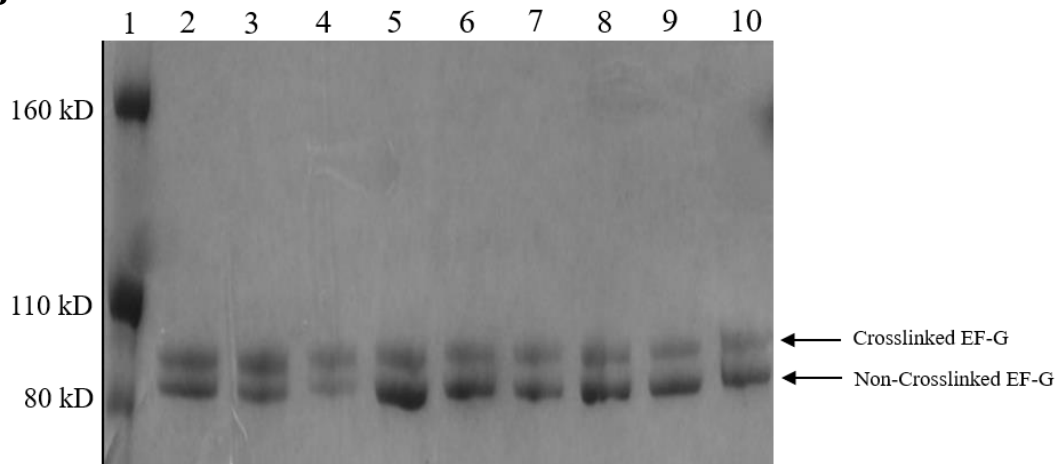
**A**, Mini-Protean TGX gel. *Lane 1* Novex sharp protein ladder, *lane 2* E413C/G528C non-crosslinked EF-G, *lane 3* E413C/G528C BM(PEG)<sub>2</sub> crosslinked EF-G, *lane 4* E413C/G528C BM(PEG)<sub>2</sub> crosslinked EF-G, *lane 5* M5 non-crosslinked EF-G

**B**, 5% tris-glycine SDS-PAGE gel with M5 BM(PEG)<sub>2</sub> crosslinked EF-G with different incubation times and crosslinker to protein ratio (cr/p) . *Lane 1* Novex sharp protein ladder, *lane 2* 1 h incubation, 2:1 cr/p, *lane 3* 1 h incubation, 4:1 cr/p, *lane 4* 1 h incubation, 8:1 cr/p, *lane 5* 2 h incubation, 2:1 cr/p, *lane 6* 2 h incubation, 4:1 cr/p, *lane 7* 2 h incubation, 8:1 cr/p, *lane 8* 3 h incubation, 2:1 cr/p, *lane 9* 3 h incubation, 4:1 cr/p, *lane 10* 8 h incubation, 8:1 cr/p

**A**



**B**



### 3.2.2 Visualization of Crosslinked M5 Elongation Factor G

Crosslinking efficiency was determined through visualization, and the crosslinked EF-G was run on SDS-PAGE gels. The optimum gel conditions for visualization of crosslinked and non-crosslinked bands were determined. 5%, 6%, and 7% tris-glycine SDS-PAGE gels were done (Figure 3.2.4 A-C). 5% and 6% gels resulted in separation of the crosslinked and non-crosslinked bands, while 7% did not. 5% provided the greatest separation of bands. The inclusion of a stacking gel was studied; however, no difference in separation was seen (Figure 3.2.5 A). The addition of 5 mM sodium thioglycolate was tested to reduce any disulfide bonds that formed spontaneously in the non-crosslinked EF-G (Figure 3.2.5 B). Based on the location of the two cysteines, it is possible for non-crosslinked EF-G to form disulfide bonds. The addition of sodium thioglycolate, however, did not produce any observable difference in the non-crosslinked band. 5% native gels, with 4% stacking gels, were done to avoid the SDS removal step that is necessary to allow EF-G to refold after purification (Figure 3.2.5 C). The native gels provided no separation of bands. 5%, 6%, 8%, and 10% bis-tris gels were tested to determine if they could result in separation of the protein (Figure 3.2.6 A-D). Separation of crosslinked and non-crosslinked EF-G was achieved only with 8% and 10% gels, and the 8% and 10% gels run for a significantly longer time compared to tris-glycine. In addition, the gels became significantly warmer, thus bis-tris was not selected. 5% tris-glycine SDS gels were chosen to determine crosslinking efficiency, as well as for purification of the crosslinked protein using electro-elution.

**Figure 3.2.4 Visualization of M5 BM(PEG)<sub>2</sub> Crosslinked EF-G Using Tris-Glycine SDS-PAGE.**

**A**, 5% tris-glycine SDS-PAGE gel. *Lane 1* Bio-Rad dual color protein ladder, *lane 2* M5 EF-G, *lane 3* M5 BM(PEG)<sub>2</sub> crosslinked EF-G, *lane 4* M5 BM(PEG)<sub>2</sub> crosslinked EF-G, *lane 5* M5 BM(PEG)<sub>2</sub> crosslinked EF-G

**B**, 6% tris-glycine SDS-PAGE gel. *Lane 1* Bio-Rad dual color protein ladder, *lane 2* M5 EF-G, *lane 3* M5 BM(PEG)<sub>2</sub> crosslinked EF-G, *lane 4* M5 BM(PEG)<sub>2</sub> crosslinked EF-G, *lane 5* M5 BM(PEG)<sub>2</sub> crosslinked EF-G, *lane 6* M5 BM(PEG)<sub>2</sub> crosslinked EF-G

**C**, 7% tris-glycine SDS-PAGE gel. *Lane 1* Bio-Rad dual color protein ladder, *lane 2* M5 EF-G, *lane 3* M5 BM(PEG)<sub>2</sub> crosslinked EF-G, *lane 4* M5 BM(PEG)<sub>2</sub> crosslinked EF-G, *lane 5* M5 BM(PEG)<sub>2</sub> crosslinked EF-G

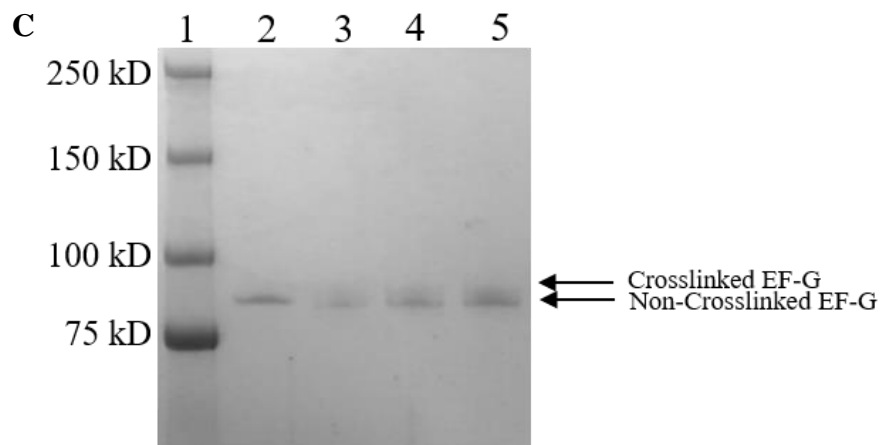
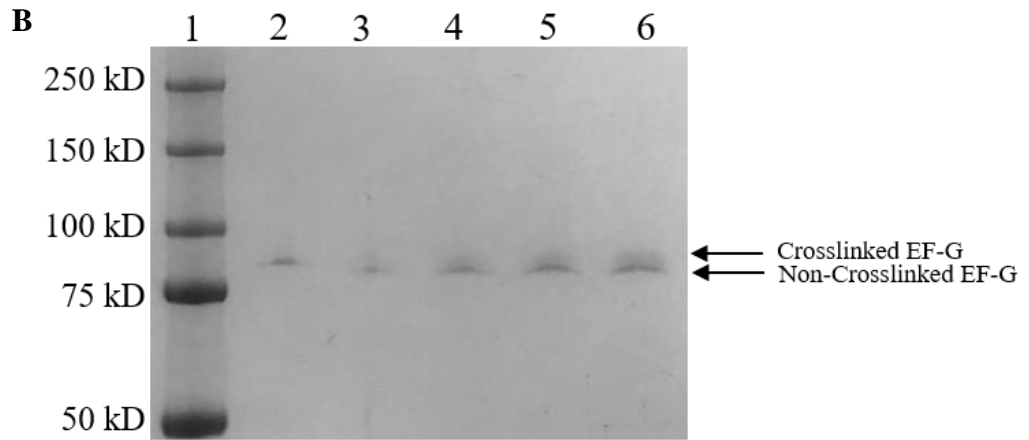
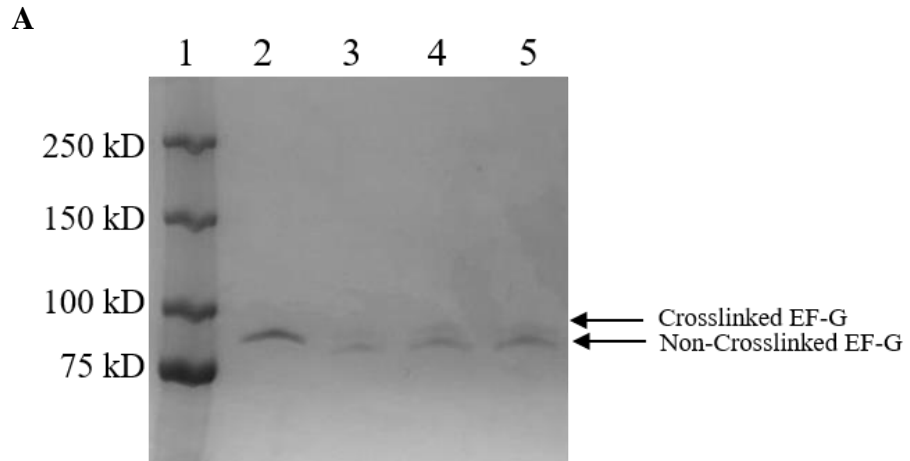


**Figure 3.2.5 Visualization of M5 BM(PEG)<sub>2</sub> Crosslinked EF-G Using Stacking and Native Gels.**

**A**, 5% tris-glycine SDS-PAGE gel with 4% stacking gel. *Lane 1* Bio-Rad dual color protein ladder, *lane 2* M5 EF-G, *lane 3* M5 BM(PEG)<sub>2</sub> crosslinked EF-G, *lane 4* M5 BM(PEG)<sub>2</sub> crosslinked EF-G, *lane 5* M5 BM(PEG)<sub>2</sub> crosslinked EF-G

**B**, 5% tris-glycine SDS-PAGE gel with 5 mM sodium thioglycolate. *Lane 1* Bio-Rad dual color protein ladder, *lane 2* M5 EF-G, *lane 3* M5 BM(PEG)<sub>2</sub> crosslinked EF-G, *lane 4* M5 BM(PEG)<sub>2</sub> crosslinked EF-G, *lane 5* M5 BM(PEG)<sub>2</sub> crosslinked EF-G *lane 6* M5 BM(PEG)<sub>2</sub> crosslinked EF-G

**C**, 5% tris-glycine Native PAGE gel with 4% stacking gel. *Lane 1* Bio-Rad dual color protein ladder, *lane 2* M5 BM(PEG)<sub>2</sub> crosslinked EF-G, *lane 3* M5 BM(PEG)<sub>2</sub> crosslinked EF-G, *lane 4* M5 BM(PEG)<sub>2</sub> crosslinked EF-G, *lane 5* M5 EF-G

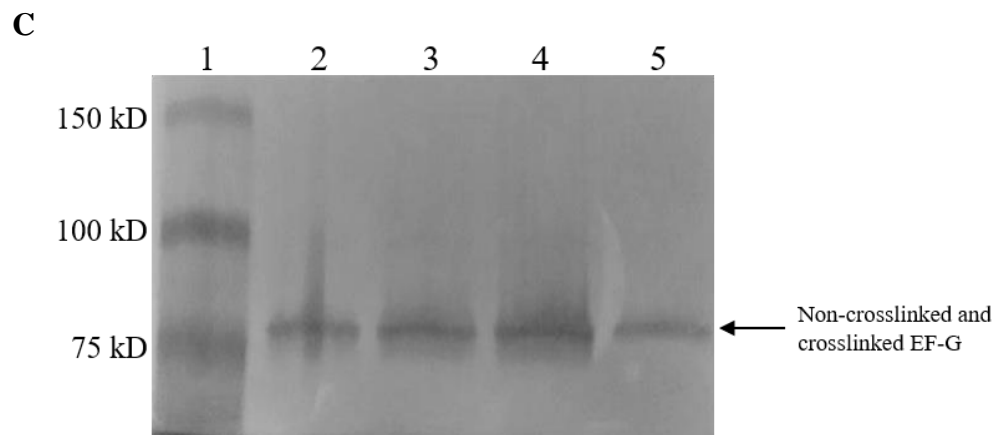
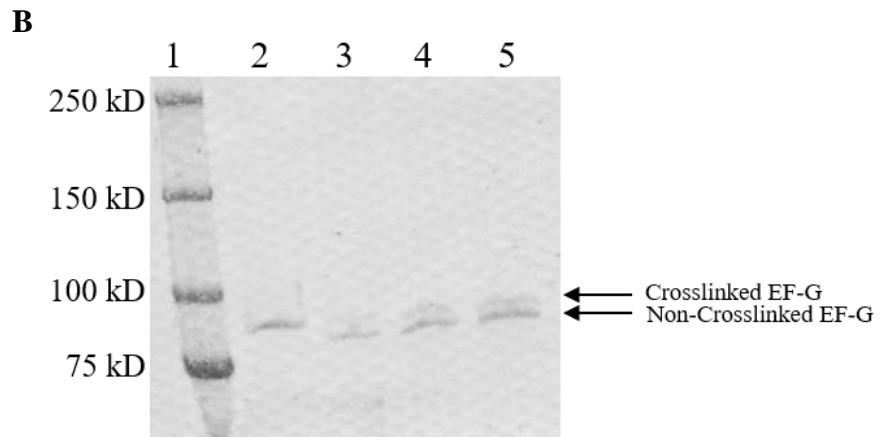
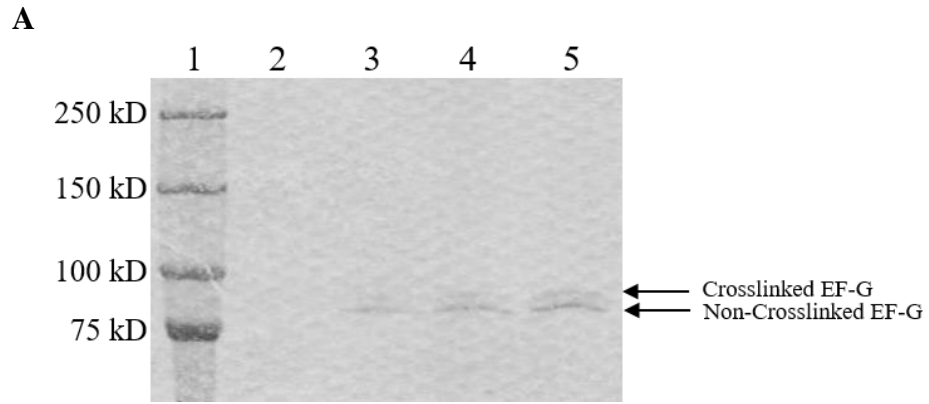


**Figure 3.2.6 Visualization of M5 BM(PEG)<sub>2</sub> Crosslinked EF-G Using Bis-Tris SDS-PAGE.**

**A**, 5% Bis-tris SDS-PAGE gel. *Lane 1* Bio-Rad dual color protein ladder, *lane 2* M5 BM(PEG)<sub>2</sub> crosslinked EF-G, *lane 3* M5 BM(PEG)<sub>3</sub> crosslinked EF-G, *lane 4* M5 BM(PEG)<sub>6</sub> crosslinked EF-G, *lane 5* M5 BM(PEG)<sub>11</sub> crosslinked EF-G, *lane 6* M5 EF-G

**B**, 6% Bis-tris SDS-PAGE gel. *Lane 1* Bio-Rad dual color protein ladder, *lane 2* M5 BM(PEG)<sub>2</sub> crosslinked EF-G, *lane 3* M5 BM(PEG)<sub>3</sub> crosslinked EF-G, *lane 4* M5 BM(PEG)<sub>6</sub> crosslinked EF-G, *lane 5* M5 BM(PEG)<sub>11</sub> crosslinked EF-G, *lane 6* M5 EF-G

**C**, 8% Bis-tris SDS-PAGE gel. *Lane 1* Bio-Rad dual color protein ladder, *lane 2* M5 BM(PEG)<sub>2</sub> crosslinked EF-G, *lane 3* M5 BM(PEG)<sub>3</sub> crosslinked EF-G, *lane 4* M5 BM(PEG)<sub>6</sub> crosslinked EF-G, *lane 5* M5 BM(PEG)<sub>11</sub> crosslinked EF-G, *lane 6* M5 BM(PEG)<sub>6</sub> crosslinked EF-G, *lane 7* M5 EF-G

**D**, 10% Bis-tris Native PAGE gel. *Lane 1* Bio-Rad dual color protein ladder, *lane 2* M5 BM(PEG)<sub>2</sub> crosslinked EF-G, *lane 3* M5 BM(PEG)<sub>3</sub> crosslinked EF-G, *lane 4* M5 BM(PEG)<sub>6</sub> crosslinked EF-G, *lane 5* M5 BM(PEG)<sub>11</sub> crosslinked EF-G

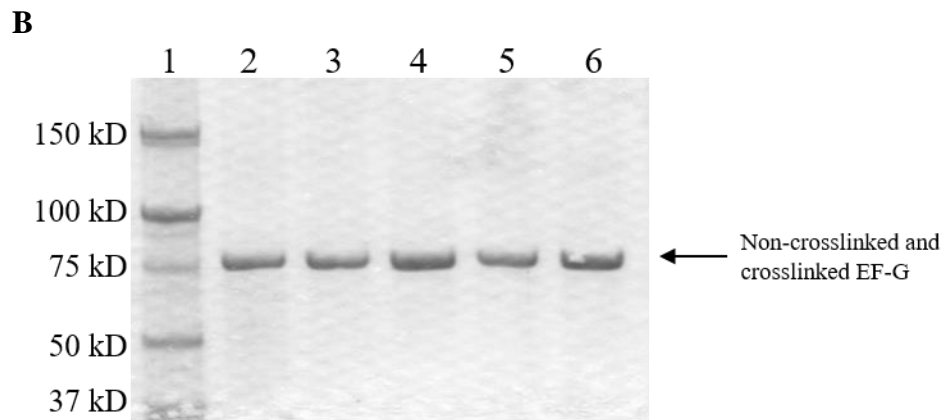
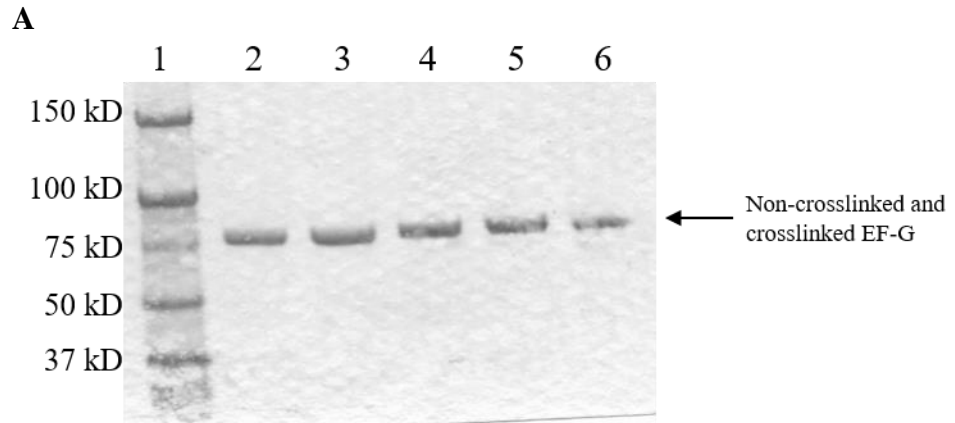
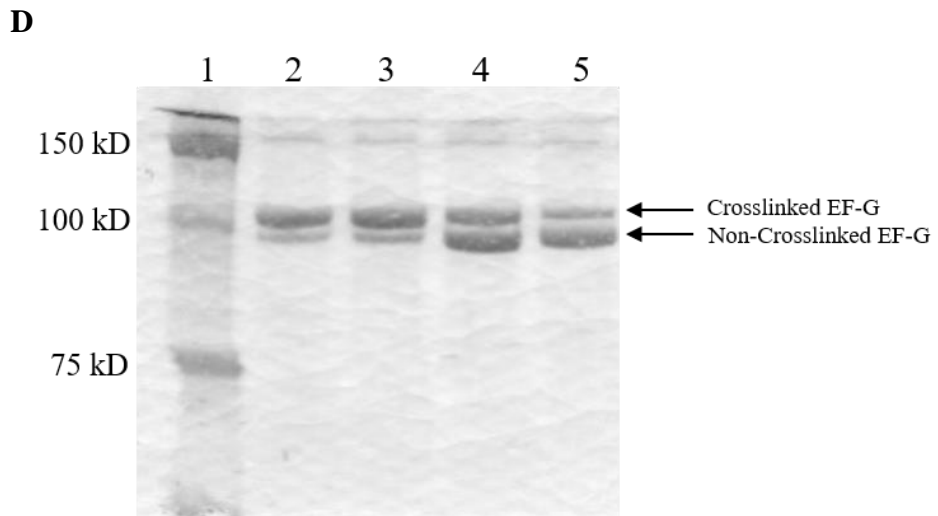
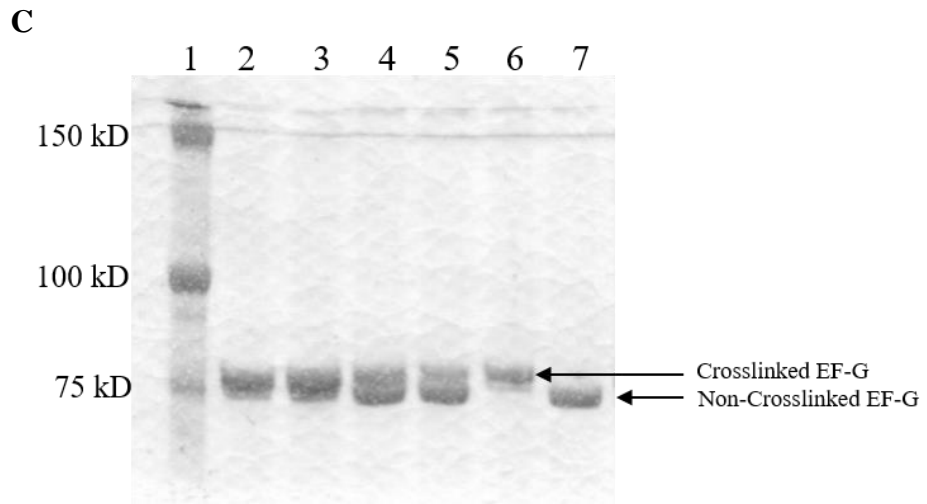


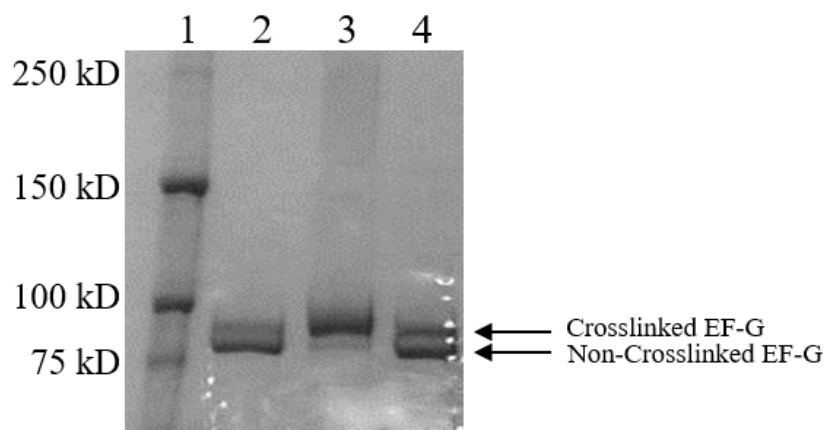
Figure 3.2.6 continued



### 3.2.3 Purification of Crosslinked M5 Elongation Factor G via Electro-Elution

Purification of crosslinked EF-G from non-crosslinked EF-G was done. To purify crosslinked M5, the Model 491 Prep Cell was used. Crosslinked and non-crosslinked EF-G ran as two separate bands on 5% tris-glycine SDS-PAGE gels, and cylindrical gels were cast in lengths of 6 cm and 10 cm. 6 cm gels were selected for further purifications, and M5 BM(PEG)<sub>2</sub> crosslinked EF-G ran for 6 h at 15 W. Fraction group 1 (G1) and fraction group 2 (G2) were pooled together to form two separate samples. G1 was determined to be non-crosslinked EF-G, while G2 was determined to be purified crosslinked EF-G (Figure 3.2.7 A). The purified crosslinked EF-G sample was confirmed via mass spectrometry. Mass spectrometry was performed on BM(PEG)<sub>6</sub> crosslinked sample to verify that the crosslinker was binding to the correct amino acids on EF-G (F411/Y534) (Figure 3.2.7 B). The molecular ion peak was 3304.58, which is equal to the sum of the two cysteine-containing peptides plus the molecular weight of the crosslinker, BM(PEG)<sub>6</sub>. Electro-elution was able to purify the crosslinked EF-G from the non-crosslinked EF-G, however, this method resulted in a low yield of crosslinked EF-G. Because of this, electro-elution was not continued as the method for crosslinked EF-G purification in later experiments, and was instead replaced with maleimide bead purification.

**A**



**B**

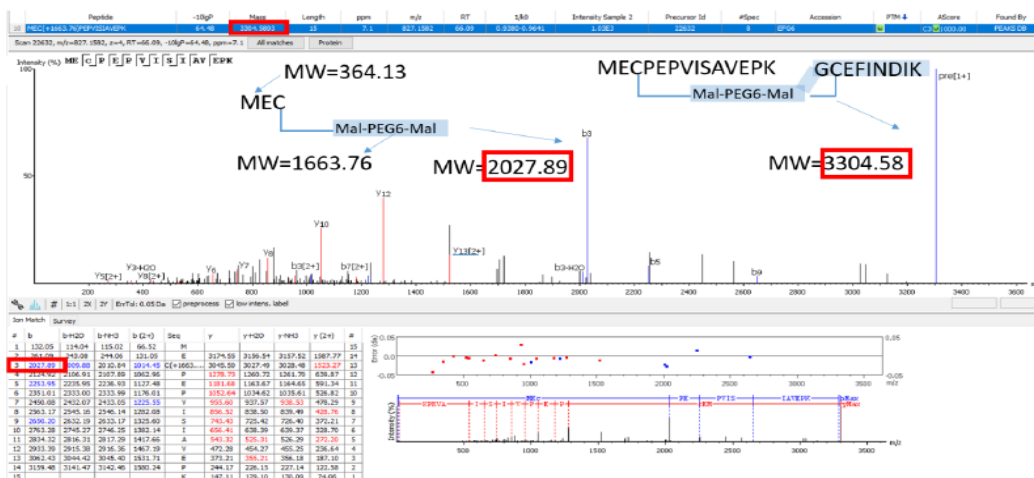


**Figure 3.2.7 Purification of Crosslinked EF-G via Electro-elution and Mass Spectrometry Confirmation of Crosslinking.**

**A**, 5% tris-glycine SDS-PAGE gel. Lane 1 Bio-Rad dual color protein ladder, lane 2 fraction group 1 (G1) of electro-elution purified M5 BM(PEG)<sub>2</sub> crosslinked EF-G, lane 3 fraction group 2 (G2) of electro-elution purified M5 BM(PEG)<sub>2</sub> crosslinked EF-G, lane 4 unpurified M5 BM(PEG)<sub>2</sub> crosslinked EF-G

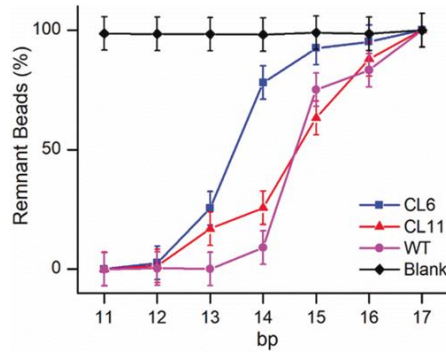
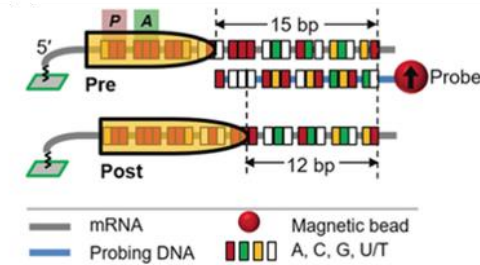
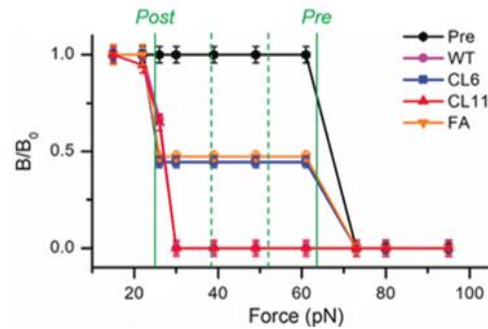
**B**, Mass Spectrum of M5 BM(PEG)<sub>6</sub> crosslinked EF-G after band excision from SDS-PAGE gel. Molecular ion peak was 3304.58 which equals the sum of the double cysteine containing peptide plus the molecular weight of the BM(PEG)<sub>6</sub> crosslinker.

### 3.3 Modulation and Visualization of EF-G Power Stroke During Ribosomal Translocation

#### 3.3.1 Power Stroke and Translocation Measurements of Maleimide Crosslinked EF-G

Power-stroke measurements of EF-G crosslinked with BM(PEG)<sub>6</sub> and BM(PEG)<sub>11</sub> were performed using microscope detection to observe the percent of particles that remained on the slide after EF-G addition (Figure 3.2.8 A). M5 BM(PEG)<sub>11</sub> crosslinked EF-G functioned similarly to wild type EF-G, and the power stroke force observed with M5 BM(PEG)<sub>11</sub> crosslinked EF-G was  $93\pm 8$  pN, while wild type power stroke force was observed to be  $87\pm 8$  pN. M5 BM(PEG)<sub>6</sub> crosslinked EF-G had an observed force of  $60\pm 6$  pN. Translocation efficiencies on the ribosome were also determined using FIRMS. The translocation scheme is shown in Figure 3.2.8 B. When the ribosome is in the pre-translocation conformation, a 15 bp probe can fully bind to the mRNA. When the ribosome moves into a post-translocation conformation, only 12 bp of the 15 bp probe can bind to the mRNA. In the case of frameshifting, 13 and 14 bp for -2 and -1 frameshifting, respectively, would be bound to the mRNA. The translocation results for M5 BM(PEG)<sub>11</sub> crosslinked EF-G, M5 BM(PEG)<sub>6</sub> crosslinked EF-G, wild type, and Fusidic acid bound EF-G can be seen, along with a pre-translocation ribosome (Figure 3.2.8 C). The pre-translocation ribosome sample did not contain EF-G. M5 BM(PEG)<sub>11</sub> crosslinked EF-G and wild type EF-G functioned similarly in that all of the ribosomes were observed to have gone into the post-translocation conformation. M5 BM(PEG)<sub>6</sub> crosslinked EF-G and the Fusidic acid bound EF-G also functioned similarly. In both cases, approximately 55% of the ribosomes reacted and went into the post-translocation conformation. The remaining 45% were maintained in the

pre-translocation conformation. No frameshifting was observed for any of the EF-G samples tested.

**A****B****C****Figure 3.2.8 Measurements of EF-G Power-stroke and Translocation Efficiencies.**

**A**, Results of particle counting for the microscope detection of the EF-G power stroke. Blank contains no EF-G.

**B**, Translocation efficiency probed by FIRMS. Probing scheme for translocation of the same ribosome complex as in the power stroke experiments.

**C**, Translocation efficiency probed by FIRMS. Translocation products for different EF-Gs. The two solid lines indicate the positions of Post and Pre, respectively. The two dashed green lines indicate the expected positions of “-1” (left) and “-2” (right) frameshifting products (58).

### 3.4 Discussion

In this study, crosslinking the M5 EF-G mutant with BM(PEG)<sub>6</sub> resulted in large reductions of both power stroke force and translocation efficiency. Previous studies had shown that EF-G exerts a force, however, until the compact state of this protein was seen, the extent of conformational changes was unknown (56,88). Before the discovery this structure, EF-G that was conformationally restricted through the use of a disulfide bridge had resulted in a variant that was unable to promote translocation on the ribosome (57). The use of a disulfide bridge, however, is limited by its length. This bond has a length of approximately 2 Å, and this restricts the use of this method only to residues that are in close proximity (94). The study on EF-G, nonetheless, had revealed that connecting two domains of EF-G abolishes translocation function. What the study failed to do, however, was explain what caused this. When the compact conformation of EF-G was discovered, more insight into the mechanism of EF-G function was obtained; however, in order to determine if the movement of EF-G truly impacts the function, a method that allowed for EF-G to partially extend was needed (56). To address this crosslinkers were used, in place of disulfide bonds, to allow EF-G to extend to varying degrees within its motion during translocation.

EF-G is an enzyme that catalyzes ribosomal translocation at a rate of  $\sim 25 \text{ s}^{-1}$  (62). Because of this, to ensure the sample contained only crosslinked protein, a purification protocol for crosslinked EF-G was successfully devised. Any amount of non-crosslinked enzyme in the sample would result in data that was not reflective of the crosslinked EF-G. Previous studies have shown that crosslinked protein migrates differently than the same protein when it is reduced, and that the model 491 prep cell can be used to successfully purify samples via SDS-PAGE (95,96). By combining the previous studies, electro-elution

successfully separated the crosslinked and non-crosslinked M5 EF-G by utilizing their differences in migration rates, something that had not previously been done for this protein. The result, however, was a yield of purified crosslinked M5 EF-G that was too low to perform multiple experiments. Because this method was successful in separating crosslinked and non-crosslinked enzyme within the same sample, with optimization it can certainly be adopted for future experiments facing a similar dilemma. Nonetheless, it was necessary to move to maleimide bead purification. In previous studies, maleimide bead purification separated protein through binding of free sulfhydryl groups, and subsequent removal of the desired protein from the beads (97). This method was utilized, in the opposite manner, to remove protein containing free sulfhydryl groups (non-crosslinked EF-G), leaving behind the desired crosslinked EF-G. The maleimide beads were easily overloaded, a problem that was solved by optimizing crosslinking conditions so the initial crosslinking efficiency was high. By using a combination of methods and properties inherent to the protein, crosslinked EF-G was successfully purified.

Using Force Induced Remnant Magnetization Spectroscopy (FIRMS) the power stroke forces and translocation efficiencies were determined for both M5 BM(PEG)<sub>6</sub> and M5 BM(PEG)<sub>11</sub> crosslinked EF-G. BM(PEG)<sub>11</sub> allowed for the full extension of EF-G during translocation, and resulted in normal EF-G function. BM(PEG)<sub>6</sub>, however, restricted EF-G from moving fully into the elongated conformation, and resulted in a lower power stroke force being exerted (Figure 3.2.8 A). As the DNA probe base pair length increases, the percentage of beads removed from the slide decreases until the critical duplex force is reached. When there is no longer a decrease in signal, the duplex force has exceeded the power stroke force. When no EF-G is added to the sample (blank), no power stroke force is applied to the system,

no decrease in signal occurs, and the percentage of beads remaining on the slide is 100%. In the case of wild type and M5 BM(PEG)<sub>11</sub> EF-G, the power stroke forces were 87±8 pN and 93±8 pN, respectively, meaning both EF-G species functioned similarly. M5 BM(PEG)<sub>6</sub> crosslinked EF-G, on the other hand, had a force of 60±6 pN. The ability of EF-G to function normally with the BM(PEG)<sub>11</sub> crosslinker supported that the crosslinker itself did not affect protein function, and the results of the M5 BM(PEG)<sub>6</sub> crosslinked EF-G are due only to the restriction of movement by the crosslinker. Based on the results obtained, the ability of EF-G to move from the compact to the elongated state is important for the function of EF-G, and the force correlates with the structural study giving relevance to the new conformation that was seen (56).

To determine if catalytic activity was affected by crosslinking, translocation efficiencies were also measured using FIRMS. Figure 3.2.8 B shows the translocation scheme. The 15 bp, 3'-probe fully binds to the mRNA when the ribosome is in the pre-translocation position. When the ribosome has translocated into the post-translocation position, 3 nucleotides of the mRNA will be covered, thus only 12 bp of the 3'-probe can bind. External forces needed to remove 15 and 12 bp probes were ~62 pN and ~25 pN, respectively. When all ribosome complexes have undergone translocation, one decrease in signal will be seen consistent with 12 bp bound. Both wild type and M5 BM(PEG)<sub>11</sub> crosslinked EF-G completely promoted translocation of ribosomal complexes from the pre- to post- translocation state, thus a single drop in signal was observed at ~25 pN (Figure 3.2.8 C). M5 BM(PEG)<sub>6</sub> crosslinked EF-G, on the other hand, resulted in two drops in signal. Approximately 55% ribosome complexes fully translocated constituting the first drop. The remaining 45% of the ribosomal complexes remained in the pre-translocation state and

resulted in the second drop. No frameshifting was observed for any EF-G species. This finding confirms previous data indicating that the ribosome itself is responsible for maintaining the mRNA reading frame, and supports that the conformational changes in EF-G do not contribute (84). While the reading frame maintenance wasn't affected, the lower translocation efficiency indicates that restricting EF-G movement did have an effect on its catalytic activity. Previous kinetic studies indicated that EF-G causes a rate-limited ribosome unlocking step preceding mRNA translocation, implying that EF-G's role is to overcome the activation energy barrier between the pre-translocation and post-translocation states (98). While EF-G accelerates the reaction, it does not directly determine the translocation stepping size, hence normal translocation can occur. Fusidic acid bound EF-G was also tested and the results were similar to that of M5 BM(PEG)<sub>6</sub> crosslinked EF-G, indicating that a possible explanation for the lower efficiency is that the crosslinker prevents EF-G from dissociating from the ribosome. In this case, EF-G would be able to undergo normal catalysis only once. Through the use of internal crosslinkers, the mechanism of translocation in which EF-G exerts a force to be utilized by the ribosome during translocation was further explored, and a reduction in power stroke and translocation efficiency were both seen when conformational changes in this protein are restricted.

## **CHAPTER FOUR: THE EFFECTS OF FUSIDIC ACID**

### **BINDING POCKET MUTATIONS**

#### **4.1 Introduction**

Within a compartment formed by domains I-III of EF-G is the region known as the Fusidic acid binding pocket. This pocket binds the antibiotic Fusidic acid and results in inactivation of EF-G by trapping it on the ribosome (99). The location of the binding pocket is within the vicinity of the GTPase center of EF-G, and potentially contains some of the earliest conformational changes in EF-G (83). Restricting movement in this region may greatly affect the function of EF-G, even so far as to completely abolish it. Mutating important residues in the pocket may also prevent Fusidic acid from binding, and thus would confer resistance to Fusidic acid. Changes in EF-G's ability to successfully promote translocation on the ribosome with, and without, Fusidic acid would provide insight into the mechanism of EF-G mediated translocation, as well as provide a deeper understanding in the mechanism of Fusidic acid resistance. This antibiotic, however, is currently banned in the United States for human use, but is very often used for research purposes (100). The reason for its banning in the United States is unclear, however, resistance to Fusidic acid is most likely a factor, as resistance has been observed for several decades (78). In research, it traps EF-G in the post-translational conformation on the ribosome (101). This antibiotic has been used to help determine EF-G structure, however, static structures cannot provide a comprehensive analysis of the mechanism of action, thus it is necessary to perform real-time experiments using Fusidic acid in order to determine its effect on EF-G's mechanism.

As done in the previous chapter, site-directed mutagenesis and crosslinking were used to insert internal crosslinkers into EF-G. Mutations of important residues was generally avoided, however, substitution of *E. coli* residue phenylalanine 95 may confer resistance to Fusidic acid, thus this variant was produced to observe changes in EF-G movement that may occur (68). Hydrophobic interaction chromatography and maleimide bead purification were done for the F95C/M682C variant, however, purification was unsuccessful. Further experimentation with this mutant were unable to be completed because of this.

## 4.2 Results

### 4.2.1 Site-Directed Mutagenesis and Crosslinking of F95C/M682C Elongation Factor G in the Fusidic Acid Binding Pocket

Phenylalanine 90 and methionine 671 were selected in *T. thermophilus* EF-G for mutation. The residues were aligned and converted to *E. coli* residues phenylalanine 95 (F95) and methionine 682 (M682), respectively. The pre-translocation distance between F95 and M682 is 19.20 Å and 22.22 Å in the post-state (Table 4.2.1).

**Table 4.2.1 Residues in *T. thermophilus* Elongation Factor G Fusidic Acid Binding Pocket Selected for Mutation to Cysteine and Their Distances in the Pre-translocation and Post-Translocation Complex**

Residue 1	Residue 2	Pre – Distance (Å)	Post – Distance (Å)	Difference (Å)
Phenylalanine 90	Methionine 671	19.30	22.22	2.92

As done previously, site-directed mutagenesis was performed to mutate F95 and M682 to cysteines. The short PCR piece had a length of 1760 bp and the long piece had a length of 5614 bp (Figure 4.2.1 A). After recombination, protein expression with different concentrations of IPTG was determined (Figure 4.2.1 B). F95C/M682C EF-G was crosslinked with four crosslinkers: BM(PEG)<sub>2</sub>, BM(PEG)<sub>3</sub>, BM(PEG)<sub>6</sub>, and BM(PEG)<sub>11</sub>. On a 5% tris-glycine SDS-PAGE gel, the upper band was determined to be the non-crosslinked EF-G, while the lower band was the crosslinked protein. Various crosslinking conditions were tested to determine the optimum conditions for crosslinking the F95C/M682C pair. The conditions tested were: 2 h at room temperature with a 2:1 ratio of crosslinker to protein (cr/p), 2 h at 37 °C then overnight at 4 °C with 2:1 cr/p, overnight at 4 °C with 2:1 cr/p, 2 h at 37 °C then overnight at 4 °C with 4:1 cr/p, and overnight at 4 °C with 4:1 cr/p (Figure 4.3.1 C). The condition of 2 h at room temperature then overnight at 4 °C with 2:1 cr/p was selected for further purification.

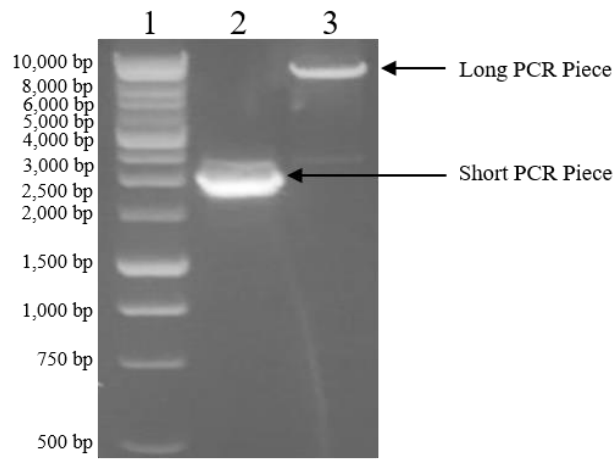
**Figure 4.2.1 Site-Directed Mutagenesis and Crosslinking of F95C/M682C EF-G.**

**A**, 1.2% agarose gel. *Lane 1* 1 Kb ladder, *lane 2* F95C/M682C EF-G short PCR piece (1760 bp), *lane 3* F95C/M682C EF-G long PCR piece (5614 bp)

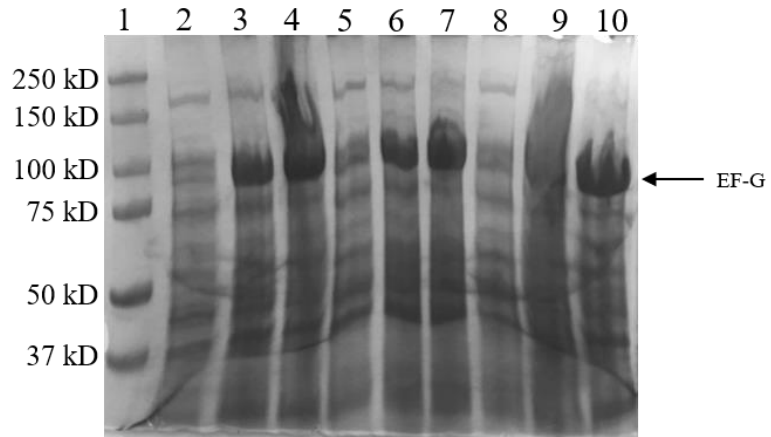
**B**, 8% tris-glycine SDS-PAGE gel. *Lane 1* Bio-Rad dual color protein ladder, *lane 2* F95C/M682C EF-G non-induced, *lane 3* F95C/M682C EF-G induced with 250  $\mu$ M IPTG 1 h, *lane 4* F95C/M682C EF-G induced with 250  $\mu$ M IPTG for 3 h, *lane 5* F95C/M682C EF-G non-induced, *lane 6* F95C/M682C EF-G induced with 500  $\mu$ M IPTG 1 h, *lane 7* F95C/M682C EF-G induced with 500  $\mu$ M IPTG for 3 h, *lane 8* F95C/M682C EF-G non-induced, *lane 9* F95C/M682C EF-G induced with 1 mM IPTG 1 h, *lane 10* F95C/M682C EF-G induced with 1 mM IPTG for 3 h

**C**, 5% tris-glycine SDS-PAGE gel. *Lane 1* Bio-Rad dual color protein ladder, *lane 2* F95C/M682C BM(PEG)<sub>3</sub> crosslinked EF-G crosslinked 2 h at room temperature, 2:1 ratio of crosslinker to protein (cr/p), *lane 3* F95C/M682C BM(PEG)<sub>3</sub> crosslinked EF-G crosslinked 2 h at 37 °C, then 4 °C overnight, 2:1 cr/p, *lane 4* F95C/M682C EF-G, *lane 5* F95C/M682C BM(PEG)<sub>3</sub> crosslinked EF-G crosslinked at 4°C overnight, 2:1 cr/p, *lane 6* F95C/M682C BM(PEG)<sub>3</sub> crosslinked EF-G crosslinked 2 h at 37 °C, then 4 °C overnight, 4:1 cr/p *lane 7* F95C/M682C EF-G, *lane 8* F95C/M682C BM(PEG)<sub>3</sub> crosslinked EF-G crosslinked at 4 °C overnight, 4:1 cr/p, *lane 9* F95C/M682C EF-G, *lane 10* F95C/M682C BM(PEG)<sub>3</sub> crosslinked EF-G crosslinked 2 h at 37 °C, then 4 °C overnight 4:1 cr/p

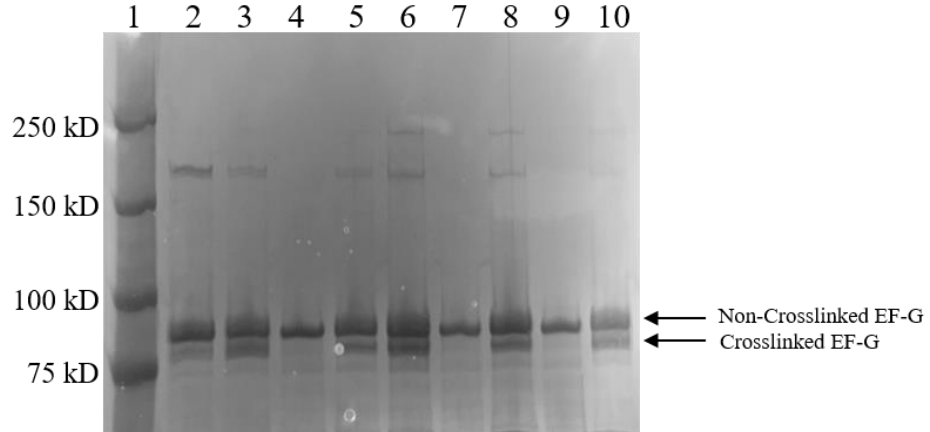
**A**



**B**



**C**



## **4.2.2 Purification of F95C/M682C Elongation Factor G via Hydrophobic Interaction Chromatography and Bead Purification**

Hydrophobic interaction chromatography using a phenyl column was tested to separate BM(PEG)<sub>3</sub> crosslinked F96C/M682C EF-G (Figure 4.2.2). The optimum concentration of ammonium sulfate was first determined by testing 1 M and 2 M ammonium sulfate. 2 M ammonium sulfate resulted in inconsistent protein peaks. 1 M ammonium sulfate produced consistent protein peaks, however, both crosslinked and non-crosslinked eluted together in the same fractions. Optimum buffer pH was determined to separate the fractions. A buffer pH of 6.5, 7.0, and 7.6 was tested with 1 M ammonium sulfate. pH's of 6.5 (Figure 4.2.2 C) and 7.6 (Figure 4.2.2 A1 and A2) resulted in one peak, while a pH of 7.0 (Figure 4.2.2 B1 and B2) resulted in two. The two peaks, however, did not contain separated crosslinked and non-crosslinked EF-G, but contained a mixture of both. Maleimide bead purification was done to separate the two samples (Figure 4.2.3 A). The unpurified F95C/M682C EF-G, crosslinked with BM(PEG)<sub>6</sub>, was reduced with TCEP prior to incubation with the beads. Five different types of beads were tested in order to purify the sample. Thiol Sepharose 4B beads and sulfoLink coupling resin resulted in the lowest amounts of purified crosslinked EF-G (Figure 4.2.3 B and C). Each sample contained approximately 10-30% crosslinked EF-G. Bioclone iodoacetyl beads produced a sample containing approximately 45% crosslinked EF-G (Figure 4.2.4 B). PureCube maleimide magnetic and agarose beads produced the highest amounts of crosslinked EF-G with each containing approximately 50% crosslinked EF-G (Figure 4.2.4 A and B). The samples still contained 50% of non-crosslinked EF-G. Unlike the M5 crosslinked EF-G, the F96C/M682C crosslinked EF-G was unable to be purified completely.

**Figure 4.2.2 Purification of F95C/M682C EF-G via Hydrophobic Interaction Chromatography.**

**A1**, Phenyl column chromatograph of purified F96C/M682C BM(PEG)<sub>3</sub> crosslinked EF-G. Buffer pH 7.6 with 1 M ammonium sulfate.

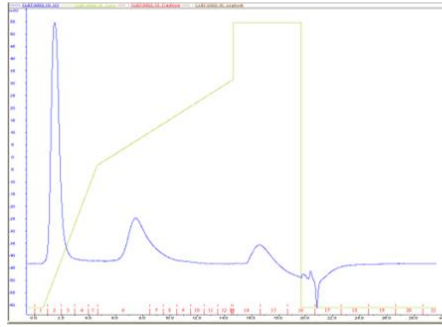
**A2**, 5% tris-glycine SDS-PAGE gel of panel A containing phenyl column fractions collected during purification of F96C/M682C BM(PEG)<sub>3</sub> crosslinked EF-G. Buffer pH 7.6 with 1 M ammonium sulfate. *Lane 1* Bio-Rad dual color protein ladder, *lane 2* phenyl column fraction 6 of purified F96C/M682C BM(PEG)<sub>3</sub> crosslinked EF-G, *lane 3* phenyl column fraction 7 of purified F96C/M682C BM(PEG)<sub>3</sub> crosslinked EF-G, *lane 4* unpurified F96C/M682C BM(PEG)<sub>3</sub> crosslinked EF-G, *lane 5* phenyl column fraction 14 of purified F96C/M682C BM(PEG)<sub>3</sub> crosslinked EF-G, *lane 6* phenyl column fraction 15 of purified F96C/M682C BM(PEG)<sub>3</sub> crosslinked EF-G, *lane 7* unpurified F96C/M682C BM(PEG)<sub>3</sub> crosslinked EF-G

**B1**, Phenyl column chromatograph of purified F96C/M682C BM(PEG)<sub>3</sub> crosslinked EF-G. Buffer pH 7.0 with 1 M ammonium sulfate.

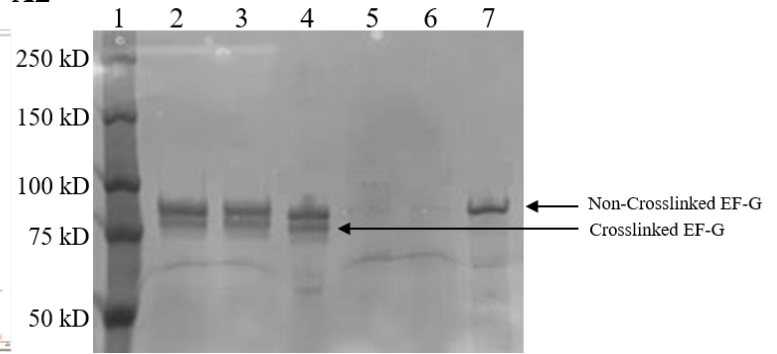
**B2**, 5% tris-glycine SDS-PAGE gel of panel C containing phenyl column fractions collected during purification of F96C/M682C BM(PEG)<sub>3</sub> crosslinked EF-G. Buffer pH 7.0 with 1 M ammonium sulfate. *Lane 1* Bio-Rad dual color protein ladder, *lane 2* phenyl column fraction 6 and 7 of purified F96C/M682C BM(PEG)<sub>3</sub> crosslinked EF-G (run 1), *lane 3* phenyl column fraction 8 and 9 of purified F96C/M682C BM(PEG)<sub>3</sub> crosslinked EF-G (run 1), *lane 4* phenyl column fraction 28 and 29 of purified F96C/M682C BM(PEG)<sub>3</sub> crosslinked EF-G (run 1), *lane 5* unpurified F96C/M682C BM(PEG)<sub>3</sub> crosslinked EF-G, *lane 6* phenyl column fraction 6 and 7 of purified F96C/M682C BM(PEG)<sub>3</sub> crosslinked EF-G (run 2), *lane 7* phenyl column fraction 8 and 9 of purified F96C/M682C BM(PEG)<sub>3</sub> crosslinked EF-G (run 2), *lane 8* phenyl column fraction 23 and 24 of purified F96C/M682C BM(PEG)<sub>3</sub> crosslinked EF-G (run 2), *lane 9* unpurified F96C/M682C BM(PEG)<sub>3</sub> crosslinked EF-G, *lane 10* F96C/M682C EF-G

**C**, Phenyl column chromatograph of purified F96C/M682C BM(PEG)<sub>3</sub> crosslinked EF-G. Buffer pH 6.5 with 1 M ammonium sulfate.

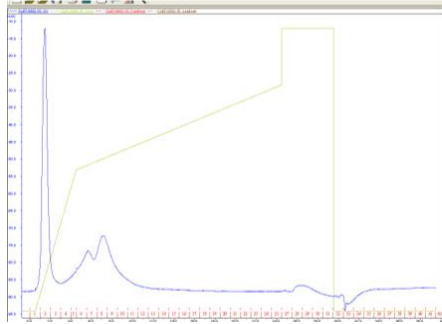
**A1**



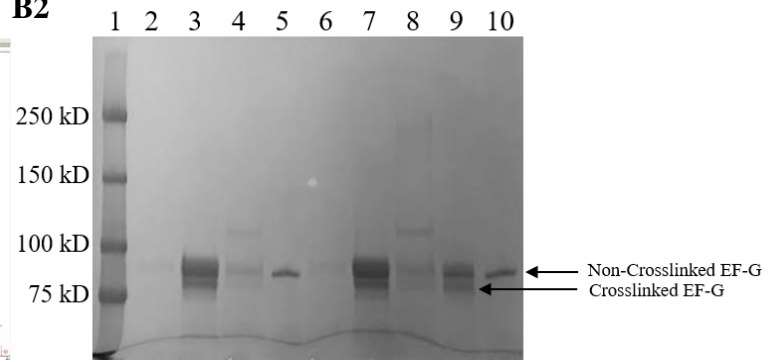
**A2**



**B1**



**B2**



**C**

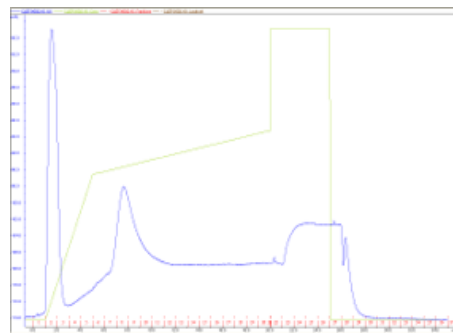


**Figure 4.2.3 Purification of F95C/M682C Crosslinked EF-G Via Thiol Sepharose 4B and Sulfolink Coupling Resin Bead Binding.**

**A**, 5% tris-glycine SDS-PAGE gel. *Lane 1* Bio-Rad dual color protein ladder, *lane 2* F95C/M682C BM(PEG)<sub>6</sub> crosslinked EF-G, *lane 3* 95C/M682C BM(PEG)<sub>6</sub> crosslinked EF-G, *lane 4* F95C/M682C EF-G, *lane 5* 95C/M682C BM(PEG)<sub>6</sub> crosslinked EF-G

**B**, 5% tris-glycine SDS-PAGE gel with thiol sepharose 4B purified F95C/M682C BM(PEG)<sub>6</sub> crosslinked EF-G. *Lane 1* Bio-Rad dual color protein ladder, *lane 2* purified F95C/M682C BM(PEG)<sub>6</sub> crosslinked EF-G fraction 1, *lane 3* purified F95C/M682C BM(PEG)<sub>6</sub> crosslinked EF-G fraction 2, *lane 4* purified F95C/M682C BM(PEG)<sub>6</sub> crosslinked EF-G fraction 1, *lane 5* purified F95C/M682C BM(PEG)<sub>6</sub> crosslinked EF-G fraction 2

**C**, 5% tris-glycine SDS-PAGE gel with SulfoLink coupling resin purified F95C/M682C BM(PEG)<sub>6</sub> crosslinked EF-G. *Lane 1* Bio-Rad dual color protein ladder, *lane 2* purified F95C/M682C BM(PEG)<sub>6</sub> crosslinked EF-G, *lane 3* unpurified F95C/M682C BM(PEG)<sub>6</sub> crosslinked EF-G, *lane 4* purified F95C/M682C BM(PEG)<sub>6</sub> crosslinked EF-G, *lane 5* unpurified F95C/M682C BM(PEG)<sub>6</sub> crosslinked EF-G

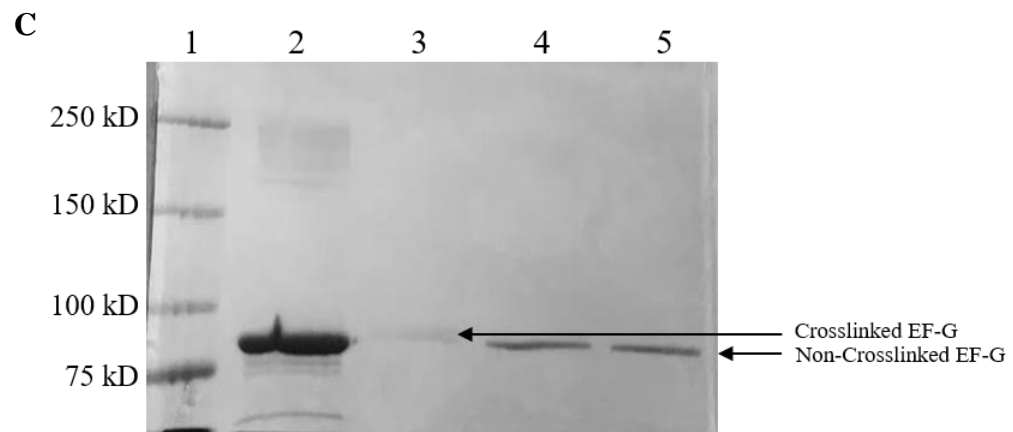
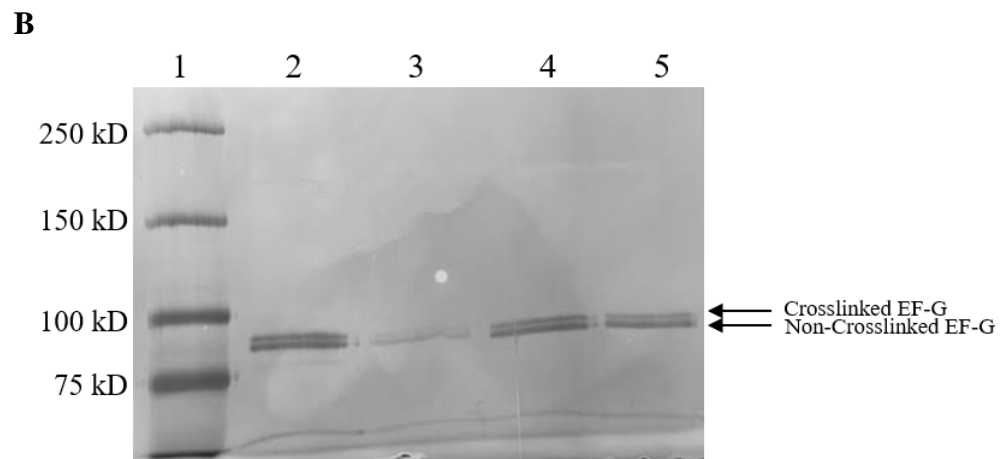
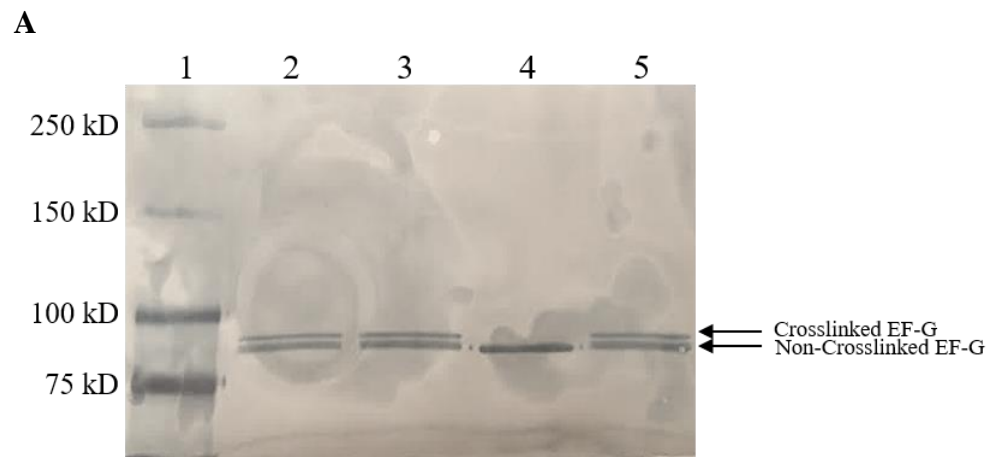
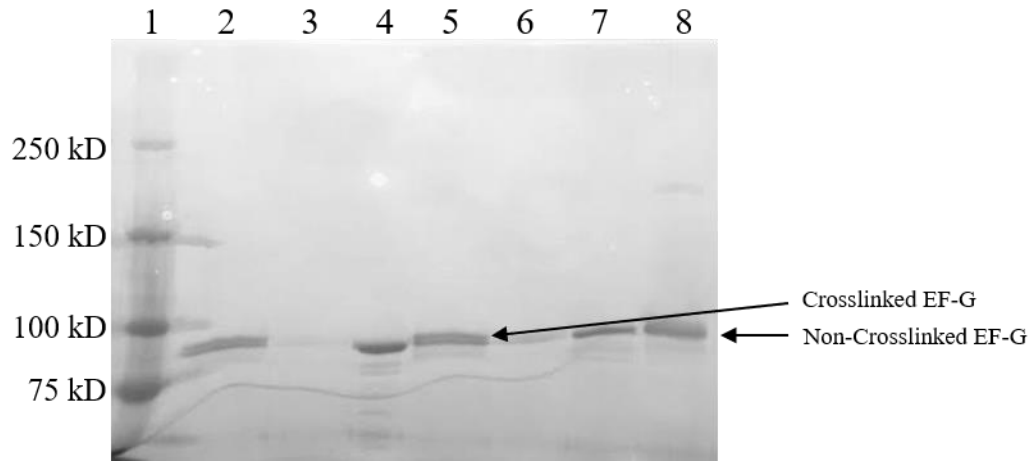


**Figure 4.2.4 Purification of F95C/M682C Crosslinked EF-G Via PureCube Maleimide Bioclone Iodoacetyl Bead Binding.**

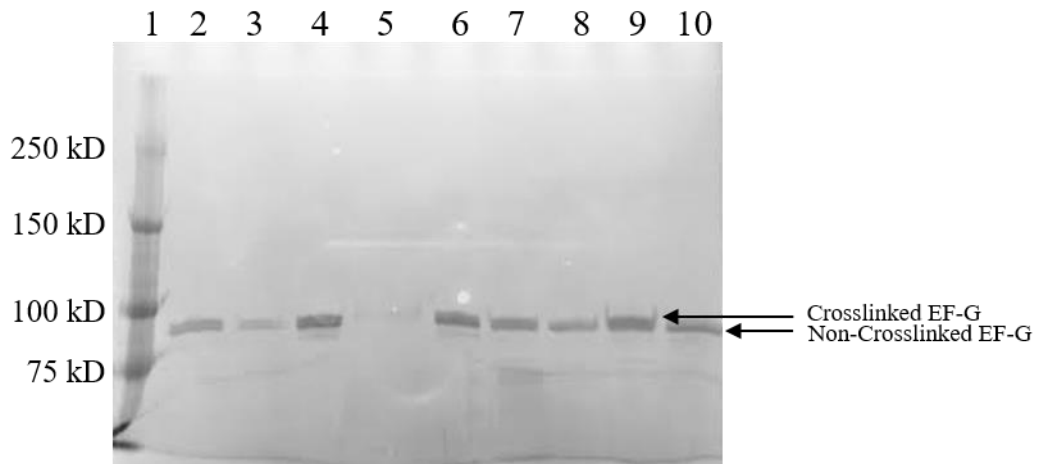
**A**, 5% tris-glycine SDS-PAGE gel with pureCube maleimide magnetic bead purified F95C/M682C BM(PEG)<sub>6</sub> crosslinked EF-G. *Lane 1* Bio-Rad dual color protein ladder, *lane 2* purified F95C/M682C BM(PEG)<sub>6</sub> crosslinked EF-G, *lane 3* purified F95C/M682C BM(PEG)<sub>6</sub> crosslinked EF-G wash fraction, *lane 4* F95C/M682C EF-G, *lane 5* purified F95C/M682C BM(PEG)<sub>6</sub> crosslinked EF-G, *lane 6* purified F95C/M682C BM(PEG)<sub>6</sub> crosslinked EF-G wash fraction, *lane 7* sulfoLink coupling resin purified F95C/M682C BM(PEG)<sub>6</sub> crosslinked EF-G, *lane 8* unpurified F95C/M682C BM(PEG)<sub>6</sub> crosslinked EF-G

**B**, 5% tris-glycine SDS-PAGE gel with pureCube maleimide agarose and Bioclone iodoacetyl bead purified F95C/M682C BM(PEG)<sub>6</sub> crosslinked EF-G. *Lane 1* Bio-Rad dual color protein ladder, *lane 2* pureCube maleimide agarose purified F95C/M682C BM(PEG)<sub>6</sub> crosslinked EF-G fraction 1, *lane 3* PureCube maleimide agarose purified F95C/M682C BM(PEG)<sub>6</sub> crosslinked EF-G fraction 2, *lane 4* pureCube maleimide agarose purified F95C/M682C BM(PEG)<sub>6</sub> crosslinked EF-G fraction 1, *lane 5* pureCube maleimide agarose purified F95C/M682C BM(PEG)<sub>6</sub> crosslinked EF-G fraction 2, *lane 6* unpurified F95C/M682C BM(PEG)<sub>6</sub> crosslinked EF-G, *lane 7* bioclone iodoacetyl bead purified F95C/M682C BM(PEG)<sub>6</sub> crosslinked EF-G fraction 1, *lane 8* bioclone iodoacetyl bead purified F95C/M682C BM(PEG)<sub>6</sub> crosslinked EF-G fraction 2, *lane 9* bioclone iodoacetyl bead purified F95C/M682C BM(PEG)<sub>6</sub> crosslinked EF-G fraction 1, *lane 10* bioclone iodoacetyl bead purified F95C/M682C BM(PEG)<sub>6</sub> crosslinked EF-G fraction 2

**A**



**B**



### 4.3 Discussion

#### Site-Directed Mutagenesis and Crosslinking of F95C/M682C Elongation Factor G in the Fusidic Acid Binding Pocket

In this investigation, mutations with two amino acid residues substituted for cysteine in the Fusidic acid binding pocket were made in an attempt to observe the effects of crosslinking on EF-G function. However, the inability to purify crosslinked EF-G resulted in the halting of this study. Studies of the antibiotic Fusidic acid have shown that it binds directly to EF-G, and was originally thought to allow one round of translocation before trapping EF-G on the ribosome (99). However, more recent studies instead propose that Fusidic Acid inhibition still allows multiple rounds of translocation before trapping EF-G on the ribosome (101). This antibiotic binds within the vicinity of the GTPase center, in a pocket formed by domains I, II, and III (68,102). Because of the proximity of this binding pocket to the GTPase center, it is possible that some of the earliest conformational changes that occur in EF-G occur here. To address the gaps in the understanding of the mechanism of Fusidic acid inhibition and the if and how of conformational change initiation, mutagenesis and crosslinking in this region was done.

Because this pocket is in such close proximity to the GTPase center, crosslinking could result in much more dramatic effects. Compared to the previous crosslinked mutant, in which conformational changes were halted in the middle of the reaction on the ribosome, the binding pocket mutant would be halted at the beginning of the translocation reaction. In this study, site-directed mutagenesis was used to mutate F95 and M682 in *E. coli* EF-G to cysteine. The mutant, F95C/M682C EF-G, was then crosslinked to itself using bis-maleimide crosslinkers. As was done in the previous chapter, the crosslinked EF-G required purification

from the non-crosslinked EF-G. Unlike the previous chapter, however, the crosslinking efficiency for the F95C/M682C EF-G was extremely low. The location of the two cysteines in the Fusidic acid binding pocket presented challenges in crosslinking. A number of reasons could result in the low crosslinking efficiency. These include the distance between the residues, the size of the crosslinker, and most importantly, the accessibility of the two cysteine residues. The Fusidic acid binding pocket is located towards the interior of EF-G, and this would result in difficulty for the crosslinker to reach the two cysteine residues.

Purification using hydrophobic interaction chromatography and maleimide beads was done for the crosslinked EF-G. By utilizing the potential differences in hydrophobicity, the crosslinked and non-crosslinked EF-G could be separated with a phenyl column. Different salt concentrations and pH's were tested; however, no amount of fine tuning was able to successfully separate the crosslinked and non-crosslinked EF-G. The differences in hydrophobicity were most likely not substantial enough to produce differences in binding to the column. Maleimide bead purification was also tested, however, purifying the crosslinked EF-G was unsuccessful. Because the initial crosslinking efficiency was low, the beads were most likely overloaded with non-crosslinked protein. Reducing the amount of sample added to the beads was not plausible, as the yield would have been inadequate for further experiments. Although this mutant was not purified, crosslinking in the Fusidic acid binding pocket still merits further studies due to the potential studies on EF-G mechanism that can be done by focusing on this binding pocket.

# CHAPTER FIVE: CHARACTERIZATION OF THE EFFECTOR LOOP OF EF-G

## 5.1 Introduction

Domain I of EF-G contains the GTPase center. Domain I is responsible for hydrolysis of GTP during translocation, and for binding interactions with the ribosome. The effector loop region spans approximately seven residues in domain I and contributes to EF-G induced movement of the tRNA-mRNA complex through the ribosome (59,89). In EF-G crystal structures, however, the effector loop region is always disordered (56). Recent structural data on EF-G in complex with the ribosome, though, finally reveals the organized effector loop region, and the loop is seen to form a cover for the GTP binding site (59). In the eukaryotic homolog of EF-G, EF2 (eEF2), phosphorylation of a threonine residue (T56) within the effector loop completely inactivates eEF2 (72,73). This type of translational control has not been reported for bacteria, however, the existence of a similar mechanism of EF-G regulation cannot be excluded. Also, the effector loop harbors an aspartate residue (D51) universally conserved through all three major domains of life in both the EF-G (EF2) and EF-Tu (EF-1A) protein families. This makes the effector loop a legitimate target for more detailed studies focused on its involvement in EF-G specific activities.

To begin characterizing the effector loop, six EF-G mutants were produced. The single mutations G46P, T49V, T49E, M50E, D51A, and W52E were introduced into the F411C/Y543C double mutant EF-G (M5 EF-G) that was first mentioned in Chapter 3. Each mutant, therefore, is a mutant of the original M5 EF-G variant. These EF-G mutants, containing a single amino acid substitution in the effector loop, were made in order to better

understand the individual contribution of each residue in the effector loop. Glycine 46 (of the G46P mutant) is conserved among bacterial EF-Gs and is expected to confer flexibility on the flank of the effector loop. Many structures of EF-G often exhibit a disordered effector loop, implying the dynamic nature of this region. By replacing the glycine with proline, the backbone mobility is anticipated to be constrained. Methionine 50 (of the M50E mutant) aligns exactly with the site of phosphorylation in the eukaryotic homolog of EF-G, eEF2. The mutation to a glutamic acid, therefore, mimics phosphorylation at this position. Threonine 49 (of the T49V and T49E mutants) is the closest threonine residue to the anticipated phosphorylation site at position 50. Mutation to glutamic acid (T49E) was selected to mimic phosphorylation on a threonine residue, as threonine is the residue that is phosphorylated in EF2. Mutation to valine (T49V) was chosen because valine is isosteric to threonine, but lacks the hydroxyl group, which might serve as a phosphorylation site. Mutation of tryptophan at position 52 (W52E) was selected because this position corresponds to a secondary site of phosphorylation in eEF2. Mutation of aspartate to alanine (D51A) was done because of its ultra-conserved nature in translational GTPases.

For each mutant produced, the ribosome-dependent GTP hydrolysis and translocation activities were determined. All of the mutants, with the exception of D51A, were able to efficiently hydrolyze GTP. However, none of the mutants were able to induce translocation on the ribosome comparable to that of M5 EF-G. Overall, this study of the effector loop has provided a better understanding of EF-G function on the ribosome.

## **5.2 Results**

### **5.2.1 GTP Hydrolysis Analysis of Effector Loop Mutants of EF-G**

The EF-G effector loop was mutagenized at six separate positions. The structure of the effector loop is shown in Figure 5.2.1. Each mutant was derived from the original M5 EF-G that was first mentioned in Chapter 3. The mutants were designated as G46P, T49V, T49E, M50E, D51A, and W52E, according to the residue mutated (Figure 5.2.2). In order to determine the GTP hydrolysis activity of the mutants, a fluorescence based GTP hydrolysis assay was used. Each hydrolysis reaction was run separately, and 20 s, 3 min, and 10 min timepoints were collected (Figure 5.2.3). T49V and T49E mutants hydrolyzed GTP at a comparable rate to M5 EF-G, considering the experimental error. M50E and W52E exhibited similar rates of GTP hydrolysis, but both being lower than that of M5 EF-G. Even slower GTP hydrolysis was seen in the case of the G46P mutant, while D51A EF-G possessed no detectable activity.

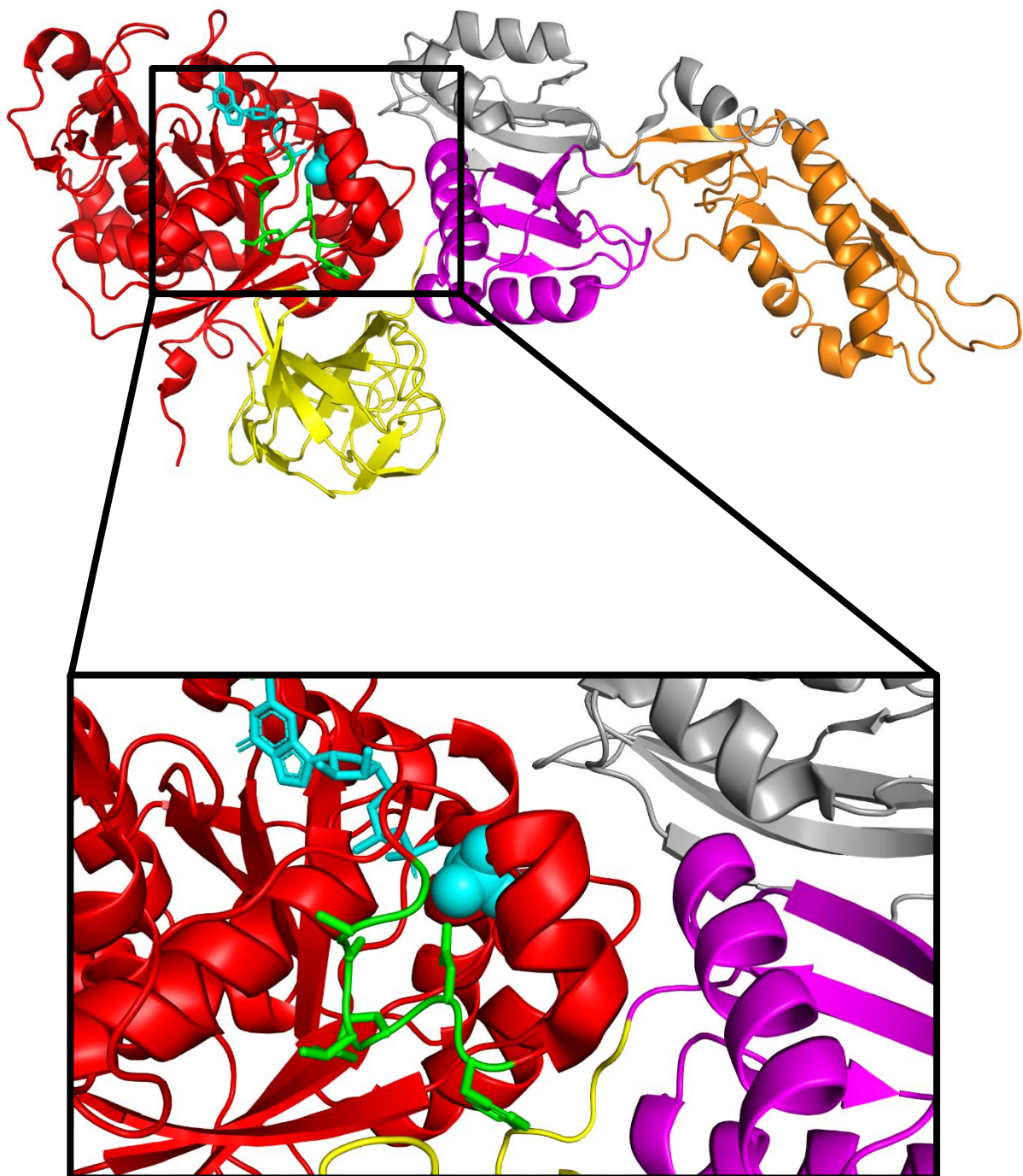


**Figure 5.2.1 Structure of the Effector Loop of EF-G.** *Top*, crystal structure of EF-G effector loop highlighted in green. domain I (red), domain II (yellow), domain III (magenta), domain IV (orange), domain V (Grey). *Bottom*, close up view of EF-G effector loop. GDP and Pi shown in cyan (PBD: 7PJV) (59).

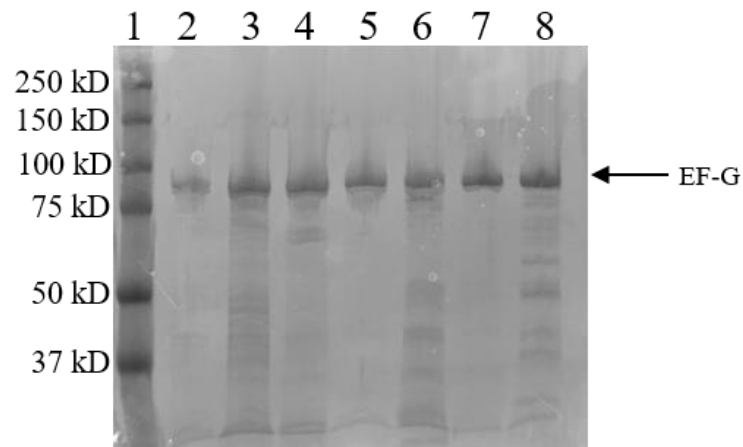


**Figure 5.2.2 Effector Loop Mutants of EF-G.** 8% tris-glycine SDS-PAGE gel. *Lane 1* Bio-Rad dual color protein ladder, *lane 2* G46P EF-G, *lane 3* T49V EF-G, *lane 4* T49E EF-G, *lane 5* M50E EF-G, *lane 6* D51A EF-G, *lane 7* W52E EF-G, *lane 8* M5 EF-G

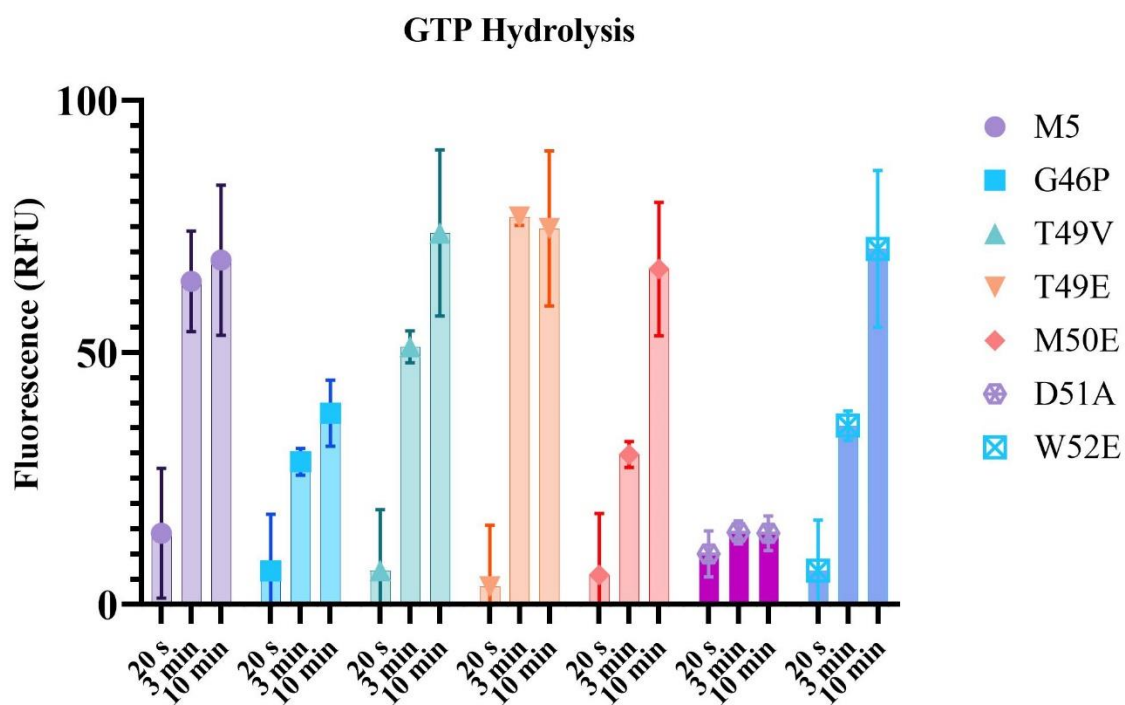


**Figure 5.2.3 GTP Hydrolysis Activities of M5 EF-G and Effector Loop Mutants of EF-G.** Fluorescence measurements by the Transcreener GDP FI assay of M5 EF-G and effector loop mutants of EF-G with timepoints taken at 20 s, 3 min, and 10 min.

### **5.2.2 Translocation Activity of Effector Loop Mutants of EF-G**

In addition to the GTPase assays, the translocation activity of M5, G46P, T49V, T49E, M50E, D51A, and W52E EF-Gs on the ribosome was studied. Polyphenylalanine synthesis assays were performed according to the standard protocol, with 20 s, 3 min, and 10 min timepoints per reaction. The highest activity was seen in the case of M5 EF-G, while the activity of the mutants was dramatically decreased (Figure 5.2.4). Of the mutants, only T49V was able to drive polyphenylalanine synthesis to detectable levels, however, the translocation rate was still much lower than that of M5 EF-G. No EF-G dependent translocation was observed with the remaining mutants. Overall, the studied mutations in the effector loop efficiently impaired EF-G activity in the translocation process.

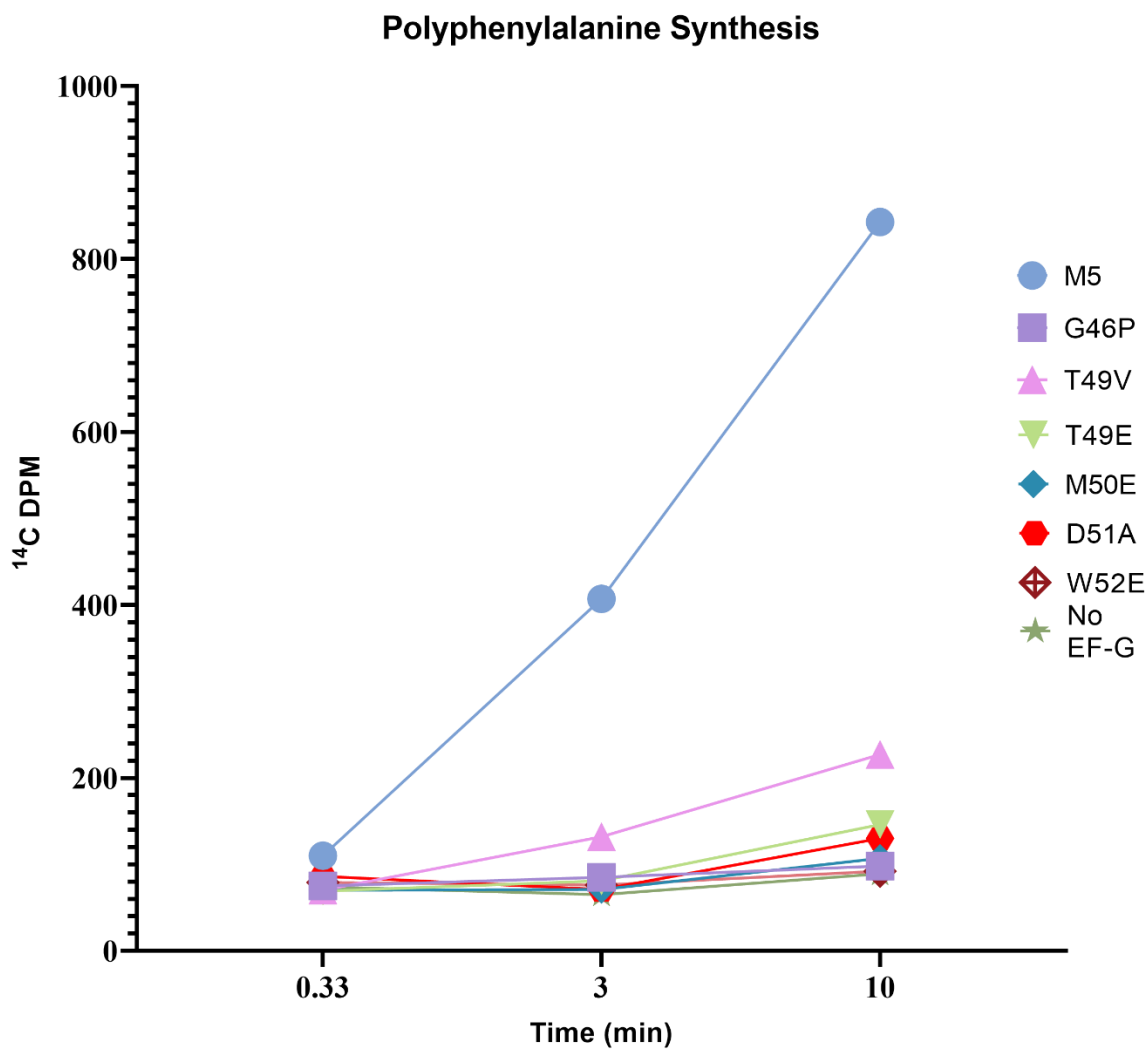


**Figure 5.2.4 Polyphenylalanine Assays of M5 EF-G and Mutants of M5 EF-G.** Radioactivity measurements by polyphenylalanine synthesis assay for M5 EF-G and effector loop mutants of EF-G with timepoints taken at 20 s, 3 min, and 10 min.

### 5.3 Discussion

In this study, the effector loop region of EF-G was investigated by introducing single amino acid substitutions, and has revealed that all of the mutations resulted in a total loss of function for EF-G. The effector loop lies within switch I in domain I of EF-G. This loop is known to contain a point of translational control in the human homolog of EF-G, eEF2 (72,103). And although the effector loop was long anticipated to be important, studies have largely ignored the region. This was possibly because it was difficult to surmise the positions of the residues within the loop since it was always disordered in EF-G structures available at that time. Without structural data, it would be problematic to assign the contributions of each residue to the function of EF-G. To fill this gap, mutations in the effector loop were generated in order to examine the role of residues in this region.

The conservation of aspartate in position 51 of EF-G spans all three domains of life, as well as in elongation factor Tu (EF-Tu) (104,105). In EF-Tu, the structure of the switch I region is often ordered, unlike in EF-G, and this residue is shown to be involved in positioning of the guanine nucleotide cofactor in its binding site. This interaction is mediated by a  $Mg^{2+}$  ion and water bridge (70). Our study has revealed that when aspartate at site 51 is mutated to alanine (D51A), a total loss of GTPase activity occurs. Recent structures of EF-G, with an ordered effector loop, imply that this aspartate residue may interact with the  $Mg^{2+}$  ion in the same way as seen in EF-Tu, possibly through a water molecule (59). The distance between the aspartate side chain and  $Mg^{2+}$  ion is approximately 4.2Å, which is consistent with their interaction via a water bridge. The loss of this interaction with the  $Mg^{2+}$  ion by replacement of aspartate with alanine is the most likely cause for the loss of GTP hydrolysis activity. Without

the ability to hydrolyze GTP, it is only natural that the D51A mutant was also unable to induce translocation on the ribosome.

The substitution of glycine at position 46 with proline was aimed at local changing of the backbone's flexibility. Glycine at this site is conserved within bacteria (52,54,106). Studies of EF-G revealed that in the course of translocation switch I moves over a long distance as a whole, and this movement requires substantial flexibility of the amino acid backbone at the flanks of this region (59). The N-terminal flank of switch I contains three spaced glycine residues, adding flexibility at these points. By imposing constraint on the backbone movement through the replacement of glycine with proline, as is done in G46P EF-G, the switch I dynamics are anticipated to be critically impaired (107,108). Experiments with G46P reveal that it hydrolyzes GTP, but at a rate noticeably lower than M5 EF-G. Thus, while the replacement of the flexible glycine residue with the inflexible proline reduced GTP hydrolysis, it did not completely abolish it. And as with the D51A mutant, G46P EF-G was also unable to catalyze translocation in polyphenylalanine synthesis assays.

Previous studies have shown that single site substitution of residues with glutamic acid can be used to mimic phosphorylation on serine and threonine residues in proteins (109). In eEF2, threonine phosphorylation in the effector loop turns off the function of EF-G at the translocation step, a mechanism not yet seen in bacterial EF-G (59). To study this, three residues were mutated to glutamic acid. Methionine 50 of *E. coli* EF-G aligns directly with the primary threonine phosphorylation site (T56) in human eEF2, while tryptophan 52 is a positional equivalent of the secondary site of phosphorylation (T58) (110). Both M50E and W52E hydrolyzed GTP at rates comparable to M5 EF-G, yet neither was able to induce translocation. This observation is consistent with previous studies on eEF2, in which

phosphorylation did not affect GTPase activity, but halted its function before the translocation step through impaired binding of the enzyme to the ribosome (73-75). While methionine 50 exactly corresponds to the phosphorylation site in human eEF2, threonine 49 is the closest threonine residue to this position in *E. coli* EF-G. When mutated to glutamic acid (T49E), no changes in the GTP hydrolysis activity were observed as compared with M5 EF-G. At the same time, a substitution of threonine 49 with valine, an isosteric residue lacking a phosphorylatable group, also didn't affect GTPase activity. Interestingly, T49V did catalyze translocation, albeit at a substantially lower rate than M5 EF-G, while T49E was totally inactive in polyphenylalanine synthesis assays. Previous studies from our lab confirmed that the mutants are able to bind GTP and GDP comparably to M5 EF-G, indicating that the mutations did not result in misfolded enzyme. Apart from D51A and G46P, mutations in the effector loop did not greatly affect GTPase activity. However, all the substitutions in this region did result in large reductions in EF-G's ability to induce translocation on the ribosome.

## CHAPTER SIX: CONCLUSIONS AND FUTURE DIRECTIONS

### 6.1 Major Conclusions

#### 6.1.1 EF-G Crosslinking and FIRMS Measurements

During translation of mRNA in protein, EF-G binds to the ribosome and promotes translocation allowing this process to proceed at a rate that is able to sustain life. Using site-directed mutagenesis and crosslinking, M5 BM(PEG)<sub>6</sub> and M5 BM(PEG)<sub>11</sub> crosslinked EF-Gs were made to determine if restricting conformational changes in EF-G would affect the force that EF-G exerts on the ribosome. The BM(PEG)<sub>11</sub> crosslinker was 42.6 Å, and did not restrict EF-G conformational changes. BM(PEG)<sub>6</sub> was 27.1 Å, and allowed EF-G to only partially extend into the elongated conformation. Using FIRMS, the power stroke force of EF-G with each crosslinker was determined. M5 BM(PEG)<sub>11</sub> crosslinked EF-G produced a force similar to wild-type EF-G. The power stroke forces were 93±8pN for crosslinked EF-G and 87±8 pN for wild type. M5 BM(PEG)<sub>6</sub> crosslinked EF-G, on the other hand, produced a lower power stroke force (60±6 pN). Translocation efficiencies with each EF-G were also determined. BM(PEG)<sub>11</sub> crosslinked EF-G exhibited a translocation efficiency similar to wild type (100% translocation of ribosomal complexes). BM(PEG)<sub>6</sub> crosslinked EF-G, on the other hand, exhibited a translocation efficiency of about 55%, meaning 45% of ribosomal complexes were left in the pre-translocation state. No frameshifting occurred as a result of the EF-G being crosslinked, indicating that the force EF-G exerts does not have an effect on reading frame maintenance. Crosslinking EF-G to restrict conformational changes resulted in a large reduction of both power stroke force and translocation efficiency, but did not induce ribosomal frameshifting.

### **6.1.2 Crosslinking in the Fusidic Acid Binding Pocket**

To continue using crosslinking to study EF-G conformational changes, a double cysteine mutant with mutations in the Fusidic acid binding pocket was produced. Initiation of conformational changes in EF-G are thought to occur near this binding pocket, which is located in the vicinity of the GTPase center. Using the same protocol as for M5 EF-G, the F95C/M682C EF-G mutant was made in order to study the conformational changes that occur at the beginning of EF-G translocation. If the initiation of conformational changes occurs in this region, internally crosslinking EF-G could potentially have more dramatic effects. Unfortunately, while the Fusidic acid binding pocket did support mutagenesis, the crosslinking efficiency was extremely low in this region. The most likely cause is the inability for the crosslinker to enter the binding pocket. Low crosslinking efficiency then resulted in poor purification of the crosslinked EF-G, and because purification was not achieved, force and translocation measurements could not be done.

### 6.1.3 Characterization of the Effector Loop of EF-G

The effector loop is located within switch I on domain I of EF-G and contains important interactions for GTP hydrolysis. Six single substitution effector loop mutants were produced in order to study the role of each residue in the function of EF-G. Each is variant of the original M5 EF-G, first mentioned in Chapter 3. The mutants produced were G46P, T49V, T49E, M50E, D51A, and W52E, and the GTP hydrolysis and translocation activity was measured for each. Substitution of *E. coli* glycine 46 with proline (G46P) resulted in GTPase activity that was considerably lower than M5 EF-G, while mutation of *E. coli* aspartate residue 51 (D51A) completely abolished activity. GTP hydrolysis by the remaining mutants was comparable to that of M5 EF-G. Polyphenylalanine synthesis assays uncovered the interesting discovery that not a single variant was able to induce translocation comparable to that of M5 EF-G. Therefore, single site substitutions in the effector loop effectively knocked out the ability of EF-G to promote translocation on the ribosome, while mostly allowing for GTPase activity to remain intact.

## 6.2 Future Directions

### 6.2.1 Crosslinking to Study Protein Conformational Changes

The purpose of crosslinking EF-G was to restrict full conformational changes in EF-G. The residues were selected on the basis of their pre-translocation and post-translocation distances, in order to have the ability to restrict EF-G within its intermediate states of translocation. By doing this, large conformational change restrictions were studied, however, the effect of crosslinking to restrict the initial conformational changes still remained to be studied. This problem had begun to be tackled by crosslinking in the Fusidic acid binding pocket. The goal was to observe the effects of restricting much more minute conformational changes at the beginning of the translocation reaction. Though the Fusidic acid crosslinked EF-G was not purified, the potential to crosslink in this region still exists. The crosslinkers used contained PEG groups to add length, however, using shorter linkers without PEG groups could result in a higher initial crosslinking efficiency. With a higher efficiency, purification should be achievable. New studies in the early stages of translocation have begun to uncover the role of GTP hydrolysis in EF-G, and the release of Pi was shown to induce conformational changes in switch I which propagate to the rest of the ribosomal complex (59). The compact conformation has been seen in solution, as well as during ribosome recycling, however the fully compact conformation in ribosomal translocation is still up for debate (4,111). Crosslinking with shorter crosslinkers would be able to provide a deeper understanding of the biological relevance of the compact conformation. Crosslinking EF-G with BM(PEG)<sub>2</sub> and BM(PEG)<sub>3</sub> was attempted, but proved to be more difficult to purify, however, a combination of the mentioned purification methods could provide the purity needed for experimentation.

In addition to the PEG crosslinkers, which are fairly flexible, exchanging for a rigid crosslinker would also provide insight into the movement of EF-G. Using rigid crosslinkers would trap EF-G in different positions, and using varying lengths of rigid crosslinkers would allow EF-G to be maintained in specific conformations. The use of crosslinkers can greatly assist in studying EF-G conformational changes, and using new insights into the movement of EF-G can guide in which areas to crosslink. The crosslinking data, combined with structural studies would provide a more comprehensive understanding of the movement of EF-G, as well as its mechanism in translocation.

### **6.2.2 Fusidic Acid Resistance**

In addition to crosslinking, studies in the Fusidic acid binding pocket had the dual purpose of examining Fusidic acid resistance. The F95C/M682C mutation was generated in order to confer Fusidic acid resistance, and the effects on EF-G were to be studied using biochemical assays and FIRMS. Though the mutant was not utilized previously, continued studies with this variant can be done. Studies with and without Fusidic acid can determine the effects on EF-G during Fusidic acid resistance. Because Fusidic acid is banned in the US, the antibiotic is only used for research purposes. Recently, however, it has been brought to the attention of clinicians for its possible use against MRSA infections. In order to bring Fusidic acid to the clinic, though, detailed studies of resistance and subsequent FDA approval would be required.

### **6.2.3 Continued Studies of the Effector loop**

Mutations in the effector loop resulted in the total abolishment of GTPase activity in one mutant (D51A), and reduction in another (G46P). Surprisingly, all of the single site substitution EF-Gs were unable to induce translocation on the ribosome. To continue the

study of these mutants, measurements of power stroke force and translocation efficiencies via FIRMS will be done. In addition to the continuation of assays with the mutants as mentioned, new substitutions to cover the entirety of the effector loop would be greatly beneficial to uncovering the precise contribution of this small region to the function of EF-G. Aspartic acid 51 was substituted with alanine which resulted in abolishment of hydrolysis and translocation activity. Studies in EF-Tu reveal that the aspartic acid may interact with a coordinated  $Mg^{2+}$  ion via a water bridge, and the same residue in EF-G may function the same (70). Substitution with glutamic acid, which contains the same functional group but also includes an added methylene group, could provide insight into the importance of distance in the interaction of D51. In addition to biochemical and FIRMS assays, the effector loop mutants can also be studied using single-molecule FRET (smFRET), because each is a variant of the original M5 EF-G which contains two known cysteines. The conformational data obtained from FRET, combined with FIRMS and biochemical assays will provide a complete understand of the effect of each mutation on the movement and function of EF-G. Three of the six mutants contain a glutamic acid substitution to mimic the phosphorylation that occurs in human eEF2. Continued studies of these mutants using the previously mentioned techniques would also provide understanding into the translational control mechanism that occurs in eEF2 through phosphorylation of threonine 56. In addition to single-site substitutions, loop replacement with the loop of human eEF2 can be studied to observe the effects on EF-G. If the replacement is successful, phosphorylation of the human eEF2 effector loop can be observed in a bacterial system. The combined studies in the effector loop will provide much needed characterization of this fairly unstudied region.

## BIBLIOGRAPHY

1. Melnikov, S., Ben-Shem, A., De Loubresse, N. G., Jenner, L., Yusupova, G., and Yusupov, M. (2012) One core, two shells: bacterial and eukaryotic ribosomes. *Nature Structural & Molecular Biology* **19**, 560-567
2. Pikó, L., and Taylor, K. D. (1987) Amounts of mitochondrial DNA and abundance of some mitochondrial gene transcripts in early mouse embryos. *Developmental Biology* **123**, 364-374
3. Chaffey, N. (2003) Alberts, B., Johnson, A., Lewis, J., Raff, M., Roberts, K. and Walter, P. *Molecular biology of the cell*. 4th edn. Oxford University Press
4. Zhou, D., Tanzawa, T., Lin, J., and Gagnon, M. G. (2020) Structural basis for ribosome recycling by RRF and tRNA. *Nature Structural & Molecular Biology* **27**, 25-32
5. Von Böhlen, K., Makowski, I., Hansen, H., Bartels, H., Berkovitch-Yellin, Z., Zaytzev-Bashan, A., Meyer, S., Paulke, C., Franceschi, F., and Yonath, A. (1991) Characterization and preliminary attempts for derivatization of crystals of large ribosomal subunits from *Haloarcula marismortui* diffracting to 3 Å resolution. *Journal of Molecular Biology* **222**, 11-15
6. Schlünzen, F., Hansen, H., Thygesen, J., Bennett, W., Volkmann, N., Harms, J., Bartels, H., Krumbholz, S., Levin, I., and Zaytzev-Bashan, A. (1995) A milestone in ribosomal crystallography: the construction of preliminary electron density maps at intermediate resolution. *Biochemistry and Cell Biology* **73**, 739-749
7. Frank, J., and Agrawal, R. K. (2000) A ratchet-like inter-subunit reorganization of the ribosome during translocation. *Nature* **406**, 318-322
8. Horan, L. H., and Noller, H. F. (2007) Intersubunit movement is required for ribosomal translocation. *Proceedings of the National Academy of Sciences* **104**, 4881-4885
9. Ban, N., Nissen, P., Hansen, J., Moore, P. B., and Steitz, T. A. (2000) The complete atomic structure of the large ribosomal subunit at 2.4 Å resolution. *Science* **289**, 905-920
10. Arnold, R. J., and Reilly, J. P. (1999) Observation of *Escherichia coli* ribosomal proteins and their posttranslational modifications by mass spectrometry. *Analytical Biochemistry* **269**, 105-112

11. Ban, N., Beckmann, R., Cate, J. H., Dinman, J. D., Dragon, F., Ellis, S. R., Lafontaine, D. L., Lindahl, L., Liljas, A., and Lipton, J. M. (2014) A new system for naming ribosomal proteins. *Current Opinion in Chemical Biology* **24**, 165-169
12. Narla, A., and Ebert, B. L. (2010) Ribosomopathies: human disorders of ribosome dysfunction. *Blood, The Journal of the American Society of Hematology* **115**, 3196-3205
13. Xia, X. (2021) Detailed dissection and critical evaluation of the Pfizer/BioNTech and Moderna mRNA vaccines. *Vaccines* **9**, 734-752
14. Polack, F. P., Thomas, S. J., Kitchin, N., Absalon, J., Gurtman, A., Lockhart, S., Perez, J. L., Marc, G. P., Moreira, E. D., and Zerbini, C. (2020) Safety and efficacy of the BNT162b2 mRNA Covid-19 vaccine. *New England Journal of Medicine* **383**, 2603-2615
15. Ramrath, D. J., Lancaster, L., Sprink, T., Mielke, T., Loerke, J., Noller, H. F., and Spahn, C. M. (2013) Visualization of two transfer RNAs trapped in transit during elongation factor G-mediated translocation. *Proceedings of the National Academy of Sciences* **110**, 20964-20969
16. Kurland, C. G. (1960) Molecular characterization of ribonucleic acid from *Escherichia coli* ribosomes: I. Isolation and molecular weights. *Journal of Molecular Biology* **2**, 83-91
17. Lane, B., and Tamaoki, T. (1967) Studies of the chain termini and alkali-stable dinucleotide sequences in 16 s and 28 s ribosomal RNA from L cells. *Journal of Molecular Biology* **27**, 335-348
18. Elela, S. A., and Nazar, R. N. (1997) Role of the 5.8 S rRNA in ribosome translocation. *Nucleic Acids Research* **25**, 1788-1794
19. Warner, J. R. (1999) The economics of ribosome biosynthesis in yeast. *Trends in Biochemical Sciences* **24**, 437-440
20. Traub, P., and Nomura, i. (1968) Structure and function of *E. coli* ribosomes. V. Reconstitution of functionally active 30S ribosomal particles from RNA and proteins. *Proceedings of the National Academy of Sciences of the United States of America* **59**, 777-784
21. Nissen, P., Hansen, J., Ban, N., Moore, P. B., and Steitz, T. A. (2000) The structural basis of ribosome activity in peptide bond synthesis. *Science* **289**, 920-930
22. Ramakrishnan, V. (2002) Ribosome structure and the mechanism of translation. *Cell* **108**, 557-572

23. Takyar, S., Hickerson, R. P., and Noller, H. F. (2005) mRNA helicase activity of the ribosome. *Cell* **120**, 49-58
24. Davies, J., Gilbert, W., and Gorini, L. (1964) Streptomycin, suppression, and the code. *Proceedings of the National Academy of Sciences of the United States of America* **51**, 883-890
25. Carter, A. P., Clemons, W. M., Brodersen, D. E., Morgan-Warren, R. J., Wimberly, B. T., and Ramakrishnan, V. (2000) Functional insights from the structure of the 30S ribosomal subunit and its interactions with antibiotics. *Nature* **407**, 340-348
26. Ogle, J. M., Murphy IV, F. V., Tarry, M. J., and Ramakrishnan, V. (2002) Selection of tRNA by the ribosome requires a transition from an open to a closed form. *Cell* **111**, 721-732
27. Oleinikov, A. V., Perroud, B., Wang, B., and Traut, R. R. (1993) Structural and functional domains of Escherichia coli ribosomal protein L7/L12. The hinge region is required for activity. *Journal of Biological Chemistry* **268**, 917-922
28. Diaconu, M., Kothe, U., Schlünzen, F., Fischer, N., Harms, J. M., Tonevitsky, A. G., Stark, H., Rodnina, M. V., and Wahl, M. C. (2005) Structural basis for the function of the ribosomal L7/12 stalk in factor binding and GTPase activation. *Cell* **121**, 991-1004
29. Hoagland, M. B., Stephenson, M. L., Scott, J. F., Hecht, L. I., and Zamecnik, P. C. (1958) A soluble ribonucleic acid intermediate in protein synthesis. *Journal of Biological Chemistry* **231**, 241-257
30. Itoh, Y., Sekine, S.-i., Suetsugu, S., and Yokoyama, S. (2013) Tertiary structure of bacterial selenocysteine tRNA. *Nucleic Acids Research* **41**, 6729-6738
31. Chládek, S., and Sprinzl, M. (1985) The 3'-end of tRNA and its role in protein biosynthesis. *Angewandte Chemie International Edition in English* **24**, 371-391
32. Ladner, J., Jack, A., Robertus, J., Brown, R., Rhodes, D., Clark, B., and Klug, A. (1975) Structure of yeast phenylalanine transfer RNA at 2.5 Å resolution. *Proceedings of the National Academy of Sciences* **72**, 4414-4418
33. Felsenfeld, G., and Cantoni, G. (1964) Use of thermal denaturation studies to investigate the base sequence of yeast serine sRNA. *Proceedings of the National Academy of Sciences of the United States of America* **51**, 818-826
34. Quigley, G. J., and Rich, A. (1976) Structural domains of transfer RNA molecules: the ribose 2' hydroxyl which distinguishes RNA from DNA plays a key role in stabilizing tRNA structure. *Science* **194**, 796-806

35. Roth, A. C. (2012) Decoding properties of tRNA leave a detectable signal in codon usage bias. *Bioinformatics* **28**, i340-i348
36. Shine, J., and Dalgarno, L. (1974) The 3'-terminal sequence of Escherichia coli 16S ribosomal RNA: complementarity to nonsense triplets and ribosome binding sites. *Proceedings of the National Academy of Sciences* **71**, 1342-1346
37. Dahlquist, K. D., and Puglisi, J. D. (2000) Interaction of translation initiation factor IF1 with the E. coli ribosomal A site. *Journal of Molecular Biology* **299**, 1-15
38. Steitz, J. A., and Jakes, K. (1975) How ribosomes select initiator regions in mRNA: base pair formation between the 3'terminus of 16S rRNA and the mRNA during initiation of protein synthesis in Escherichia coli. *Proceedings of the National Academy of Sciences* **72**, 4734-4738
39. Hussain, T., Ll acer, J. L., Wimberly, B. T., Kieft, J. S., and Ramakrishnan, V. (2016) Large-scale movements of IF3 and tRNA during bacterial translation initiation. *Cell* **167**, 133-144. e113
40. Agrawal, R. K., Spahn, C. M., Penczek, P., Grassucci, R. A., Nierhaus, K. H., and Frank, J. (2000) Visualization of tRNA movements on the Escherichia coli 70S ribosome during the elongation cycle. *The Journal of Cell Biology* **150**, 447-460
41. Korostelev, A., Asahara, H., Lancaster, L., Laurberg, M., Hirschi, A., Zhu, J., Trakhanov, S., Scott, W. G., and Noller, H. F. (2008) Crystal structure of a translation termination complex formed with release factor RF2. *Proceedings of the National Academy of Sciences* **105**, 19684-19689
42. Laurberg, M., Asahara, H., Korostelev, A., Zhu, J., Trakhanov, S., and Noller, H. F. (2008) Structural basis for translation termination on the 70S ribosome. *Nature* **454**, 852-857
43. Freistroffer, D. V., Pavlov, M. Y., MacDougall, J., Buckingham, R. H., and Ehrenberg, M. (1997) Release factor RF3 in E. coli accelerates the dissociation of release factors RF1 and RF2 from the ribosome in a GTP-dependent manner. *The EMBO journal* **16**, 4126-4133
44. Wilson, D. N. (2014) Ribosome-targeting antibiotics and mechanisms of bacterial resistance. *Nature Reviews Microbiology* **12**, 35-48
45. Goldman, R. A., Hasan, T., Hall, C. C., Strycharz, W. A., and Cooperman, B. S. (1983) Photoincorporation of tetracycline into Escherichia coli ribosomes. Identification of the major proteins photolabeled by native tetracycline and tetracycline photoproducts and implications for the inhibitory action of tetracycline on protein synthesis. *Biochemistry* **22**, 359-368

46. Brodersen, D. E., Clemons Jr, W. M., Carter, A. P., Morgan-Warren, R. J., Wimberly, B. T., and Ramakrishnan, V. (2000) The structural basis for the action of the antibiotics tetracycline, pactamycin, and hygromycin B on the 30S ribosomal subunit. *Cell* **103**, 1143-1154
47. Wisseman Jr, C., Smadel, J., Hahn, F., and Hopps, H. (1954) Mode of action of chloramphenicol I: action of chloramphenicol on assimilation of ammonia and on synthesis of proteins and nucleic acids in *Escherichia coli*. *Journal of Bacteriology* **67**, 662-673
48. Dunkle, J. A., Xiong, L., Mankin, A. S., and Cate, J. H. (2010) Structures of the *Escherichia coli* ribosome with antibiotics bound near the peptidyl transferase center explain spectra of drug action. *Proceedings of the National Academy of Sciences* **107**, 17152-17157
49. Wilson, D. N. (2009) The A–Z of bacterial translation inhibitors. *Critical Reviews in Biochemistry and Molecular Biology* **44**, 393-433
50. Krásný, L., Vacík, T. s., Fučík, V. r., and Jonák, J. i. (2000) Cloning and characterization of the str operon and elongation factor Tu expression in *Bacillus stearothermophilus*. *Journal of Bacteriology* **182**, 6114-6122
51. Bourne, H. R., Sanders, D. A., and McCormick, F. (1991) The GTPase superfamily: conserved structure and molecular mechanism. *Nature* **349**, 117-127
52. Czworkowski, J., Wang, J., Steitz, T., and Moore, P. (1994) The crystal structure of elongation factor G complexed with GDP, at 2.7 Å resolution. *The EMBO Journal* **13**, 3661-3668
53. Wilden, B., Savelsbergh, A., Rodnina, M. V., and Wintermeyer, W. (2006) Role and timing of GTP binding and hydrolysis during EF-G-dependent tRNA translocation on the ribosome. *Proceedings of the National Academy of Sciences* **103**, 13670-13675
54. Ævarsson, A., Brazhnikov, E., Garber, M., Zheltonosova, J., Chirgadze, Y., Al-Karadaghi, S., Svensson, L., and Liljas, A. (1994) Three-dimensional structure of the ribosomal translocase: elongation factor G from *Thermus thermophilus*. *The EMBO Journal* **13**, 3669-3677
55. Savelsbergh, A., Matassova, N. B., Rodnina, M. V., and Wintermeyer, W. (2000) Role of domains 4 and 5 in elongation factor G functions on the ribosome. *Journal of Molecular Biology* **300**, 951-961
56. Lin, J., Gagnon, M. G., Bulkley, D., and Steitz, T. A. (2015) Conformational changes of elongation factor G on the ribosome during tRNA translocation. *Cell* **160**, 219-227

57. Peske, F., Matassova, N. B., Savelsbergh, A., Rodnina, M. V., and Wintermeyer, W. (2000) Conformationally restricted elongation factor G retains GTPase activity but is inactive in translocation on the ribosome. *Molecular Cell* **6**, 501-505
58. Yin, H., Gavriiliuc, M., Lin, R., Xu, S., and Wang, Y. (2019) Modulation and visualization of EF-G power stroke during ribosomal translocation. *ChemBioChem* **20**, 2927-2935
59. Petrychenko, V., Peng, B.-Z., de AP Schwarzer, A. C., Peske, F., Rodnina, M. V., and Fischer, N. (2021) Structural mechanism of GTPase-powered ribosome-tRNA movement. *Nature Communications* **12**, 5933-5941
60. Katunin, V. I., Savelsbergh, A., Rodnina, M. V., and Wintermeyer, W. (2002) Coupling of GTP hydrolysis by elongation factor G to translocation and factor recycling on the ribosome. *Biochemistry* **41**, 12806-12812
61. Inoue-Yokosawa, N., Ishikawa, C., and Kaziro, Y. (1974) The role of guanosine triphosphate in translocation reaction catalyzed by elongation factor G. *Journal of Biological Chemistry* **249**, 4321-4323
62. Rodnina, M. V., Savelsbergh, A., Katunin, V. I., and Wintermeyer, W. (1997) Hydrolysis of GTP by elongation factor G drives tRNA movement on the ribosome. *Nature* **385**, 37-41
63. Rodnina, M. V., and Wintermeyer, W. (2011) The ribosome as a molecular machine: the mechanism of tRNA–mRNA movement in translocation. *Biochemical Society Transactions* **39**(2), 658-662
64. Conway, T. W., and Lipmann, F. (1964) Characterization of a ribosome-linked guanosine triphosphatase in Escherichia coli extracts. *Proceedings of the National Academy of Sciences of the United States of America* **52**, 1462-1469
65. Rohrbach, M. S., and Bodley, J. W. (1976) Studies on translocation. 21. Steady state kinetic analysis of the mechanism of guanosine triphosphate hydrolysis catalyzed by Escherichia coli elongation factor G and the ribosome. *Biochemistry* **15**, 4565-4569
66. La Cour, T., Nyborg, J., Thirup, S., and Clark, B. (1985) Structural details of the binding of guanosine diphosphate to elongation factor Tu from E. coli as studied by X-ray crystallography. *The EMBO journal* **4**, 2385-2388
67. Saraste, M., Sibbald, P. R., and Wittinghofer, A. (1990) The P-loop—a common motif in ATP- and GTP-binding proteins. *Trends in Biochemical Sciences* **15**, 430-434
68. Gao, Y.-G., Selmer, M., Dunham, C. M., Weixlbaumer, A., Kelley, A. C., and Ramakrishnan, V. (2009) The structure of the ribosome with elongation factor G trapped in the posttranslocational state. *Science* **326**, 694-699

69. Stouten, P. F., Sander, C., Wittinghofer, A., and Valencia, A. (1993) How does the switch II region of G-domains work? *FEBS letters* **320**, 1-6
70. Song, H., Parsons, M. R., Rowsell, S., Leonard, G., and Phillips, S. E. (1999) Crystal structure of intact elongation factor EF-Tu from *Escherichia coli* in GDP conformation at 2.05 Å resolution. *Journal of Molecular Biology* **285**, 1245-1256
71. Kolesnikov, A., and Gudkov, A. (2002) Elongation factor G with effector loop from elongation factor Tu is inactive in translocation. *FEBS letters* **514**, 67-69
72. Hizli, A. A., Chi, Y., Swanger, J., Carter, J. H., Liao, Y., Welcker, M., Ryazanov, A. G., and Clurman, B. E. (2013) Phosphorylation of eukaryotic elongation factor 2 (eEF2) by cyclin A–cyclin-dependent kinase 2 regulates its inhibition by eEF2 kinase. *Molecular and Cellular Biology* **33**, 596-604
73. Ryazanov, A. G., and Davydova, E. K. (1989) Mechanism of elongation factor 2 (EF-2) inactivation upon phosphorylation Phosphorylated EF-2 is unable to catalyze translocation. *FEBS letters* **251**, 187-190
74. Carlberg, U., Nilsson, A., and Nygard, O. (1990) Functional properties of phosphorylated elongation factor 2. *European Journal of Biochemistry* **191**, 639-645
75. Dumont-Miscopein, A., Lavergne, J.-P., Guillot, D., Sontag, B., and Reboud, J.-P. (1994) Interaction of phosphorylated elongation factor EF-2 with nucleotides and ribosomes. *FEBS letters* **356**, 283-286
76. Bodley, J. W., Zieve, F. J., Lin, L., and Zieve, S. T. (1969) Formation of the ribosome-G factor-GDP complex in the presence of fusidic acid. *Biochemical and Biophysical Research Communications* **37**, 437-443
77. Koripella, R. K., Chen, Y., Peisker, K., San Koh, C., Selmer, M., and Sanyal, S. (2012) Mechanism of elongation factor-G-mediated fusidic acid resistance and fitness compensation in *Staphylococcus aureus*. *Journal of Biological Chemistry* **287**, 30257-30267
78. Turnidge, J., and Collignon, P. (1999) Resistance to fusidic acid. *International Journal of Antimicrobial Agents* **12**, S35-S44
79. Falagas, M. E., Grammatikos, A. P., and Michalopoulos, A. (2008) Potential of old-generation antibiotics to address current need for new antibiotics. *Expert Review of Anti-Infective Therapy* **6**, 593-600
80. Bulkley, D., Brandi, L., Polikanov, Y. S., Fabbretti, A., O'Connor, M., Gualerzi, C. O., and Steitz, T. A. (2014) The antibiotics dityromycin and GE82832 bind protein S12 and block EF-G-catalyzed translocation. *Cell Reports* **6**, 357-365

81. Pestka, S. (1968) Studies on the formation of transfer ribonucleic acid-ribosome complexes: III. The formation of peptide bonds by ribosomes in the absence of supernatant enzymes. *Journal of Biological Chemistry* **243**, 2810-2820
82. Moazed, D., and Noller, H. F. (1989) Intermediate states in the movement of transfer RNA in the ribosome. *Nature* **342**, 142-148
83. Ratje, A. H., Loerke, J., Mikolajka, A., Brünner, M., Hildebrand, P. W., Starosta, A. L., Dönhöfer, A., Connell, S. R., Fucini, P., and Mielke, T. (2010) Head swivel on the ribosome facilitates translocation by means of intra-subunit tRNA hybrid sites. *Nature* **468**, 713-716
84. Zhou, J., Lancaster, L., Donohue, J. P., and Noller, H. F. (2014) How the ribosome hands the A-site tRNA to the P site during EF-G-catalyzed translocation. *Science* **345**, 1188-1191
85. Dorner, S., Brunelle, J. L., Sharma, D., and Green, R. (2006) The hybrid state of tRNA binding is an authentic translation elongation intermediate. *Nature Structural & Molecular Biology* **13**, 234-241
86. Ermolenko, D. N., and Noller, H. F. (2011) mRNA translocation occurs during the second step of ribosomal intersubunit rotation. *Nature Structural & Molecular Biology* **18**, 457-462
87. Liu, T., Kaplan, A., Alexander, L., Yan, S., Wen, J.-D., Lancaster, L., Wickersham, C. E., Fredrick, K., Noller, H., and Tinoco Jr, I. (2014) Direct measurement of the mechanical work during translocation by the ribosome. *Elife* **3**, e03406
88. Yao, L., Li, Y., Tsai, T. W., Xu, S., and Wang, Y. (2013) Noninvasive Measurement of the Mechanical Force Generated by Motor Protein EF-G during Ribosome Translocation. *Angewandte Chemie International Edition* **52**, 14041-14044
89. Ticu, C., Nechifor, R., Nguyen, B., Desrosiers, M., and Wilson, K. S. (2009) Conformational changes in switch I of EF-G drive its directional cycling on and off the ribosome. *The EMBO Journal* **28**, 2053-2065
90. Lagerkvist, U., and Waldenström, J. (1964) Structure and function of transfer RNA: I. Species specificity of transfer RNA from *E. coli* and yeast. *Journal of Molecular Biology* **8**, 28-37
91. Rodnina, M. V., and Wintermeyer, W. (1995) GTP consumption of elongation factor Tu during translation of heteropolymeric mRNAs. *Proceedings of the National Academy of Sciences* **92**, 1945-1949

92. Rodnina, M. V., Peske, F., Peng, B.-Z., Belardinelli, R., and Wintermeyer, W. (2019) Converting GTP hydrolysis into motion: versatile translational elongation factor G. *Biological Chemistry* **401**, 131-142
93. Zengel, J. M., Archer, R. H., and Lindahl, L. (1984) The nucleotide sequence of the *Escherichia coli* fus gene, coding for elongation factor G. *Nucleic Acids Research* **12**, 2181-2192
94. Chaney, M. O., and Steinrauf, L. K. (1974) The crystal and molecular structure of tetragonal L-cystine. *Acta Crystallographica Section B: Structural Crystallography and Crystal Chemistry* **30**, 711-716
95. Schmidt, H. H.-J., Genschel, J., Haas, R., and Manns, M. P. (1997) Preparative electrophoresis: An improved method for the isolation of human recombinant apolipoprotein AI. *BioTechniques* **23**, 778-779
96. Griffith, I. (1972) The effect of cross-links on the mobility of proteins in dodecyl sulphate–polyacrylamide gels. *Biochemical Journal* **126**, 553-560
97. Yamanaka, T., Tosaki, A., Miyazaki, H., Kurosawa, M., Furukawa, Y., Yamada, M., and Nukina, N. (2010) Mutant huntingtin fragment selectively suppresses Brn-2 POU domain transcription factor to mediate hypothalamic cell dysfunction. *Human Molecular Genetics* **19**, 2099-2112
98. Savelsbergh, A., Katunin, V. I., Mohr, D., Peske, F., Rodnina, M. V., and Wintermeyer, W. (2003) An elongation factor G-induced ribosome rearrangement precedes tRNA-mRNA translocation. *Molecular Cell* **11**, 1517-1523
99. Kaziro, Y. (1978) The role of guanosine 5'-triphosphate in polypeptide chain elongation. *Biochimica et Biophysica Acta Reviews on Bioenergetics* **505**, 95-127
100. Kraus, C. N., and Burnstead, B. W. (2011) The safety record of fusidic acid in non-US markets: a focus on skin infections. *Clinical Infectious Diseases* **52**, S527-S537
101. Seo, H.-S., Abedin, S., Kamp, D., Wilson, D. N., Nierhaus, K. H., and Cooperman, B. S. (2006) EF-G-dependent GTPase on the ribosome. Conformational change and fusidic acid inhibition. *Biochemistry* **45**, 2504-2514
102. Carbone, C. E., Loveland, A. B., Gamper, H., Hou, Y.-M., Demo, G., and Korostelev, A. A. (2021) Time-resolved cryo-EM visualizes ribosomal translocation with EF-G and GTP. *Nature Communications* **12**, 7236-7248
103. Connell, S. R., Takemoto, C., Wilson, D. N., Wang, H., Murayama, K., Terada, T., Shirouzu, M., Rost, M., Schüler, M., and Giesebrecht, J. (2007) Structural basis for interaction of the ribosome with the switch regions of GTP-bound elongation factors. *Molecular Cell* **25**, 751-764

104. Wang, Y., Jiang, Y., Meyering-Voss, M., Sprinzl, M., and Sigler, P. B. (1997) Crystal structure of the EF-Tu EF-Ts complex from *Thermus thermophilus*. *Nature Structural Biology* **4**, 650-656
105. Jørgensen, R., Merrill, A. R., and Andersen, G. R. (2006) The life and death of translation elongation factor 2. *Biochemical Society Transactions* **34**(1), 1–6
106. Finstad, K. M., Probst, A. J., Thomas, B. C., Andersen, G. L., Demergasso, C., Echeverría, A., Amundson, R. G., and Banfield, J. F. (2017) Microbial community structure and the persistence of cyanobacterial populations in salt crusts of the hyperarid Atacama Desert from genome-resolved metagenomics. *Frontiers in Microbiology* **8**, 1435-1444
107. Jacob, J., Duclohier, H., and Cafiso, D. S. (1999) The role of proline and glycine in determining the backbone flexibility of a channel-forming peptide. *Biophysical Journal* **76**, 1367-1376
108. D'aquino, J. A., Gómez, J., Hilser, V. J., Lee, K. H., Amzel, L. M., and Freire, E. (1996) The magnitude of the backbone conformational entropy change in protein folding. *Proteins: Structure, Function, and Bioinformatics* **25**, 143-156
109. Maciejewski, P. M., Peterson, F. C., Anderson, P. J., and Brooks, C. L. (1995) Mutation of serine 90 to glutamic acid mimics phosphorylation of bovine prolactin. *Journal of Biological Chemistry* **270**, 27661-27665
110. Redpath, N. T., Price, N. T., Severinov, K. V., and Proud, C. G. (1993) Regulation of elongation factor-2 by multisite phosphorylation. *European Journal of Biochemistry* **213**, 689-699
111. Salsi, E., Farah, E., Netter, Z., Dann, J., and Ermolenko, D. N. (2015) Movement of elongation factor G between compact and extended conformations. *Journal of Molecular Biology* **427**, 454-467